NORTHWESTERN UNIVERSITY

Role of HCN channels in Behavioral Responses to Psychosocial Stress

A DISSERTATION

SUBMITTED TO THE GRADUATE SCHOOL IN PARTIAL
FULFILLMENT OF THE REQUIREMENTS

for the degree

DOCTOR OF PHILOSOPHY

Field of Neuroscience

By

Daniel W. Fisher

EVANSTON, ILLINOIS

December 2017

ABSTRACT

Psychosocial stress is part of everyday life, and while ubiquitous, stress plays a huge role

disease development and treatment. Though the stressor's intensity, predictability, and frequency (acute

vs chronic) are important determinants of disease development, interactions with one's genetic and

epigenetic make-up also play a causal role. Major Depressive Disorder (MDD) is influenced by stress,

and MDD is best described as a disease of aberrant neural connectivity. Hyperpolarization-activated

Cyclic Nucleotide-gated (HCN) channels are important molecular regulators of neural excitability

influencing connectivity, and ablation of HCN channels in the dorsal hippocampus lead to antidepressant-

like behavior in mice. However, HCN channels' role in response to psychosocial stress is unknown. In this

thesis, hippocampal HCN channels and their behavioral effects are characterized after acute and chronic

stress in mice. Data presented here suggests that HCN channels do not change expression or function

after Chronic Social Defeat (CSD) in the dorsal hippocampus of mice, nor does loss of HCN channel

localizing protein, Tetratricopeptide repeat-containing Rab8b-interacting protein (TRIP8b), protect mice

from CSD. However, loss of TRIP8b or HCN channels in the dorsal CA1 leads to persistent active coping

behavior, which in humans prevents the development of certain diseases while improving outcomes to

treatment. In all, the data shown here suggest that HCN Channels may not be specific targets for MDD

but instead may more broadly applied to numerous disease where improving adaptive responses to

stress would greatly benefit patients.

This thesis additionally explores the phenotype of a novel HCN2 mutation in mice that leads to

complete ablation of this protein. Like other HCN2 ablation mice, these mice display ataxia, tremor,

infertility, persistent absence epilepsy-like spike-wave discharges, antidepressant-like behavior, and

severe growth restriction. Data here shows that the extreme growth restriction is unlikely to be due to

hormone dysfunction of the pancreas, pituitary, or thyroid and more likely to be due to malnutrition

secondary to slowed GI motility.

ACKNOWLEDGEMENTS

They say it takes a village to raise a child, and it took an entire campus worth of people to get me through my PhD. While I will undoubtedly forget multiple people who helped out greatly, I'd like to take this space to thank a few who were completely indispensable for my growth and maturation as a scientist.

First and foremost, I'd like to give my sincerest thanks to my mentor, Dr. Dane Chetkovich. I think I may have been the most difficult graduate student of all time, and Dane did a remarkable job in keeping me focused and getting me to graduate. I can only imagine that having such an opinionated and passionate student was difficult for Dane, but Dane stretched himself to his own personal limits in guiding me as best he could to success. For all Dane's students, he demonstrates an incredible ability to foster their growth in any way he can, which is a rare quality in scientific mentors and one that makes him one of the best Principal Investigators on the whole Northwestern University Campus. There is no doubt in my mind that I would not have been more successful in any other lab, and I'm very fortunate to have landed in such a nurturing environment as Dane's lab for my PhD.

In addition to Dane, my labmates Kyle Lyman, Ye Han, Robert "BJ" Heuermann, Jonathan Kurz, Kendall Timmons, Xiangying Cheng, Annie Ismail, and Phillip Luu all contributed greatly to my training in ways I have difficulty enumerating. Both Kyle and BJ were great sources of feedback during troubleshooting experiments and immensely helpful in improving my understanding of electrophysiology. Ye helped train me on many of the techniques in the lab, and I would not have been able to complete my project without her assistance. I was especially lucky to have Jon as a teacher and role model, and I owe all my knowledge about EEGs to him. Finally, the rest of the lab has been supportive of me and my projects, being quick to lend a hand when needed, and I thank all of you for your help during my training.

Outside of my lab specifically, there were numerous others who helped me develop myself scientifically, and I would not have graduated without their help. I'd like to specifically point out the help I received from the Kessler, Opal, Garcia-Anoveros, Dong, Goldman, Miller, Disterhoft, and Hunter labs, as all of these groups greatly aided the completion of the work displayed in this thesis. In addition, I would like to thank my thesis committee: Chair Dr. Jack Kessler MD, Dr. Richard J. Miller PhD, and Dr. Hongxin Dong MD PhD. The guidance given by this committee was greatly appreciated in creating this final work,

of which I'm very proud. In particular, I'd like to give a special mention to Hongxin, who has been an incredible friend throughout this process and an even better mentor. There were multiple times where her guidance and generosity led to me to exactly what I needed, and I am lucky to have been embraced by her incredible spirit and giving nature.

Finally, I'd like to thank my family for their support. In some ways, I feel like what really needs to be written is an apology to them, but I suppose this acknowledgement is the best I can do for now. Though completion of any PhD is tumultuous, the effect that this process had on me was especially overwhelming. The long hours, high stress, and constant failures that are imperative to personal and professional growth also led me to turn inwards, and no one suffered more from this than the ones I love. Still, they had the incredible strength of character and compassion to accept my withdrawal as a feature of a difficult time in my life and lift me up gently when I didn't even know I was down. It would be hard to write enough words about these people in my life – and I suspect that if I tried I'd have an even longer document than the one here, though maybe with less tables and graphs. So I'll say this: To Dad, Mom, Kara, and Jill; I love you all very much. And to Tory, the only one in my family who had a choice, may you never be cured of the insanity which leads to your love for me. G-d only knows what I'd be without you.

DEDICATION

To my family and friends, but especially Dad, Mom, Kara, Jill, and Tory.

TABLE OF CONTENTS

LIST OF FIGURES

CHAPTER 1

Introduction

1.1 <u>Understanding Acute and Chronic Stress</u>

As organisms interact with their environment, a complex interplay between environmental stimuli and biological responses rapidly develop, often leading to bidirectional changes between that organism and the world around them. Of these responses, higher organisms' (i.e. vertebrates') behavioral responses to psychosocial stress are among the most complex and least understood by biologists and physicians. Though many of the body's stress responses are mediated through the Hypothalamus-Pituitary-Adrenal (HPA) axis and the Autonomic Nervous System (ANS), increasing evidence is beginning to demonstrate that the nuanced responses to stress over time are shaped by many other pathways, including the immune system and the intrinsic connectivity of various regions of the brain. In addition, the quality and quantity of responses from these systems depend on the modality and timing of the psychosocial stressors encountered by the individual organism, and the interactions between these biological systems is also likely to change depending on the stress stimuli. For this reason, it makes sense to differentiate between stress responses of short duration (acute) and those that are shaped by repeated stress over time (chronic), as their impact is quite divergent in terms of the individual's behavioral and biological response.

In general, acute psychosocial stress has an 'activating' response both behaviorally and biochemically. With an acutely stressful situation, the sympathetic nervous system is activated, peripheral and central stress hormone signaling is increased, many cognitive centers of the brain become more excitable, and the individual tends to display an adaptive response that is ultimately shaped by all of these factors[1-3]. Evolutionarily, acute stresses tend to alert the organism to potentially threatening changes in the environment, and the increase in these biological symptoms prepares the individual for a dynamic response. In this way, many researchers have indicated that moderate, acute stressors lead to better performance on cognitive tasks and increased physical abilities. Still, an extremely intense stressor may have negative effect on both these behavioral domains, leading to a loss of focus or inability to perform goal-directed actions quickly and efficiently, and in some cases, may lead to later aberrant

behavior, such as seen in Post-Traumatic Stress Disorder. For this reason, much of the complexity in understanding the acute stress response lies in the relationship between an individual' s natural response to stress and the modality and intensity of the stress response encountered[1-3].

Similar to acute stress, chronic stress can have both advantageous and deleterious consequences on behavior[2]. Though the biological adaptations to chronic stress are by definition less immediate and longer lasting, modality and intensity of stressors are again central to understanding how an individual responds[3,4]. Unimodal, predictable, and mild stressors can often lead to adaptation and a reduced stress response that is often pro-resilient in terms of pathological behavior. This is especially true of early life stress, which has been shown by many to be adaptive if the intensity of the stressor is low and if resolution of the stressor is relatively swift. However, chronic stress often leads to increasingly more maladaptive responses, especially when repeated stress is multimodal, unpredictable, and uncontrollable[2,4]. In these situations, an individual's response is almost opposite of the adaptive, acute stress response, including blunting of HPA axis activation and feedback, imbalance between sympathetic and parasympathetic nervous systems, and aberrant connectivity within important corticolimbic structures[2,5,6]. As chronic stress is a salient feature of everyday life, numerous diseases are worsened by chronic stress, among them Major Depressive Disorder (MDD).

Because of the huge impact that psychosocial stress has on health and disease, our lab has extensively studied how psychosocial stress impacts pre-clinical models of disease in mice. In particular, our lab hope to develop new approaches to reducing maladaptive behavior associated with MDD and other diseases that are heavily influenced by psychosocial stress. In this thesis, I will present an in depth characterization of a group of ion channels, known as Hyperpolarization Activated Cyclic Nucleotide-Gated (HCN) channels, and their role in the murine behavioral response to both acute and chronic stress. It is our hopes that this work will someday lay the groundwork for future therapies designed to benefit patients who suffer from stress-related diseases.

In order to give the context for the experiments described in this thesis, I will outline what is currently known about psychosocial stress, MDD, and HCN channels in the following sections.

1.2 The Connectivity/Excitability Hypothesis of Depression

In the United States, there is a 1 in 4 risk of developing MDD by age 75[7]. While it is known that MDD causes significant cognitive impairment[8], MDD also increases the risk of developing other diseases, including type 2 diabetes[9], cardiovascular disease, Alzheimer's Disease, and substance abuse[7,10]. MDD worsens glycemic control in diabetic patients, worsens prognoses after myocardial infarction and stroke, lowers adherence to HIV medications, complicates dementia, and demonstrates high co-morbidity with other psychiatric disorders, especially substance abuse[7,10]. Though the prevalence and burden of MDD are enormous, the current medications available to treat this disease – which consist almost exclusively of monoamine-manipulating drugs targeting serotonin, dopamine, and norepinephrine – have not changed for the past half century[11]. Unfortunately, first-line SSRIs are often ineffective, with response rates of 30-50%, leaving millions of people without relief[11,12]. Worse, those with the most severe symptoms are the least likely to respond to current treatments[12].

Significant resources have been devoted to the exploration of monoamines in MDD pathology – without many new therapeutic advances. However, within the last two decades, new models of MDD that highlight brain-wide connective and synaptic dysfunction have surfaced[11,13-15]. Most recently, fMRI and FDG-PET imaging have been used to characterize specific functional connections between a number of brain regions that consistently differ between depressed and healthy control patients[16,17], often showing increased inhibition of cortical structures by the limbic system[18]. These characteristic differences in connectivity have further been shown to disappear with effective antidepressant treatment[19,20].

Though compelling, these associations uncovered by functional imaging lack the ability to resolve the connections between individual neurons or small populations of similar neurons. Further, any fMRI evidence for differences in connectivity between brain regions is derived indirectly through associative changes in blood oxygenation levels, concurrent to predicted neural activation. The paucity of research on causal changes in specific neural circuits is likely due to the technological unfeasibility of studying such changes in humans. Fortunately, rodent models of depression and stress induction[21] have been used extensively to document region-specific changes in transcription[22,23], dendritic morphology[24-26], and synaptic transmission[27-29]. Importantly, there is a give-and-take aspect to the transcriptional patterns, plasticity, and excitability between connected brain regions that strongly support the role of altered circuitry in MDD.

For example, in mice that have undergone Chronic Mild Stress (CMS), a daily stress induction paradigm that rotates mild stressors unpredictably and results in depression-like behaviors in rodents, it was shown that distinct and largely non-overlapping transcriptional patterns were identified in three brain regions implicated as being important in MDD etiology: the amygdala, dentate gyrus (DG), and the cingulate cortex[22]. In addition, treatment with the SSRI fluoxetine reversed gene expression from 28% in the DG to 70% in the amygdala with <10% of gene changes overlapping. It's important to note that while some of these non-overlapping changes constitute changes in separate genes, there were some changes that were opposite in different brain regions, supporting the give-and-take of these circuits. Perhaps one of the most salient example of this is with the regulation of BDNF, a neurotrophin that has recently shown great importance in MDD pathogenesis and treatment [for two contrasting reviews, see Duman 2012[11] and Krishnan 2008[15]]. In a review of MDD, Krishnan and Nestler[15] point out that while preclinical stress paradigms have shown a decrease in BDNF in the Prefrontal Cortex (PFC) and hippocampus, BDNF is increased in the Nucleus Accumbens (NAc), an area innervated by connections from the hippocampus and the dopaminergic cells of the Ventral Tegmental Area (VTA). Further, they notice that while direct infusion of BDNF into the hippocampus promotes antidepressant-like behavior, direct infusion of BDNF into the VTA-NAc pathway increases depression-like behavior.

Though the previous examples highlight the transcriptional differences that may underlie changes in abnormal circuitry in MDD, specific electrophysiological alterations have been noted in humans and preclinical models of MDD as well. As one example, hyperactivtiy of the amygdala has been shown by numerous human functional imaging studies as central to MDD[30]. In accordance with this, it has been shown that optogenetic stimulation of the principal cells of the Basolateral Amygdala (BLA) that synapse in the ventral hippocampus (vHC) can drive depression-like and anxiety-like behavior in mice. In addition, optogentic inhibition of the BLA-vHC pathway can promote antidepressant-like and anxiolytic-like behavior in mice[31]. Further, this behavior was shown to extend to social interactions, as stimulation of this pathway leads to social avoidance and inhibition of this pathway leads to more normal social interactions in mice[32]. Importantly, electrophysiological assessment of socially interacting rodents show increased firing of a subset of BLA neurons during social interaction events[27]. Approaches to determining causality in MDD, as

suggested in this example, are quickly validating functional imaging studies and continue to support the connectivity/excitability hypothesis of MDD.

1.3 The Hippocampus in Major Depressive Disorder

The mounting evidence of abnormal connectivity of brain circuitry in MDD has pushed the field into understanding how the reported morphological, molecular, and electrophysiological changes may interact. In particular, the hippocampus has been implicated structurally[33-35], functionally[18,19], and pharmacologically[36-39] as contributing to MDD pathogenesis and treatment response[40], making it a very attractive place to investigate these interactions. The hippocampus, which is perhaps best known for its contributions to short-term and spatial memory, is central to the limbic-to-cortical inhibition that is characteristic of MDD[18,19,41]. Complex changes in hippocampal activity occur in responders to the SSRI fluoxetine but not in those who are treatment resistant[20]. Interestingly, functional imaging studies rarely show the hippocampus as being hyper- or hypoactive in MDD patients, though hippocampal grey matter reduction is often described in MDD patients[41]. However, more recent functional imaging that measure functional connectivity have begun to show abnormalities in connections between the hippocampus and other regions[42-44].

One major drawback to the results displayed in functional imaging studies is the lack of attention to sub-regions of the hippocampus. Classically, the hippocampus is described as a trisynaptic circuit, with input from the entorhinal cortex (EC) flowing through the DG, CA3, CA1, and then back to the entorhinal cortex. In addition, the hippocampus can be divided into sections along its dorso-ventral axis by its patterns of inputs and outputs to and from other brain regions as well as by sharp demarcations developed from abrupt changes in gene expression from one region to another[45,46]. In particular, regions implicated in regulating emotional responses tend to connect with the vHC, while those involved in cognition and spatial memory tend to connect with the dorsal hippocampus (dHC)[46]. Though highly simplified, dissection of the hippocampus into these subregions along the trisnaptic circuit or dorso-ventral axis begins to lay a framework for understanding the complexity of the changes in hippocampal function in MDD. Morphologically, differences in dendritic branching and spines have been noted between the DG, CA1, and CA3 regions with either chronic early life stress or adult stress that results in depression-like behavior in

rodents[24-26]. These differences in morphology are sometimes contrasting and are also subject to change during development[47], though different morphological changes are also likely to be dependent on the stress induction paradigm and possibly the sex of the subject[26].

In addition to the morphological differences caused by stress in hippocampal subregions, stress-induced changes in gene expression show region specificity. One study of transcriptional changes in post-mortem samples from depressed patients shows distinct patterns of monoamine receptor, ion channel, and scaffolding protein gene expression between the CA1 and DG[23]. In line with this, changes in histone modifications, histone deacetylases, and sirtuin activity have been shown to be subregion-specific following CMS or Chronic Restraint Stress in rodents, representing region specific epigenetic modifications that underlie changes in transcription[48,49].

But perhaps most importantly, electrophysiological differences in synaptic plasticity have been reported after acute and chronic stress in rodents in a subregion specific manner. With CMS, specific changes in the Schaffer Collateral (SC) pathway from the CA3 to the stratum radiatum (SR) of the CA1 have shown to be dependent on the time of stress induction[28]. CMS was administered for 1, 2, or 3 weeks in rats with progressively increasing anxiety- and depression-like behavior with increasing CMS duration. In particular, depression-like behavior tended not to develop until the 3rd week of CMS. Interestingly, LTP was enhanced with 2 weeks of CMS but inhibited at 3 weeks of CMS, and this change correlated with a decrease in Kalirin-7 and loss of CA1 and CA3 spine density at 3 weeks but not 2 weeks. In corroboration, another group showed a decrease in LTP magnitude after 3 weeks of CMS in both the SC-CA1 pathway and Perforant Pathway (PP) of the EC to the DG[50]. These results demonstrate that stress duration has a large impact on plasticity and that differences between acute and chronic stress lead to specific changes in plasticity that mirror the development of symptoms.

While the CA3 has connections to the proximal CA1 dendrites in the SR, another important set of connections stem from the EC to the distal dendrites of the CA1 in the Stratum-Lacunosum Moleculare (SLM), termed the Temporo-Ammonic (TA) pathway. This pathway is known to have a large influence over spatial memory, which can also be impaired with chronic, though rarely acute, stress[29]. In rats that were subjected to CMS, a deficit in AMPA-mediated responses but not relative LTP was detected only at the TA-CA1 and not the SC-CA1[29]. Interestingly, biochemical analysis showed that a specific reduction in GluA1

and PSD95 but not GluA2 or GluN1 was associated with this change in synaptic strength and that these changes were restricted to the SLM, not the SR. These changes in synaptic strength were also associated with specific changes in spatial memory consolidation demonstrated in the Morris Water Maze (MWM). This group also showed that SSRI or TCA administration can reverse these changes in synaptic strength through the actions of 5HTR2B, a G_q/G_{11} GPCR, and GluA1 phosphorylation and surface upregulation[51]. These results still held true after treating CMS rats with an SSRI, with concomitant improvement of depression-like behavior on the Sucrose Preference Test (SPT) and Novelty Suppressed Feeding Test (NSFT). While the negative results in the SC-CA1 pathway contrast with those mentioned above, there were significant differences in electrophysiology protocols: the study that showed a difference in the SC-CA1 used *in vivo* anesthetized recordings while the negative result study used *ex vivo* slice preparations with the CA3 and DG removed. Regardless, reductions in synaptic strength and plasticity are evident with CMS, and such findings strongly suggest that changes in inter- and intra-hippocampal connectivity are likely to underlie MDD mechanistically.

1.4 Ketamine as a Fast Acting Antidepressant

Excitingly, the connectivity/excitability hypothesis of MDD has been accompanied by a novel class of drugs: glutamate receptor antagonists[11] and partial agonists[52]. The most well studied of these is ketamine, a putative non-competitive NMDA receptor antagonist. Unlike SSRIs, a sub-hypnotic dose of ketamine improves mood within hours and last for up to two weeks without increasing suicidal behavior in patients with MDD[53-57]. One study showed that at day 3, there was a 70% improvement and nearly 50% remission in ketamine-treated patients who previously failed an average of five other treatment modalities[56]. While ketamine's downstream mechanism of action is still unclear, preclinical studies have demonstrated that plasticity related proteins are likely necessary for ketamine's antidepressant effect. In particular, the neurotrophin BDNF is upregulated in the hippocampus and mPFC and has been implicated as being necessary for ketamine's mechanism of action[54,58]. In addition, downstream mTOR phosphorylation and downstream signaling, including EF-2 activation, seems necessary for ketamine's antidepressant-like effect in rodents, as are AMPARs[54,58-60]. These promising pharmacological data on ketamine help support the

hypothesis that affecting excitability and connectivity, especially in the hippocampus, is a promising approach for developing novel antidepressants and understanding MDD pathogenesis.

While exciting, the characterization of ketamine as a fast acting antidepressant is incomplete. The well-known role of ketamine is to block NMDAR signaling, but both preclinical studies and clinical trials have shown that memantine, a well tolerated NMDAR antagonist, does not have the same antidepressant properties[61,62]. Upon closer inspection, it was shown that memantine fails to elicit the same changes in BDNF and EF-2 as ketamine and that these differences may be mediated in part by memantine's less potent blockade of NMDAR when Mg2+ is present[63]. However, the absence or presence of Mg2+ was not shown to be correlated with the downstream changes in BDNF signaling, so another mechanism may better explain these differences.

Importantly, while ketamine blocks the NMDAR, it has also been reported to affect other receptors. Ketamine has been shown to block D2R, one of the main dopamine receptors[64]. Further, ketamine, but not MK-801 or PCP, has some ability to block certain GABA-A receptors with α6 or σ subunits[65]. Finally, ketamine has been reported to selectively block a subunit of the Hyperpolarization-activated Cyclic Nucleotide gated (HCN) channel, HCN1[66,67].

1.5 HCN Channels

The HCN channels are important regulators of intrinsic excitability through its current, I_h[68-72]. HCN channels are a non-selective cation channels that are mainly permeable to Na^+ and K^+ and are open when the cell is at rest[73]. Their propensity for opening at rest results in a driving force that facilitates a depolarizing leak current, mainly driving Na^+ into the cell and depolarizing the resting membrane potential (RMP)[73]. The unique ability of these channels to support a resting depolarization makes them an incredibly important regulator of intrinsic excitability in neurons[69-71,74,75]. In general, HCN channel activity supports a specific set of electrophysiological properties within the neuron: 1) As mentioned, HCN channels depolarize the RMP, 2) their ability to provide a depolarizing leak current reduces the input resistance (R_N) of the cell[71,72,76], 3) shortens the after-hyperpolarization (AHP) of action potentials[77,78], and 4) accelerates the intrinsic membrane resonance frequency at hyperpolarized voltages[69,70].

However, the subcellular localization of these channels in conjunction with co-localization of other ion channels dictates the resulting influences of these channels to the overall excitability of the cell[73,79]. In this way, HCN channels can be dynamically expressed to bidirectionally change the excitability of the cell[69]. Comparing the distal dendrites, proximal dendrites, and soma reveals this bidirectionality: In pyramidal neurons located in layer 5 of the cortex or in the CA1 of the hippocampus, HCN subunits are trafficked in a preferentially distal dendritic pattern[80-83]. In the apical dendrites of CA1 pyramidal cells, a gradient of increasing expression is evident from the SR to the SLM, so that the majority of cells exist at the distal SLM and the least are found at the proximal SR. The consequences of this distal dendritic enrichment are striking: At the distal dendrites, HCN channels both depolarize the RMP and decrease the R_N of local synaptic inputs. Though the depolarization of the membrane is likely to promote firing, the contribution of the decreased R_N overshadows the change in RMP, and the influence of these distal synaptic inputs greatly weaken their ability to excite the cell, as shown in layer 5b pyramidal cells[84]. Electrophysiologically, a decrease in temporal summation is evident at these distal synaptic sites as well as an increase in the frequency of membrane resonance[69-71]. Interestingly, this same pattern of reducing excitability in the distal dendrites does not extend to the proximal dendrites; in fact, the opposite is true. As shown in layer 5b pyramidal cells, the depolarization of the RMP at the distal dendrites is able to extend to the proximal dendrites, but the local decrease in R_N distally is not transferred proximally[84]. As a consequence, the depolarized RMP has a greater influence than the small decrease in R_N, and synaptic input to the proximal dendrites is strengthened[84]. In concurrence, the frequency of membrane resonance is also slower at the proximal dendrites[69]. The bidirectional effects of HCN channel distal dendritic trafficking on the electrophysiological properties of the cell has prompted some to describe HCN channels' role as being an intrinsic regulator of neuronal excitability[69]. In fact, when coupled with the ability of HCN channels to influence subthreshold membrane resonance, one group has hypothesized that HCN channels are able to "tune" a neuron to the frequencies of various inputs, acting as a band-pass filter[69].

By contrast to distal dendritic HCN channels, a general pattern for somatic HCN has a strong role in regulating the firing frequency of a cell[77,78,85,86], though possible exceptions may exist[87]. In general, when I_h is increased somatically, the AHP that results after the firing of an action potential (AP) is diminished due to HCN channels' ability to rapidly depolarize the cell at voltages below the RMP[77]. Therefore, in cells where

somatic I_h is increased, the firing frequency also increases[78,85,86]. When considering the differences in somatic vs dendritic I_h, it becomes very clear that HCN channels act as a master regulator of intrinsic neuronal excitability and that dynamic expression and trafficking of HCN channels are likely to have significant effects on neuronal connectivity.

One of the most well studied regulators of HCN channel trafficking is the Tetratricopeptide repeat-containing Rab8b-interacting protein (TRIP8b)[80,88,89]. TRIP8b has at least 9 known spliceforms, and transcription of TRIP8b is driven by at least two different promoters, 1a and 1b, that result in different mRNAs and protein sequences[80]. In the hippocampus, spliceforms *Trip8b(1a)* and *Trip8b(1a4)* are the most predominantly expressed transcripts in neurons, and these two spliceforms make up the majority of *Trip8b* in the hippocampus[89]. These two spliceforms strongly influence the upregulation of HCN channels on the plasma membrane of cells *in vitro* and *in vivo,* and the rest of the 1a promoter driven spliceforms do the same[80,88]. Importantly, these two spliceforms are also sufficient to establish the distal dendritic trafficking of HCN channels in the apical dendrites of CA1 pyramidal cells, and loss of TRIP8b in mice abolishes the distally enriching gradient of HCN expression from the proximal SR to the distal SLM[74,90]. As enriched I_h reduces the excitability of distal dendrites and regulates temporal and spatial properties of synaptic integration[69,83,89,91,92], TRIP8b is imperative for normal function[74]. In addition, the *Trip8b(1a)* and *Trip8b(1a4)* spliceforms protect HCN subunits from lysosomal degradation[74].

In contrast to the 1a spliceforms, the 1b spliceforms are likely to be expressed in much greater amounts in oligodendrocytes[89]. In addition, unlike the 1a spliceforms, not all of the 1b spliceforms upregulate HCN channels to the plasma membrane. In particular, the spliceform *Trip8b(1b2)* removes HCN subunits from the plasma membrane[80,88] and leads to loss of HCN channel protein when expressed ectopically in CA1 pyramidal neurons (see Chapter 3).

Taken together, TRIP8b's role in trafficking HCN channels subcellularly has a large influence on how HCN channels influence the excitability of neurons. In addition, the incredibly diverse effects of HCN channels on intrinsic plasticity have led many to investigate what role HCN channels might play in pathogenesis of disorders typified by altered excitability. One of these diseases is MDD.

1.6 HCN Channels' role in psychological stress and MDD

HCN channel function is significantly altered in various preclinical models of psychosocial stress and MDD. Corticotropin Releasing Factor (CRF), a centrally acting stress hormone, has been shown to increase I_h and subsequent firing of excitatory cells in regions highly implicated in depression pathogenesis, including the BLA[86], VTA[78], and Periventricular Nucleus (PVN) of the hypothalamus[85]. In addition, it has been shown that NPY, an anxiolytic protein, is able to reduce I_h and firing frequency in the BLA[86]. Importantly, the amygdala and VTA have been shown to be hyperactive in MDD[30,93]. Though many of these groups acutely administered CRF, it's possible that some of the HPA axis dysfunction that is evident in MDD is due to abnormalities in CRF-mediated increases in I_h in these cell populations.

The role of HCN channels in MDD pathogenesis has also been studied in more physiologically relevant, chronic stress models. In particular, I_h in the VTA has been shown to play a large role in stress susceptibility and resilience[94,95]. The Chronic Social Defeat (CSD) model of stress induction is unique in that it identifies two groups of mice that are either susceptible or resilient to CSD stress[96-98]. The mice that are susceptible to stress develop a multitude of depression-like phenotypes while mice that are resilient behave similar to unstressed controls. Interestingly, the amount of I_h in VTA cells is significantly different between control, susceptible, and resilient mice. Unstressed mice's VTA cells have a low basal level of I_h that is associated with a relatively low firing frequency. In contrast, susceptible mice's VTA cells have increased I_h and firing frequencies. Strikingly, however, resilient mice's VTA cells have even higher levels of I_h but have a firing frequency comparable to controls. This was shown to be mediated through A-type potassium channel compensation, which reduces the firing frequency when I_h increases very strongly. These results were confirmed by pharmacological or viral increase in I_h, which were able to induce a resilient behavioral phenotype in previously susceptible mice[95]. In addition, it was shown that chronic fluoxetine decreased I_h in these VTA cells[94]. These results not only demonstrate how HCN channels may be altered by chronic stress, but also begin to hint at the complex regulation of these channels and subsequent intrinsic plasticity with psychosocial stress.

While the results mentioned so far have described brain regions where affected cells have somatic I_h, other studies have shown that regions where excitatory cells express HCN channels predominantly in dendrites may also have a role in MDD. Specifically, our lab has recently shown that knock-out (KO) of HCN1, HCN2, or TRIP8b produces a very clear antidepressant-like phenotype on FST and TST[74].

Interestingly, this antidepressant-like phenotype could be recapitulated with acute shRNA knock-down of HCN1 in the murine dorsal CA1[74,76]. Mechanistically, the antidepressant-like phenotype induced by HCN1 knockdown was accompanied by increases in BDNF signaling and mTOR phosphorylation in a manner very similar to ketamine's fast-acting antidepressant effect[76]. It is important to note that many studies have shown pathway specific changes in hippocampal excitability in rodent models of chronic stress and differences in plasticity have been noted between the SR and SLM[28,29,50,51], where HCN channel localization is highly regulated.

In addition, HCN channel expression and localization changes dramatically during postnatal development[81,99,100], and Early Life Stress (ELS) can have a long-lasting impact on adult responses to stress[24,25,101-103]. It has been shown that early life SSRI administration to mice, which facilitates depression-like development in adulthood, is able to change the transcription of HCN1 persistently through adulthood[104]. Still, little is known about whether HCN channel expression or localization is preferentially changed with stress during this early developmental period.

Given the many lines of evidence that suggest HCN channels may be altered with chronic stress in MDD, we hypothesized that HCN channels are likely to be altered in the hippocampus with MDD pathogenesis and treatment.

1.7 Coping style and disease

While much has been said about the deleterious effects of chronic stress and the development of MDD, it is well-accepted that the behavioral response an individual has towards acute stress can greatly influence whether chronic stress will lead to significant pathology[2-4]. One of the major factors in humans that leads to disease resilience is the ability of an individual to take appropriate steps in lessening the impact of a stressor[105-107]. In general, the response someone takes to mitigate the effects of stress is known as 'coping,' and almost all individuals tend to show patterns in how they cope, termed 'coping style.' As with almost any goal-oriented response, the coping style employed by an individual greatly shapes how deleterious the effect of a stressor may be. Those that have more adaptive coping styles tend to be able to surmount every day stress with relative ease, while those with ineffectual coping styles tend to have their stressors compound and often develop pathological behaviors as a result.

In general, two styles of coping are discussed at length in the literature: Active and Passive Coping[108,109]. Sometimes called 'problem-centered' or 'proactive coping,' an Active Coping style seeks to directly modulate the environment in order to reduce the impact of the stressor. In humans, this can take the form of devising solutions to solve upcoming issues, taking pro-active steps to minimize the impact of potential stressors before they happen, or directly confronting issues when they present to avoid compounding of multiple stressors. As the yin to Active Coping's yang, Passive Coping, also called 'emotion centered' or 'reactive coping,' tends to be typified by less adaptive responses to stress that often leads to an inability to solve problems in a timely manner, often leading to the development of new stressors and the compounding impact of multiple, unresolved issues. For humans, this style of coping can take the form of procrastination and avoidant behavior, "lashing out", or escape behavior, such as using alcohol and other addictive, psychoactive substances.

As might be inferred from coping styles' ability to mitigate stress, those with Active Coping styles fair significantly better in terms of disease. Compared to Passive Copers, Active Copers have lower risks of developing many different diseases and have more favorable outcomes upon treatment[105-107]. Though it may be almost self-evident that Active Coping improves disease outcomes where stress is a major etiology, like MDD[108,110,111], Bipolar Disorder Disorder[112], PTSD[113], Schizophrenia[114], and Substance Abuse[115,116], it is perhaps less obvious but no less true that Active Coping improves outcomes for those with numerous chronic illnesses[117], including Cardiovascular Disease[118], Diabetes[119], HIV infection[120], and stroke[121]. Thus, many psychological therapies are designed to increase coping habits, independent of a specific disease process.

Though Active Coping habits can be reinforced with appropriate counseling, and personal experiences are likely to shape coping style, individuals have an intrinsic propensity for one style of coping or another based on their genetic (and likely epigenetic) make-up[122]. Thus, though current research has focused greatly on genes that enhance resilience[105], it remains unknown if these genes do so by promoting more adaptive responses to acute stressors or lessen the biological and psychological impact of stressors independent of the response taken. This distinction, while slight, may be important for understanding disease conversion and prognosis. For example, if an individual gene or molecular pathway reduces the likelihood of developing MDD independent of the action taken, then two important clinical aspects emerge.

First, while the patient may show resilience for MDD, they may still harbor inadequate coping skills which may put them at risk for other stress-related disorders. Though the genetic background of this individual does lend some resilience for one disease, this patient may still lack certain Active Coping habits that would aid this patient greatly. This leads to the second point of note. A patient under extreme amounts of stress may not develop MDD, but if their coping habits are sub-optimal, they may still be at risk for other neuropsychiatric disorders and thus benefit from psychological counseling aimed at promoting active coping. Contrast this situation, with an individual who has a natural propensity for active coping. They may be protected from numerous stress-related disorders because of their natural propensity for active coping, making their likelihood of developing MDD less, similar to the patient in the previous example. However, if this patient were to develop MDD, they would be less likely to benefit from psychotherapeutic approaches designed to increase active coping and may show better responses to pharmacotherapy or other psychotherapeutic styles. While this strict dichotomy may not exist as clearly as described above, nuanced propensities towards one condition or the other are likely. In this way, understanding the genetic background of the individual along with the knowledge of how certain genes influence coping style or intrinsic resiliency would be of great value to helping patients in all branches of medicine. Still, disambiguating these two different forms of resilience is a challenging task that has yet to be fully addressed by researchers.

1.8 Neurobiology of Coping Style

Just as many different neuropsychiatric diseases overlap in affected neural circuitry, so too do many of these same neural pathways influence coping style. Though most research defining these circuits are in rodent models, similar neural pathways are found to be perturbed across different coping assays, most notably the ventral medial prefrontal cortex (vmPFC), nucleus accumbens, dorsal raphe nucleus, hypothalamus, periaqueductal gray, amygdala, lateral septum, and hippocampus[4,122]. As may be expected, the corticolimbic circuitry in coping is very similar to aberrant circuitry that develops with MDD[105].

While some studies have looked at transient activation via c-fos expression after tasks involved in coping, most of these studies have examined the balance of neurotransmitters and their receptors in these areas[4,109,122-124]. Though many neurotransmitters or neurosteroids have been studied, including

acetylcholine, dopamine, norepinephrine, oxytocin, vasopressin, glutamate, GABA, allopregnanolone, and CRF, most of the work has focused on serotonergic neurotransmission[109,124]. The vast majority of publications assessing coping style have demonstrated that increased serotoninergic signaling during stress promotes active coping[125,126]. In particular, increased signaling through 5-HT1A receptors promotes more proactive coping, and increased 5HT1A expression is a hallmark of predominantly active copers[127,128]. Additionally, increased serotonergic activity in the Lateral Septum (LS) leads to similar increases in active coping[129,130]. Intriguingly, the dHC makes prominent connections with the LS, suggesting that connectivity between these two regions may result in regulation of coping behaviors, with mutual serotonergic control from the Raphe Nucleus[130-132].

Despite the putative role of the dHC in spatial and contextual memory[46], the dHC has also been implicated in regulating coping style. For instance, pharmacologically increasing acetylcholine signaling in the dHC leads to decreased burying (active coping) in the Shock Probe Burying Test (SPBT), a test where neither active nor passive coping are reinforced[133]. Similarly, using two rat lines with different propensities towards territorial aggression and subsequent coping styles, an increase in c-fos signaling was seen in the dHC of the more aggressive males compared to the less aggressive males during an agonistic encounter[134], and similar results were seen in two mouse lines bred for high and low aggressiveness[135].

The anatomical pathways whereby the dHC could affect emotional regulation, such as coping behavior, are sparse, as the dHC makes few direct connections to the limbic system[46]. For this reason, it seems likely that the connections between the dHC and LS are responsible for influencing coping behavior, as not only are both regions under prominent serotonergic regulation but the LS serves as an intermediate for dHC signaling to the VTA[132]. However, while this pathway has been shown to be involved in contextual reward processing[132], it remains unclear if the basal connectivity between the dHC and LS influences intrinsic responses to environmental stimuli, such as coping style.

1.8 Conclusion to Chapter 1

As research into neuropsychiatric disorders returns to its roots, namely in understanding how different neural groups connect together and underlie behavior (as opposed to investigating changes in neurotransmitter levels), a greater emphasis on the intrinsic excitability of these neurons is more likely to

be appreciated. Already, advances in temporal and spatial precision in neural activation, such as opto- and chemo-genetics, are demonstrating circuit level perturbations in disease that represent new targets for drug treatment[136]. Along this same line, understanding how molecular regulators of excitability in key sub-regions and in key cell types influence connectivity should lead to similar advances.

As described in this chapter, HCN channels are likely candidates to be involved in neuropsychiatric disease, as they prominently influence the intrinsic excitability of neurons in many limbic system regions. Importantly, given the dynamic relationship between HCN channel subcellular localization and subsequent regulation of neuronal excitability, the complex regulation of these channels in terms of expression and subcellular trafficking is ideal for tight regulation of neuronal circuits, especially those that are influenced by rhythmic activations[73,79]. Therefore, it is likely that these channels are dynamically regulated in response to environmental stimuli, especially psychosocial stress.

Whether these channels are involved in the acute or chronic stress response, however, remains to be seen. Certainly, within the mouse's dorsal CA1, where they constrain excitability through decreasing R_n, a loss of these channels has profound effects on behavior, eliciting a clear antidepressant-like phenotype[76,137]. However, it remains unknown exactly how these channels may change during the development of adaptive, maladaptive, and aberrant behaviors induced by stress.

As such, the majority of this thesis will investigate how HCN channels change in the hippocampus with psychosocial stress and how changing these channels may influence behaviors that are shaped by stress. Importantly, these investigations will take place using both acute and chronic stress modalities in mice. Through the work presented here, I hope to leave the reader with a more complete view of how HCN channels in the dHC may be involved in stress regulation and further hope that future investigations will build on these findings to understand more about stress responses and how we can better shape them to treat human disease.

1.9 HCN2 in mouse models

In the adult hippocampus, HCN1 and HCN2 are the predominate HCN channel subunits expressed[99,138], and throughout the brain, these two subunits regulate neuronal excitability in complex ways[73]. However, despite their common localization in distal dendrites of pyramidal cells, these two subunits

have very different characteristics in terms of their gating and activation kinetics[73,139]. While HCN1 is relatively insensitive to cAMP and is activated relatively quickly, HCN2's gating properties are much more dependent on cAMP, and HCN2 opens and closes much more slowly than HCN1[73]. In addition, while the co-expression in pyramidal cells suggests a common function in regulating this cell's excitability, their divergent expression in other cells types and brain regions hints at completely different functions of the two subunits[139].

Nowhere is this more apparent than in the KO mice of either subunit: While HCN1-KO mice show mild motor learning defects, enhanced spatial memory, lower seizure threshold, and antidepressant-like behavior[74,140,141], HCN2-KO mice are very sick and display a wide array of phenotypes that are cell-type specific[87,142]. Most notably, HCN2-KO mice display cardiac dysrhythmias, persistent spike-wave discharges similar to absence epilepsy, ataxia, tremor, reduced neuropathic and inflammatory pain, antidepressant-like behavior, infertility, and severely restricted growth[74,87,142,143]. While the cell-types involved in these phenotypes are known for quite a few of these sequelae, the reason for the small size of these mice has yet to be determined. In fact, KO of HCN2 specifically in the heart[87], forebrain pyramidal cells[144], forebrain interneurons[144], Dorsal Root Ganglia (DRG)[145,146], and oligodendrocytes (unpublished data) have all been unable to recapitulate the small size of these mice.

HCN2 is expressed in non-neuronal tissue, and previous reports have found functional roles of this channel in the heart[87], pancreas[147], pituitary gland[148,149], GI tract[150-154], carotid bodies[155], and kidneys[156-158]. Of these tissues, many could be the potential locus of pathology for the growth restriction in HCN2-KO mice. Dysregulation of glucose through inappropriate insulin secretion is one potential mechanism, and HCN2 has been found to regulate insulin secretion upon glucose stimulation[147]. Reduced pituitary hormone secretion, especially of ACTH, TSH, and GH, could be another possible mechanism, as HCN2 has been implicated in regulating the exocytosis of certain pituitary hormones[149]. Carotid body dysregulation could impair normal respiratory responses, and the persistent hypoxia or hypercapnia could impair growth considerably. Finally, paresis of the GI tract could cause early satiety, and HCN2 has been shown to be in both parasympathetic nerve terminals[159] and Enteric Nervous System (ENS) at all levels of the digestive system[153].

In Chapter 4, I will present experiments that attempt to uncover why these mice are growth restricted, as identification of the tissues involved may have therapeutic implications for patients. If HCN2 regulates a vital function that is compromised in disease, HCN2 channel manipulation may represent a target for these diseases. Depending on the cause of the growth restriction in these mice, this could have implications for treating patients with gastroparesis or slow GI motility, such as in diabetes and Parkinson's Disease, respiratory dysfunction, such as in COPD or Congenital Central Hypoventilation Syndrome, or hormonal dysfunction, such as primary hypopituitarism.

CHAPTER 2

HCN channels and chronic stress

Abstract

Chronic, psychosocial stress can lead to numerous psychiatric diseases, including MDD. As diseases like MDD have bene shown to be caused by aberrant connectivity among key limbic system brain regions, understanding how molecular regulators of neuronal excitability influence MDD pathogenesis during chronic stress is essential for the development of future treatments. One such molecular regulator of excitability is the Hyperpolarization activated Cyclic-Nucleotide gated (HCN) channels, and ablation of these channels in the dorsal hippocampus (dHC) leads to reduced immobility on the Forced Swim Test (FST) and Tail Suspension Test (TST) at baseline. However, little is known about the interplay between HCN channel expression, chronic stress, and stress-induced behaviors. In this chapter, HCN channel expression is shown to be unchanged in numerous limbic system brain regions after Chronic Social Defeat (CSD) stress in mice, including the dHC. Further, HCN channel localization and function in CA1 pyramidal cells is unaltered by CSD, though an I_h-independent reduction in intrinsic excitability is evident in dorsal CA1 pyramidal cells from defeated mice. In addition, knockout of the HCN channel localizing protein Tetratricopeptide Repeat-containing Rab8b-Interacting Protein (TRIP8b) is unable to protect mice from CSD-induced, aberrant behaviors, though decreased immobility on FST remains. Finally, the rapid acting antidepressant ketamine reduces *Hcn1* and *Trip8b* mRNA 2 hours after injection, though the significance of this decrease is unclear. Overall, CSD stress in mice and HCN channels do not seem to affect each other on a behavioral or molecular level.

Introduction

While psychosocial stress is part of everyday life, persistent stress and genetic susceptibility to psychiatric disease can synergize to facilitate the development of numerous neuropsychiatric diseases, such as Major Depressive Disorder (MDD), General Anxiety Disorder, and Post-Traumatic Stress Disorder[5]. Of these, MDD in particular is quite prevalent[7,8,160,161] and has a burdensome impact economically[8]. In addition, successful MDD treatment rates are still low relative to other diseases in medicine and relapse is common[11,12].

Two very common antidepressant screening assays, the Tail Suspension Test (TST) and the Forced Swim Test (FST) are used ubiquitously in rodents, and almost all new antidepressant therapies are first tested for efficacy in these assays[162]. Therefore, it was of great interest when it was shown that knockout (KO) of certain Hyperpolarization activated Cyclic-Nucleotide gated (HCN) channels conferred robust antidepressant-like behavior in mice on these assays[74,76,137]. In particular, loss of HCN1, HCN2, or its localizing protein, Tetratricopeptide Repeat-containing Rab8b-Interacting Protein (TRIP8b), can all lead to the same antidepressant-like behavior in mice[74]. Further work has shown that the brain region responsible for this behavior is the dorsal CA1 region of the hippocampus[76,137].

HCN channels in pyramidal cells of the hippocampus, which are the predominate excitatory neurons of the CA1-4 regions, express HCN channels in a very characteristic, distal dendritic pattern along the apical dendrites of the hippocampus[74,81-83]. This enrichment of HCN channels at these dendrites plays an important role in regulating the excitability of these neurons by reducing the input resistance and thus requiring greater depolarizing current to increase the cell's membrane voltage[71,72,76]. Importantly, the localization of these channel at the distal dendrite, which is facilitated through TRIP8b, seems to be uniquely tied to the antidepressant-like behavior found with HCN channel ablation[74,137].

Despite the potential of HCN channels for treating MDD, little is known about how chronic stress may regulate these channels. While work in the VTA has shown that HCN channels respond dynamically to Chronic Social Defeat (CSD) stress[94,95], and that the quantity of current passed through these channels (I_h) confers both susceptibility and resistance to CSD stress in terms of depression-like behaviors[95], it is unclear if similar processes occur with HCN channels in the hippocampus. Therefore, to better understand how HCN channels may lead to MDD, we characterized HCN channel expression and function in the hippocampus of mice that had gone through CSD. We also used a transgenic mouse model of Early Life Stress (ELS)[163] to see if HCN channel alteration during development impacted adult depression-like behaviors. In addition, we determined if TRIP8b-KO mice would be protected from numerous chronic stress-induced behaviors after subjecting them to CSD. Finally, we determined if HCN channel expression changes with an exciting new MDD treatment, a sub-anesthetic dose of ketamine, which has been shown to reverse MDD-related behaviors in both mice and humans within hours of

administration[53-58]. In aggregate, these studies serve to identify how HCN channels in the hippocampus respond to numerous aspects of pre-clinical, MDD-like behavior development and treatment.

Materials and Methods

Animals

Male 8-16 week old C57BL/6J mice (Jackson Laboratories; Bar Harbour, ME) were used for all CSD experiments, excepting those utilizing *Trip8b* transgenic mice.. Male mice were used for all experiments, unless otherwise specified, since CSD is only appropriate for males, as females seldom show territorial aggression and males seldom attack female mice. Global *Trip8b*^{-/-} mice creation and genotyping have been previously described[74]. Although we have previously referred to these animals by the name of the gene encoding TRIP8b protein (*Pex5l*), we have elected to refer to them as *Trip8b* in this manuscript for clarity. Male 8 to 16 week-old *Trip8b*^{+/+} and *Trip8b*^{-/-} mice were used for all studies. To study ELS-like mice, two transgenic mouse lines were bred together, CAMKII-tTA and Tet-CRF, as previously described[163]. When both transgenes are expressed, CRF is overexpressed in forebrain regions and is sensitive to doxycycline repression of transcription. Double transgenic tTA[+]/CRF[+] and tTA[+] mice were used as test and control mice for subsequent western blot and qRT-PCR experiments between 8 – 12 weeks of age. Doxycycline was fed to all mice post-weaning to restrict CRF overexpression to the early developmental period, which has been shown to lead to depression-like behaviors in adulthood[163]. Mice were maintained on a 12:12 hour light:dark cycle with food and water given *ad libitum.* All animal experiments were performed according to protocols approved by the Institutional Animal Care and Use Committees of Northwestern University.

Drug Injections

Ketamine was administered at 10mg/kg (i.p.) in normal saline, and saline alone was used in control experiments at equal volumes to ketamine administrations. Mice were euthanized at two hours after administration to assess changes in mRNA expression.

Immunohistochemistry

Mice were anesthetized with isoflurane and perfused with phosphate buffered saline (PBS) followed by 4% paraformaldehyde (PFA) in PBS. Brains were then removed and fixed in 4% PFA overnight at 4°C. After 48-72 hours, 30 µm coronal sections were made on a vibratome (Leica, Buffalo Grove, IL) at room temperature. Antigen retrieval was performed with 10 mM Na-citrate, pH 9.0, for 10 minutes at 80°C, and the tissue was then allowed to cool for 30 minutes back to room temperature. Afterward, the tissue was blocked in PBS with 5% normal goat serum and 0.03% Triton X-100 for 1 hour at room temperature. Primary antibodies were diluted in blocking solution and applied overnight at 4°C with gentle agitation. The next day, sections were washed 3 times in PBS with 0.03% Triton X-100 (PBS-T) prior to a 1 hour incubation at room temperature in secondary antibody, followed by 3 additional washes in PBS-T. 1mM DAPI was included in the final PBS-T wash, and tissue was then mounted on glass slides with PermaFluor (Thermo Fisher Scientific, Fremont, CA). All imaging was performed at the Northwestern University Center for Advanced Microscopy on a Nikon A1R confocal microscope using NIS Elements software (Nikon, Melville, NJ). Primary antibodies used were custom[80,142,164,165] rabbit and guinea pig anti-HCN1, rabbit and guinea pig anti-HCN2, and rabbit and guinea-pig anti-TRIP8b. Monoclonal anti-TRIP8b antibodies (Neuromab; Davis, CA) and polyclonal rabbit anti-MAP2 (Millipore; Temecular, CA) were also used. All secondary antibodies were purchased from Invitrogen. For quantification of images, custom written routines in MATLAB (Mathworks, Natick, MA) were used, as in our previous report[137]. Briefly, regions of interest (ROI) were drawn over the stratum oriens (SO) and stratum pyramidale (SP). A larger ROI was also drawn over the region encompassing the stratum radiatum (SR) and stratum lacunosum moleculare (SLM) and then subdivided into ten equally spaced ROIs. The mean intensity of the staining within each ROI was then used for subsequent downstream analyses. Within each slice, the staining intensity of the injected hemisphere was divided by the intensity of the staining in the corresponding ROI from the contralateral (uninjected) hemisphere.

Brain Tissue Isolation

Mice were deeply anesthetized by isoflurane and rapidly decapitated. Brain tissue was quickly removed and put in aCSF (in mM: 125 NaCl, 2.5 KCl, 1.25 NaH_2PO_4, 25 $NaHCO_3$, 2 $CaCl_2$, 1 $MgCl_2$, and 25 dextrose) with bubbled 95% O_2/5% CO_2 on ice to help clear blood contaminants. Brain tissue was then

isolated via micropunch technique with 1mm punches (Stotling punch set). One hemisphere was

dissected in aCSF at 4C, put into ice cold RIPA buffer (150mM NaCl, 1% NP-40, 0.5% deoxycholic acid,

0.1%SDS, 50mM TRIS, pH8.0) in a 1.5mL tube for protein extraction, followed by flash freezing on dry

ice. The other hemisphere was dissected in RNA-Later (Qiagen) and flash frozen in a 1.5mL tube on dry

ice. Samples were stored at -80C until use. For ventral and dorsal hippocampus tissue, the hippocampus

was removed from the rest of the brain and spit down the middle, leaving a ventral and dorsal pole for

later experiments.

Western Blotting

Western blotting was performed as previously described[80,137]. Samples were homogenized and then

sonicated briefly on ice. Sample were then centrifuged at 21000g for 10min, supernatant was collected,

and sample buffer containing β-mercaptoethanol was added. Samples were resolved on a 10% SDS-

PAGE gel and transferred to PVDF. All blots were blocked with 5% Milk in TBS with Tween-20 (0.1%)

before adding primary antibodies in blocking buffer at 4C overnight. Primary antibodies used were the

same as for immunohistochemistry but also included mouse anti-tubulin (Millipore Temecular, CA). Band

intensities were quantified using ImageStudio (Li-Cor, Lincoln, NE) software and normalized to the anti-

tubulin signal for each sample.

qRT-PCR

RNA was extracted from samples using Pure Link RNA Mini Kit (Life Technologies), and cDNA was

synthesized using High Capacity cDNA Synthesis Kit (Applied Biosystems). qPCR reactions were

performed using Power SyBr Green Master Mix (Applied Biosystems) and reactions were facilitated by

use of a RealPlex2 thermocycler (Eppenedorf). We used primers designed by Santoro 2009[88] or

commercial qPCR primers from Biorad (Hercules, CA). Before beginning experiments, the efficiencies of

all primer sets were optimized to be between 85-110% with r >0.98. Relative quantifications of cDNA

samples measured in triplicate were achieved using the $\Delta\Delta C_t$ method, and GAPDH was used as a

housekeeping gene.

Electrophysiology

Electrophysiology was performed as previously described[137]. Mice were anesthetized with isoflurane,

decapitated, and the whole brain was rapidly dissected into ice-cold sucrose solution containing (in mM):

190 sucrose, 10 NaCl, 2.5 KCl, 25 $NaHCO_3$, 1.25 NaH_2PO_4, 0.5 $CaCl_2$, 7 $MgCl_2$, 25 dextrose; pH 7.4 with

continuous bubbling with 95% O_2/5% CO_2. 300 μm sagittal slices were made using a vibratome (Leica)

and immediately transferred to a 35ºC holding chamber containing ACSF (125 NaCl, 2.5 KCl, 25

$NaHCO_3$, 1.25 NaH_2PO_4, 2 $CaCl_2$, 1 $MgCl_2$, 25 dextrose; pH 7.4) for a 25 min incubation period.

Afterward, the chamber was allowed to equilibrate to room temperature for ≥30 min before recording

began. Individual slices were transferred to a custom chamber perfused with oxygenated, room

temperature (22±1ºC) ACSF at a rate of 1-2 mL/min. Electrodes (4-6 MΩ) were pulled on a Sutter P87

pipette puller and filled with intracellular solution containing: 115 K-gluconate, 20 KCl, 10 HEPES, 10 Na-

phosphocreatine, 2 Mg-ATP, 0.3 Na-GTP, 0.2% biocytin. KOH was added to pH 7.3. Whole-cell

recordings were made with a PC-ONE amplifier (Dagan), filtered at 3 kHz, and digitized at 20 kHz using

an InstruTECH ITC16. A calculated liquid junction potential of 13 mV was compensated prior to

approaching each cell. Series resistance was monitored throughout each experiment, and cells were

discarded if the series resistance exceeded 30 MΩ. Data acquisition and analysis was performed in

IgorPro 6 (WaveMetrics) using custom macros. I_h density at -130 mV was obtained by subtracting the

instantaneous current after the capacitive transient from the steady-state current at the end of a 2 s step.

Current clamp recordings were performed with a holding current to maintain cells at -70mV.

Chronic Social Defeat (CSD)

CSD was performed similar to as described previously[98]. Briefly, we identified aggressor mice as defined

by demonstrating a shortened attack latency (<60s) in two separate confrontations out of three daily 180s

trials. A further criterion used to evaluate these mice was the presence of at least three separate bouts

(~1/minute) in two of these confrontations. Once identified, these mice were paired with experimental

C57BL/6J mice in a cage that is separated by a clear, plexiglass divider with small holes. This allows both

mice to be able to observe each other but prevents physical contact. Separate food and water bottles

were provided for each mouse on each side of the plexiglass divider. For five minutes daily, the

experimental mouse was placed on the aggressor's side of the cage, and the aggressor physically

defeated the experimental mouse. Signs of defeat were the experimental mouse's vocalizations, flight

attempts, and submissive posture. After this defeat, the experimental mouse was put on the other side of

the plexiglass divider for the next 24 hours. This continued for 10 days, and any mouse showing serious

wounding was removed from the experiment and euthanized.

Behavioral Testing

Before each behavioral task, the mice were acclimated to the behavioral testing room for at least 1 hr. All

tests were performed in an isolated room under quiet conditions, and all behavioral experiments took

place during the light part of the light:dark cycle. For experiments with multiple trials over many days,

each trial occurred within 2 hours of the same time each day. For serial behavioral tasks, at least 4 days

were allowed for the mice to recover before the next test started. All behavioral testing apparatuses were

cleaned with 70% ethanol between trials. All experimenters were blinded to the subjects' groups during

testing and analysis.

Social Interaction Test (SIT)

After a 10 day cycle, the conditioned mice were assayed on the SIT. SIT has two phases: First, the mice

were placed in an arena with an empty cage in the middle. The arena was split into an "interaction zone,"

located around the cage and an "avoidance zone" at the corners. The mouse was given 2.5 minutes to

explore, and the time spent in each zone was recorded with video tracking software (LimeLight 3). The

second phase had an unfamiliar mouse in the arena's cage. A social interaction ratio (SI) was calculated

and was defined as the time the mouse spends in the interaction zone during the second phase divided

by the time in the interaction zone during the first phase. Stress susceptible mice had an SI<1 and so

spend less time in the interaction zone in the second phase. Stress resilient mice were defined as mice

with an SI>1 and so spend more time in the interaction zone in the second phase. The time spent in the

opposite corners of the arena from the cage (avoidance zones) was also measured, and an Avoidance

Ratio (AR) was calculated from the time the mouse spent in these avoidance zones divided by the total

time in the arena. As very few resilient mice were generated with our protocol, these mice were excluded from further analysis.

Open Field Test (OFT)

The OFT was performed as previously described[137]. Briefly, each mouse was placed in a 60cm plastic arena with white light illuminating the center of the arena. Mice were allowed to explore the arena for 10 minutes, and the time spent in the center and periphery of the arena as well as total distance traveled were recorded with overhead cameras and analyzed with Limelight 4.0 software (Coulbourne).

Zero Maze (ZM)

Each mouse was placed in a circular apparatus with 4 quadrants containing 2 closed and 2 open arms that alternated. The mouse was placed in the closed arms, and the time spent in each arm was recorded for 5 minutes with an overhead camera. Behavior was analyzed with Limelight 4.0 software. If a mouse leapt from the zero maze, the mouse was not included in the later analysis.

Sucrose Preference Test (SPT)

The SPT was performed similar to previous publications, with minor deviations[74]. Briefly, the mice were acclimated to the two water bottle choice for two days prior to testing. The amount drank from a 1% sucrose and a water-only bottle were measured by weight after a 36 hour period, with the bottle position in the cage being switched after 18 hours to prevent side bias. The Sucrose Preference endpoint was defined as the amount of sucrose water consumed divided by the total consumption of liquid in either bottles.

Tail Suspension (TST) and Forced Swim Tests (FST)

We tested the mice on the TST and FST to assess antidepressant-like behavior, as previously described[74]. We suspended the mice by their tails for 6 minutes and measured the amount of time they spent without struggling, noted as immobility time. Struggling for this assay is defined as moving their fore or hind limbs. Next for the FST, we placed the mice in 24C +/- 1C tap water for 6 minutes. After 2 minutes

had passed, we measured the amount of time spent immobile for the remaining 4 minutes. Immobility was defined as cessation of purposeful movement, except for small twitches necessary to keep the mouse upright.

Z-score normalization

To create the Behavior Induced by Chronic Stress (BICS) index, z-score normalization of the SIT, OFT, ZM, SPT, and FST were undertaken (z-score normalization process described in detail in Chapter 3). For the SIT, the social interaction and avoidance ratios were used as primary endpoints. For the OFT, the time spent in the center and center crossings were used as endpoints. For the ZM, the time spent in the open arms and open arm crossings were used as endpoints. For the SPT, the preference for sucrose was used as the final endpoint. For the FST, the total time spent immobile was used as the final endpoint. The OFT and ZM were combined before being averaged into the BICS to avoid overweighting of similar behavior tested by these assays. The Anxiety Subscale was created from the OFT and ZM. The Depression Subscale was created from the SIT, SPT, and FST.

Statistics

All statistical calculations were performed using GraphPad 6 and MATLAB. Principal Component Analysis (PCA) was completed using R-studio using the "prcomp()" function, and graphs were created using ggplot2 for this data. Raw data for PCA was z-score normalized to give a common "unit" and consisted of data from the SIT, OFT, ZM, SPT, and FST. All behavioral data that followed a normal distribution had outliers removed if they were > 2 standard deviations away from the population mean to avoid Type II errors[166]. For pairwise comparisons, a two-tailed student's T-test was performed. For comparisons with two factors, a Two-Way ANOVA was used. Significance was denoted with an asterisk, representing a p-value < 0.05, and all values were reported as mean±S.E.M.

Results

HCN channel and TRIP8b protein do not change with CSD

As chronic stress is a major determinant of MDD pathogenesis[2], we sought to characterize HCN channels after application of a well-validated stress modality in mice, CSD[98]. CSD consists of daily 5 minute aggressive bouts where the intruder male mouse is defeated by a larger, aggressive, resident male. The mice are then co-housed for 24 hours with a plexiglass divider between them, allowing for social interaction but no physical interaction between the mice. After 10 days of CSD stress, mice were then tested in the SIT to determine if they were susceptible or resilient to CSD stress. In this test, mice that are susceptible to CSD will spend less time investigating a novel aggressive male and more time avoiding this male in the corner. The SIR is derived from the time spent around the novel conspecific divided by the time spent around an inanimate target, while the AR is similarly derived from the time spent in the corner when a conspecific is present divided by the time spent in the corner when it is absent. As expected, we observed clear differences in the SIR and AR between control and defeated mice, and due to the extremely aggressive nature of the residents in the CSD, few resilient mice were observed (**Figure 1A**). Subsequently, these mice were removed from analysis.

After the SIT, mice were euthanized, and the CA1 was isolated for western blot experiments. Since HCN1 and HCN2 are the predominate subunits expressed in the hippocampus[138], expression of these subunits was assayed. In addition, the localizing protein TRIP8b as well as its most highly expressed isoform, TRIP8b(1a-4), were also assayed. Finally, since HCN4 is expressed in greater quantities during development[99], this subunit was also assayed to ensure that an aberrant upregulation during adulthood was not present. However, despite our hypothesis, none of these subunits were expressed differently in the CA1 of defeated mice compared to undefeated controls (**Figure 1B**). Because HCN channels are expressed in the amygdala and medial prefrontal cortex (mPFC)[167], which are important brain regions that are altered by chronic stress, we also investigated HCN channel expression in these regions 1 day after CSD. Similar to the CA1, however, neither HCN1, HCN4, total TRIP8b, nor TRIP8b(1a4) were altered in the amygdala, and neither HCN1, HCN2, HCN4, total TRIP8b, nor TRIP8b(1a4) were altered in the mPFC (**Figure 2**).

While the classical DG – CA3 – CA1 loop is often referred to when describing information flow through the hippocampus, there are also distinct changes in connectivity and gene expression along the dorsoventral (also known as the septotemporal) axis[46]. In particular, while the dorsal hippocampus (dHC)

has been shown to be involved most in memory related processes, the ventral hippocampus (vHC) plays

a much more prominent role in emotional regulation[46]. Because of this, we reasoned that changes in HCN

channels with chronic stress may be restricted to one pole or the other. While our previous experiments

have shown that dHC manipulation of HCN channels is sufficient to cause changes in antidepressant-like

behavior[137], it's possible that chronic stress only alters vHC channels. Therefore, we again subjected a

cohort of mice to CSD and confirmed that defeated mice showed changes in SIR and AR on the SIT

(**Figure 3A**). Then, we isolated the vHC and dHC and used western blots to quantitate the expression of

HCN1, HCN2, HCN4, and total TRIP8b after CSD. However, similar to our results in the CA1, there were

no changes in any of these proteins in either the dHC or vHC (**Figure 3B, C**).

The pathogenesis of depression-like behavior after CSD is multifaceted in terms of gene

expression, and it has been shown that gene expression in limbic system brain regions change over time

after CSD[168]. This suggests that while many of the depression-related behaviors associated with CSD

exist at both early and late time points, it's possible that short-term changes that facilitate these behaviors

are solidified through dynamic changes in gene expression and subsequent changes in neural

architecture. For this reason, we assessed whether changes in HCN1, HCN2, HCN4, or total TRIP8b may

manifest at 28 days after CSD in the dHC and vHC. We confirmed that mice that underwent CSD showed

robust changes in the SIR and AR in the SIT when tested 28 days after defeat (**Figure 4A**). However,

similar to the 1 day time point, we did not observe changes in HCN channel subunits in the dHC or vHC

(**Figure 4B, C**). Thus, it seems unlikely that CSD stress in mice leads to changes in HCN channel

expression in the hippocampus (**Table 1** summarizes brain regions and times tested).

Previous studies have shown that the localization of HCN channels in the distal dendrites of CA1

pyramidal cells is especially important for both the excitability of these cells and subsequent

antidepressant-like behavior[74]. In particular, it has been shown that loss of distal dendritic HCN channels

is sufficient to reproduce the antidepressant-like phenotypes observed in other HCN ablation mice and

that restoration of this enrichment reverses this increase in antidepressant-like behavior[137]. Because of

this, we reasoned that while the expression of HCN channel protein is unchanged with CSD, it's possible

that the localization of the protein is altered. Therefore, we subjected another cohort to CSD and

measured the expression of HCN1, HCN2, and TRIP8b along the apical dendrites of CA1 pyramidal cells

from the dHC and vHC. However, similar to our protein expression studies, we did not observe a change in HCN channel localization in either the dHC or vHC (**Figure 5, 6**). Since apical dendrite retraction in the CA3 has been reported as a sequelae of chronic stress[5], we repeated these experiments and normalized the expression of these channels to dendritic marker MAP2. However, the results still remained unchanged and reproduced previous results that CA1 dendritic branching does not change with chronic stress (**Supplementary Figure 1**)[169]. Overall, these results suggest that CSD stress in mice does not alter HCN channel expression in the hippocampus.

ELS-like mice do not show differences in HCN channels as adults

ELS can be an important precipitant of later psychiatric dysfunctions in adults, and similar phenomena have been seen in rodents that undergo extreme ELS. One paper showed that while neonatal SSRI administrations in mice, which cause adulthood depression-like behaviors, upregulated hippocampal *Hcn1* mRNA in adulthood, this was not seen with SSRIs given to adults[104]. As psychosocial stress leads to upregulation of the HPA axis, which ultimately influences the molecular adaptations that result in aberrant behavior during MDD[2,5], increasing the centrally active stress hormone Corticotropin Releasing Factor (CRF) should have a similar impact to administration of psychosocial stress[163]. Recently, this hypothesis was tested with mice that had CRF expressed exclusively in the forebrain during the pre-weaning period only[163] (termed "ELS-like mice"), and as predicted, these mice had many depression-like behaviors in adulthood.

To assess if HCN channel dysfunction is a consequence of ELS but not adult stress, we measured the expression of HCN1, HCN2, and TRIP8b via western blot from adult ELS-like mice and their littermate controls. Similar to the CSD experiments, however, we did not find a change in male or female HCN channels in the CA1 (**Figure 7A, B**). Because there are many different TRIP8b spliceforms which encode different proteins, we determined if there was a change in the balance of these spliceforms by qRT-PCR. Rather surprisingly, we noticed that while spliceforms driven by the 1a promoter were upregulated in ELS-like mice, a subsequent downregulation of 1b promoter driven spliceforms was also observed (**Figure 7C**). However, as putative expression of 1a spliceforms are neuronal while 1b spliceforms are oligodendroglial[89], and downregulation of oligodendrocytes and oligodendrocyte genes

are observed with MDD [170], we believe that this difference in TRIP8b expression is due to a difference in the relative survival of various cell types within the hippocampus. Therefore, our data suggests that HCN channel expression does not change with ELS.

CSD causes an I_h-independent loss of CA1 pyramidal cell excitability

The evidence presented so far does not support a change in HCN channel protein expression or localization with CSD, but it is possible that HCN channel function may be altered independent of protein expression after chronic stress. If HCN channels were increased, it would be expected that a hypoexcitable state in these cells would be typified by an increase in the resting membrane potential (RMP) and a decrease in the input resistance[71]. A potential change in I_h that would be independent of protein expression could be facilitated by direct post-translational modifications on HCN channels or TRIP8b or differences in local neuromodulator concentrations, such as cAMP.

In order to examine if I_h was altered by chronic stress, we subjected another cohort to CSD and performed whole cell patch clamp electrophysiology on acutely sliced CA1 pyramidal cells up to two weeks after CSD was completed. As expected, our CSD paradigm led defeated mice to have similar differences in the SIR and AR in the SIT as previously (**Figure 8A**). We observed that CA1 pyramidal cells from defeated mice had an increase in their rheobase, which means that more current needed to be injected at the soma in order for an action potential to be elicited (**Figure 8B**). However, the RMP was hyperpolarized and the input resistance was unchanged in these cells (**Figure 8C, D**). In addition, we saw no changes in sag ratio, the after-hyperpolarization (AHP), voltage threshold to fire an action potential, or capacitance (**Figure 8 E, F, G, H**). Similar to the change in rheobase, defeated CA1 pyramidal cells needed more current to reach the maximum number of action potential fired, though the maximum number of action potentials was unchanged (**Figure 8I, J**). Lastly, we noticed that while increasing current in control cells led to an eventual depolarization block, we did not observe this same depolarization block in cells from defeated animals (**Figure 8K**). These data suggest that while CA1 pyramidal cells become hypoexcitable with CSD stress, HCN channels are unlikely to mediate this change in excitability (summarized in **Table 2**), as an increase in I_h would cause a depolarization of the membrane potential, a decrease in the input resistance, and an increase in the sag ratio.

The most salient electrophysiological features of the cells from defeated animals were the increase in rheobase, hyperpolarization of the RMP, and loss of the depolarization block. These electrophysiological changes could be achieved through increasing K^+ leak channel current, voltage gated K^+ channel current, or GABA-B signaling. For this reason, we used qRT-PCR to screen CA1 tissues from control and defeated animals for changes in some of these channels as well as the GABA-A receptor subunits that are constitutively active. Specifically, we assayed *Gababr1, Gababr2, Sk2, Sk3, Kv4.1, Kv4.2, Kv.3, Gabra5, and Gabrad*. While some subtle changes in *Gabrad, Sk3, and Kv4.1* were detected, the expression of these channels was reduced instead of increased (**Figure 9**). While alterations of these channels may also occur at the protein expression or post-translational modification level, we were unable to confirm the mechanism of CA1 hypoexcitability induced by CSD.

TRIP8b-KO mice are not protected from developing aberrant behaviors induced by CSD

Though HCN channels do not seem to be altered by CSD in adults or ELS, it is still possible that HCN channel ablation may be protective against CSD. As reduced excitability in CA1 pyramidal cells were seen with CSD, we hypothesized that HCN channel loss could increase the excitability of this brain region and therefore prevent the aberrant behavior induced by CSD.

In order to test this hypothesis, we subjected *Trip8b^+/+* and *Trip8b^-/-* mice to CSD, while keeping another cohort undefeated as controls. We then assessed whether or not the mice developed chronic stress-induced behavior on 5 different assays. First, we examined the mice's tendency towards social avoidance on the SIT. Next, we determined if mice showed anxiety-like behaviors on the OFT and ZM. We then performed an in-cage test for anhedonia with the SPT. Finally, we measured antidepressant-like behavior with the FST.

From the SIT, stress was shown to decrease the SIR, as a two-way ANOVA showed a significant effect of condition but not of genotype nor an interaction between condition x genotype. Similarly, two-way ANOVA revealed an effect of condition but not genotype nor an interaction between condition and genotype for the AR, demonstrating that stress increased the AR (Figure 10A). As no effect of genotype nor a condition x genotype interaction were detected, these results suggest that *Trip8b^-/-* mice are not protected from increases in social avoidance after CSD.

From the OFT, stress was shown to decrease time spent in the center, as a two-way ANOVA showed a significant effect of condition but not of genotype nor an interaction between condition x genotype. Similarly, two-way ANOVA revealed a trend for a condition effect (p = 0.14) but not genotype nor an interaction between condition and genotype for the AR, demonstrating that stress increased the AR (**Figure 10B**). By contrast on the ZM, there was no differences between groups in terms of time spent in the open arms crossings (**Figure 10C, D**). While these results are unclear as to whether there was a change in anxiety-like behavior with stress, these results do not imply that *Trip8b*$^{-/-}$ mice were protected against anxiety-like behavior after CSD.

From the SPT, stress was shown to decrease the preference for sucrose, as a two-way ANOVA showed a significant effect of condition but not of genotype nor an interaction between condition x genotype (**Figure 10E**). Again, while stress clearly caused anhedonia in this task, the *Trip8b*$^{-/-}$ mice were not protected from developing these behaviors after CSD.

Interestingly, CSD stress did not cause a change in immobility time on the FST, as there was no effect of condition by two-way ANOVA. This result, however, is in line with previous publications that have shown no difference in FST with this particular stress paradigm in mice[171]. However, consistent with previous reports, *Trip8b*$^{-/-}$ mice still displayed reduced immobility, as evident by an effect of genotype but not a condition by genotype interaction via two-way ANOVA. Thus, CSD stress does not reverse the changes in FST seen in *Trip8b*$^{-/-}$ mice.

As high variability in mouse behavior can make interpretation of these assays difficult, means of combining like assays in a particular behavioral domain can help to more clearly assess the behavior of a particular cohort on many behavioral tasks. One method of doing this is through the use of z-score normalization, which uses the mean and standard deviation of the control population to define how different each individual is from controls. In addition, this allows each test in a particular domain to be averaged together, as the performance relative to the control population creates a "standard unit" of sorts[172]. Therefore, in tests with multiple endpoints, we used z-score normalization to yield a final z-score for each test, and then combined these z-scores into a Behavior Induced by Chronic Stress (BICS) index. For the BICS, we detected a very significant effect of condition but not genotype nor condition by genotype via two-way ANOVA. This suggests that stress did impact the behavior of these mice but that

Trip8b^{-/-} mice were not protected from this stress (**Figure 11A**). To get a clearer assessment of this

cohort's behavior in terms of anxiety-like and depression-like behavior, we split the BICS into two

subscales: an anxiety subscale that included the OFT and ZM and a depression subscale that included

the SIT, SPT, and FST. Similar to the BICS in its entirety, both the anxiety and depression subscales

were significant for an effect of condition but not an effect of genotype nor an interaction between

condition x genotype (**Figure 11B, C**).

Despite these clear results on the BICS, we implemented a PCA to get an unbiased grouping of

the data, thus investigating if clusters emerged along the axes with most variation. As expected, when we

plotted the first and second principal components, we saw a clear split between the control and defeated

groups along the first principal component (**Figure 11D**). By contrast, when looking at the data by

genotype, there was no clear separation of the wildtype and KO groups (**Figure 11E**). Statistically, we

determined that there was a very significant difference between the control and defeated groups in terms

of first principal component values while no significant differences were seen by splitting the groups by

genotype, though a trend at the last principal component was seen ($p = 0.14$; **Table 2**). In total, these

data suggest that *Trip8b*^{-/-} mice are not protected from developing aberrant behaviors following CSD.

Ketamine decreases Hcn1 *and* Trip8b *expression*

Ketamine is emerging as a promising, fast-acting antidepressant, and increases in BDNF in the

mPFC and hippocampus seem to be integral to ketamine's mechanism of action[54,58]. HCN1 knockdown in

the dHC also increases BDNF[76], and it has been shown that ketamine blocks HCN1 at physiologically

relevant doses[67]. For this reason, we wondered if reduction in HCN channels were similarly reduced by

ketamine at antidepressant doses.

We injected adult, wildtype mice with ketamine at 10mg/kg i.p. and collected the CA1 for qRT-

PCR experiments at 2 hours, an early time point when ketamine has shown to decrease immobility on the

FST[54]. We found that both *Hcn1* and *Trip8b* mRNA were reduced at this timepoint while *Hcn2* expression

was unchanged (**Figure 12A**). We next sought to identify which of the Trip8b spliceforms may be affected

and found trends towards reduction in *Trip8b(1a-4)* and *Trip8b(1a)* but no change in *Trip8b(1b-2)* (**Figure

12B**). Thus, ketamine seems to affect HCN channel expression at an early time point after injection.

Discussion

      In this chapter, we used CSD in mice to show that HCN channel expression, localization, and function do not change in the dHC with chronic stress. However, similar to other reports, dorsal CA1 pyramidal cells were hypoexcitable after CSD, though the exact mechanism remains unclear. We also show that ELS does not cause significant changes in HCN channel protein expression in the dHC of adult mice. In addition, we demonstrated that while *Trip8b*^{-/-} mice retain reduced immobility on FST after CSD, they fail to be protected from developing other chronic stress-induced behaviors such as social avoidance, anhedonia, and anxiety-like behavior. Finally, we demonstrate that the NMDA antagonist ketamine reduces *Hcn1* and *Trip8b* mRNA at therapeutic doses two hours after injection. In all, while loss of HCN channels in the dHC may influence antidepressant-like behavior, it seems unlikely that these channels are mechanistically involved in other depression-like behaviors in mice undergoing CSD.

CSD causes dorsal CA1 cells to be hypoexcitable but is not dependent on I_h

      Previous literature has suggested that deficits in plasticity and excitability in the hippocampus accompany aberrant behavior induced by chronic stress[6,29,51] and reductions in hippocampal volume are often seen in MDD patients[33-35]. Interestingly, the vHC seems to follow a different pattern, with increased excitability leading to more anxiety-like and depression-like behavior while reducing vHC excitability leads to less anxiety-like and depression-like behavior[31,32]. In both these subregions of the hippocampus, HCN channels are expressed in the apical dendrites of CA1 pyramidal cells in a distally enriching pattern[74,81-83]. HCN channels reduce the excitability of these cells, especially at the temporoammonic pathway terminating in the stratum lacunosum moleculare, through decreasing input resistance and thus needing more current to cause a similar change in membrane voltage[71,72,76]. Thus, if HCN channels are an integral part of MDD pathogenesis, it would be expected for these channels to increase in the dHC with chronic stress, decrease in the vHC with chronic stress, or both. In accordance with this, it has already been shown that dHC reduction of HCN1 is sufficient to induce antidepressant-like behavior on the FST[76] and that restoration of the distal dendritic gradient of HCN in the dHC of TRIP8b-KO mice causes a reversal in

this behavior[137]. Thus, we reasoned that HCN channels would be increased in the dHC with chronic

stress in mice and be correlated with development of aberrant behavior induced by this stress.

However, the experiments detailed above clearly suggest that hippocampal HCN channels are

not involved in depression pathogenesis after CSD. We could not find a change in HCN channel protein

in the CA1, dHC, or vHC one day after CSD, when depression-like behavior manifests. In addition, we

saw no changes in these channels at a later timepoint in the vHC or dHC, when many of the depression-

like behaviors are solidified. These results were further extended to two other limbic system areas, the

mPFC and the amygdala. We found no change in HCN channel localization in either the dorsal or ventral

CA1 after CSD, even when accounting for changes in possible dendrite morphology. Finally, we

demonstrated that dorsal CA1 pyramidal cells do not have changes in parameters influenced by I_h after

CSD. Though there still is the possibility that local subcellular concentrations of cAMP or another HCN

modulator affect HCN function, it seems unlikely that this stress modality in mice causes dynamic

changes in HCN channels.

While this result was surprising, it is far from definitive. For one, CSD stress does not cause

changes in FST with the protocol we employed[98,171], and it is possible that HCN channels in the dHC have

a strong influence on this behavior. It could be that stress paradigms that induce increases in immobility,

such as chronic mild stress or restraint stress, would increase HCN channel expression in the dHC.

However, it should be noted that these stress paradigms rely on non-social types of stress and have been

described by some as conditioning for passive coping strategies[173]. It is possible that mice are not the

best model for evaluating the changes in chronic stress and that use of different vertebrate models, such

as rats, would yield different results. Regardless of these caveats, the lack of HCN channel change with

CSD seems to be very reproducible.

Though HCN channel function was not found to be altered, we did detect a change in dorsal CA1

cell excitability that was consistent with previous reports of reduced excitability in this region after chronic

stress[29,51]. This loss of excitability seemed to be driven by a reduction in the RMP, which subsequently

required the cell to raise its voltage more drastically to induce firing of an action potential, as the voltage

threshold for firing was unaltered. This increase in current needed was reflected in the increased

rheobase and increased current needed to elicit the maximum number of spikes. Finally, the normal

depolarization block seen in CA1 pyramidal cells with large current injections was lost in cells from

defeated animals. With these characteristics, a handful of mechanisms are suggested, including increase

in potassium leak current or constitutive inhibitory conductance. Interestingly, when these recordings

were repeated with GABA-A and GABA-B receptor blockers in the bath, the differences between the

control and susceptible mice were lost, though proper controls without synaptic blockers from this cohort

of mice were not employed, and so the results remain difficult to interpret (data not shown). These

findings are interesting given recent reports that blocking or ablating both constitutive GABA-A subunits

and GABA-B cause increases in hippocampal excitability and exhibit antidepressant-like effects after

chronic stress[174,175]. In addition, chronic stress upregulates GABA-B in the dorsal CA1 with chronic stress

in mice[174]. Thus, these changes in GABA receptor signaling are plausible mechanisms for the

hypoexcitability observed after CSD in dorsal CA1 pyramidal cells. Still, HCN channels do not seem to be

involved in this process.

TRIP8b-KO mice are not protected from CSD

　　　　Though the antidepressant-like behavior on the TST and FST after HCN channel ablation has

been shown reproducibly[74,76,137], it remained unclear if these tendencies extended to other depression-like

behaviors after CSD. Thus, we put *Trip8b*^{+/+} an *Trip8b*^{-/-} mice through CSD and assayed their behavior on

5 anxiety-like or depression-like behavioral tasks. As expected based on previous reports[171], CSD caused

increased social avoidance, increased anxiety-like behavior, decreased sucrose preference, and no

change in immobility on the FST. However, *Trip8b*^{-/-} mice developed similar behavior on the SIT, OFT,

and SPT. The decreased immobility seen in non-stress conditions with these mice persisted after CSD,

though without chronic stress increasing the immobility time in defeated wildtype mice, it's difficult to

conclude whether or not *Trip8b*^{-/-} mice were protected from chronic stress in terms of FST behavior.

　　　　Given the mixed findings from these assays, we sought to clarify whether our chronic stress

paradigm really had a broad effect on stress-induced behavior and whether TRIP8b-KO mice were

protected in some way in this behavioral domain. To investigate this, we employed z-score normalization

of these five assays to create an index for aberrant behaviors induced by chronic stress, BICS. On this

index, it became clear that both *Trip8b*^{+/+} and *Trip8b*^{-/-} mice developed aberrant behaviors from CSD and

that these increases in aberrant behavior remained even when looking at subscales for depression-like or anxiety-like behaviors. Still, as this form of indexing pre-supposes a common behavioral domain, we sought an unbiased assessment of these behaviors with PCA to see if mice were grouped into clusters based on either genotype or stress condition. Similar to the BICS, we found that the first principal component split mice by stress condition nearly perfectly, while a non-significant trend (p = 0.14) towards genotype differentiating the two groups was found only at the fifth principal component. By comparison, the first principal component represented 38% of the variability while the fifth represented 9.6%. Thus, while *Trip8b*^{-/-} mice may still show antidepressant-like behavior on the FST, it seems unlikely that these mice are protected from CSD.

Again, the results here are far from conclusive and follow many of the same caveats as with the lack of HCN channel alteration with CSD. First, the CSD paradigm's inability to increase immobility in the FST may suggest that *Trip8b*^{-/-} mice would be protected more broadly from a different stress paradigm that increased immobility in this test. Second, mice may not be a suitable model and different vertebrate models of chronic stress related behaviors may yield different results. Lastly, as TRIP8b was ablated through the development of the mouse and into adulthood, it could be that acute reduction in TRIP8b either right before or right after CSD may cause broader antidepressant-like effects, as compensatory changes in excitability may develop due to constitutive HCN channel loss throughout development. Future research will be needed investigate these possibilities.

The role of HCN channels in ketamine's mechanism of action are unclear

Though the NMDA antagonist ketamine has emerged as a promising, fast-acting antidepressant[54,56,58], there has been some question about how this drug exerts its antidepressant effects. Most notably, it was shown that ketamine is actually not the active compound that causes antidepressant-like behavior in rodents but that its metabolite 2R,6R-hydroxynorketamine achieves these same results in an NMDA independent manner[176]. Before this result was found, ketamine's antidepressant-like effects in mice became very difficult to elicit in lab's that had previously reported its efficacy (personal correspondence) and may have been due to changes in synthesis or purification of the compound that excluded 2R,6R-hydroxynorketamine.

In our own laboratory, while we saw a reduction in *Hcn1* and *Trip8b* mRNA at the two hour time point post ketamine injection, we also failed to reproduce the antidepressant-like findings on FST (data not shown). This was true even when checking the 24 hour time point for antidepressant-like behavior (data not shown). Similar to other labs, it's very likely that we were not treating with the correct psychoactive compound, and thus the changes in *Hcn1* and *Trip8b* are difficult to interpret in terms of the antidepressant-like actions of ketamine. While it remains unknown if, like ketamine[67], 2R,6R-hydroxynorketamine is also a potent blocker of HCN channels, future experiments will need to be done to determine if HCN channels are involved in the fast acting antidepressant-like effects of this compound.

A

Figure 1: HCN channel expression does not change in the CA1 after CSD. A) After 10 days of CSD, defeated mice showed significantly less time in the interaction zone and more time in the avoidance zone, yielding lower SIRs and ARs than undefeated controls. **B)** No change in HCN1, HCN2, HCN4, total TRIP8b, nor TRIP8b(1A4) was detected by western blot from CA1 tissue after CSD. Student's T-test; *p < 0.05; $n_{control}$ = 8, $n_{defeated}$ = 13.
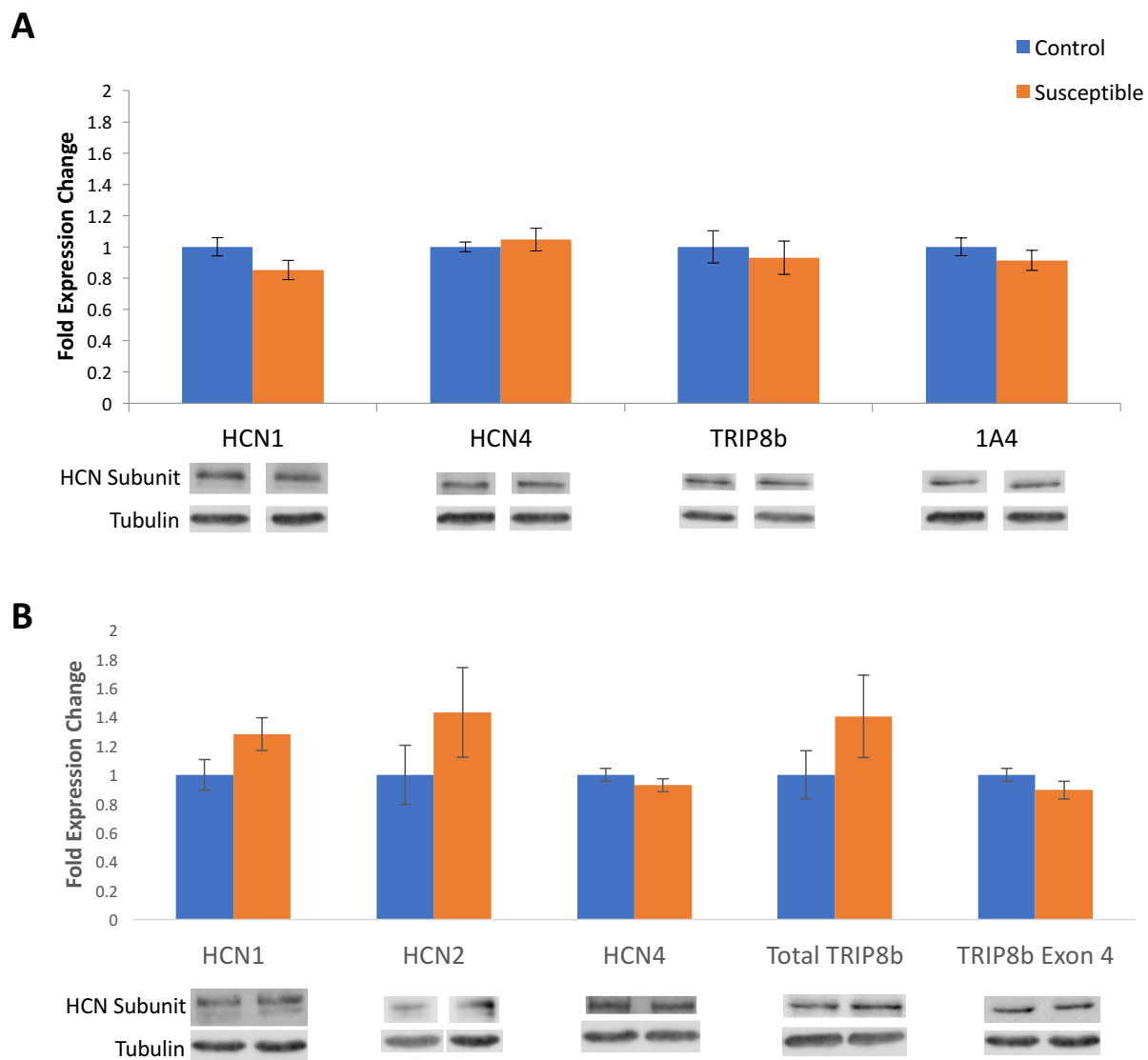
Figure 2: HCN channel expression does not change in the Amygdala or mPFC after CSD. A) Amygdala and mPFC tissue was isolated from mice used in the CA1 HCN channel expression experiment detailed in Figure 1. No change in HCN1, HCN4, total TRIP8b, nor TRIP8b(1A4) was detected by western blot from the amgydala after CSD. **B)** No change in HCN1, HCN2, HCN4, total TRIP8b, nor TRIP8b(1A4) was detected by western blot from the mPFC after CSD. Student's T-test; ncontrol = 8, ndefeated = 13.
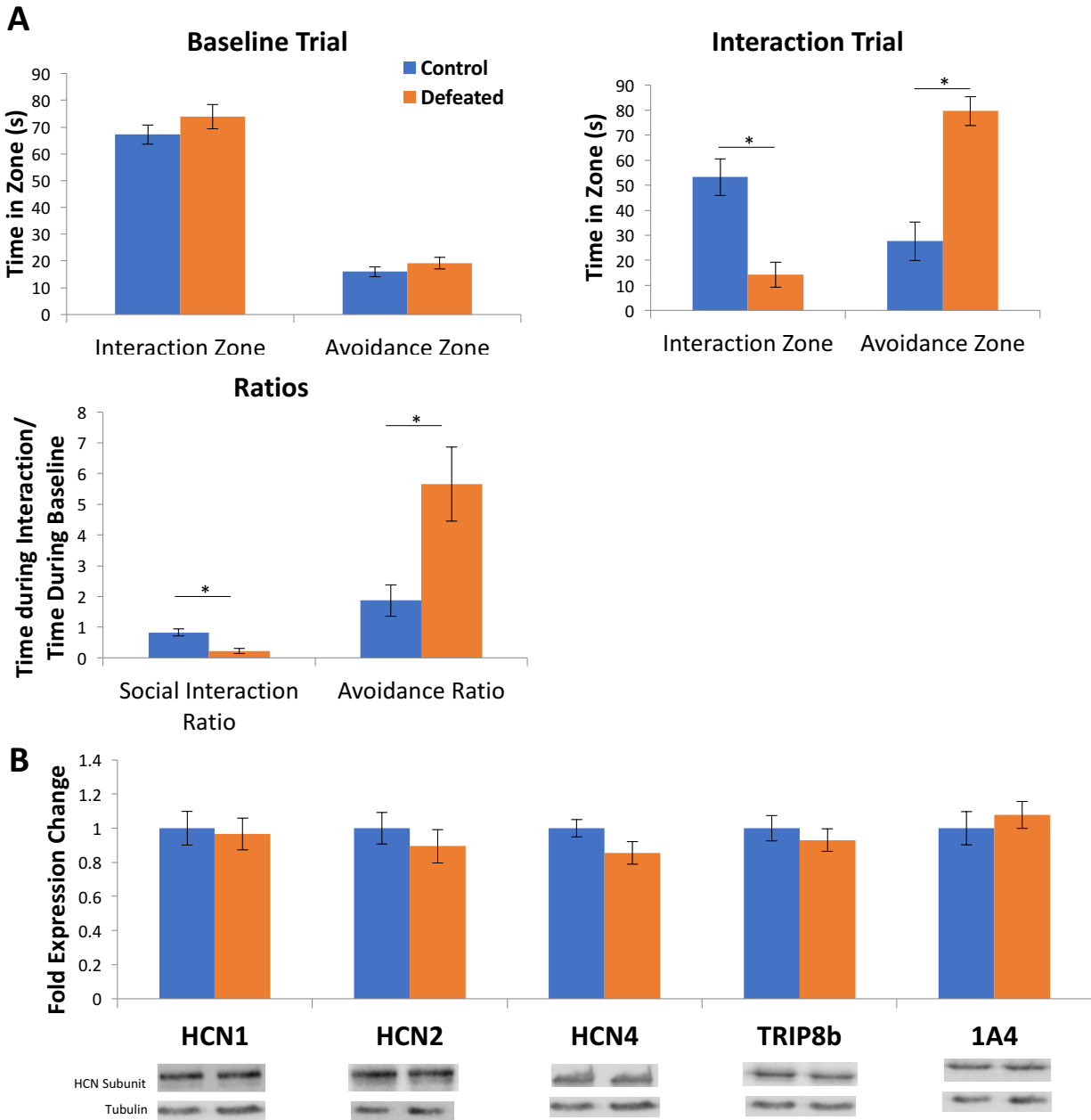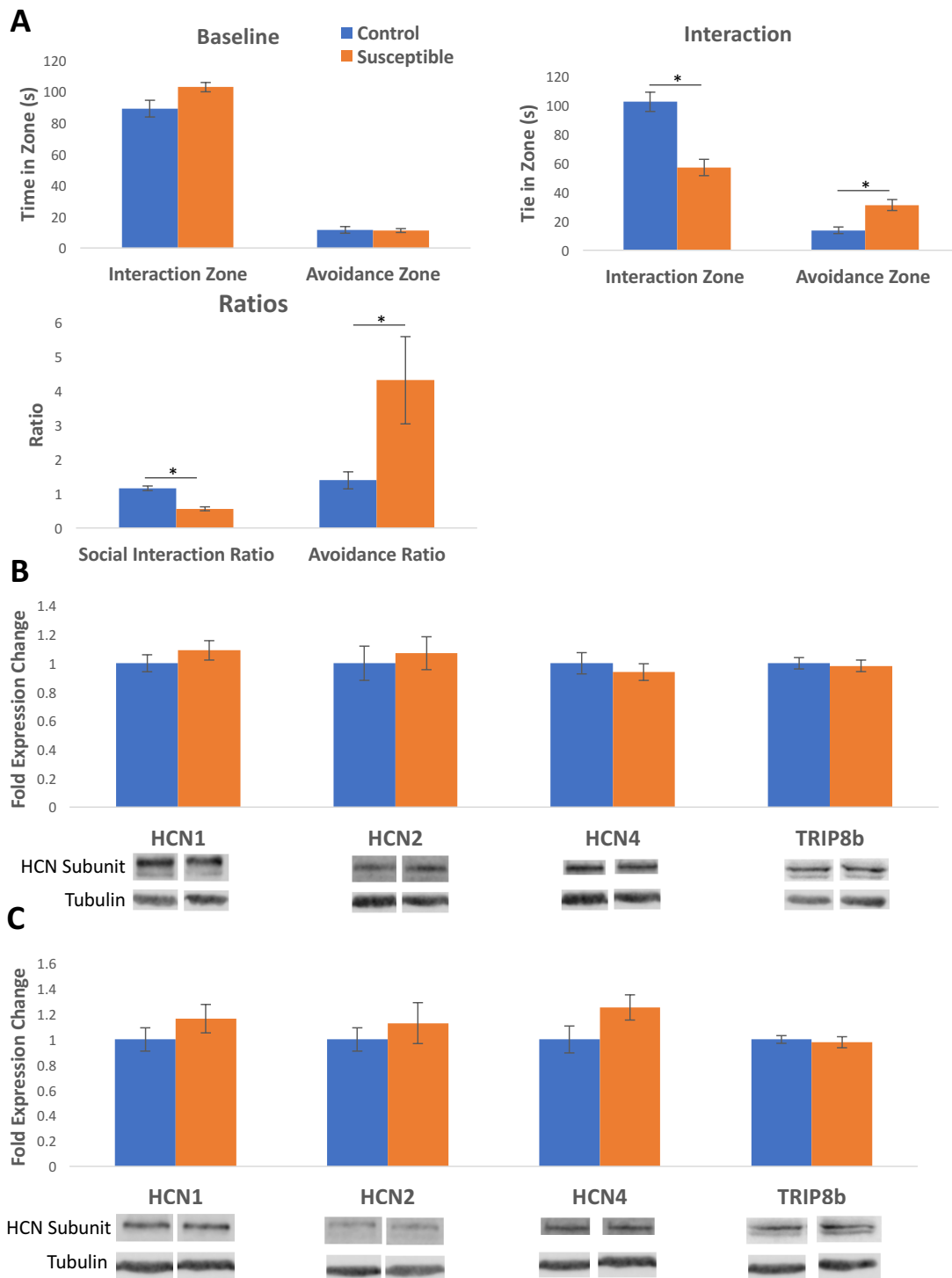
Figure 3: HCN channel expression does not change in the vHC or dHC 1 day after CSD. A) After 10 days of CSD, defeated mice showed significantly less time in the interaction zone and more time in the avoidance zone, yielding lower SIRs and ARs than undefeated controls. **B)** No change in HCN1, HCN2, HCN4, nor total TRIP8b was detected by western blot from dHC tissue 1 day after CSD. C) No change in HCN1, HCN2, HCN4, nor total TRIP8b was detected by western blot from vHC tissue 1 day after CSD. Student's T-test; *p < 0.05; ncontrol = 10, ndefeated = 17.

A
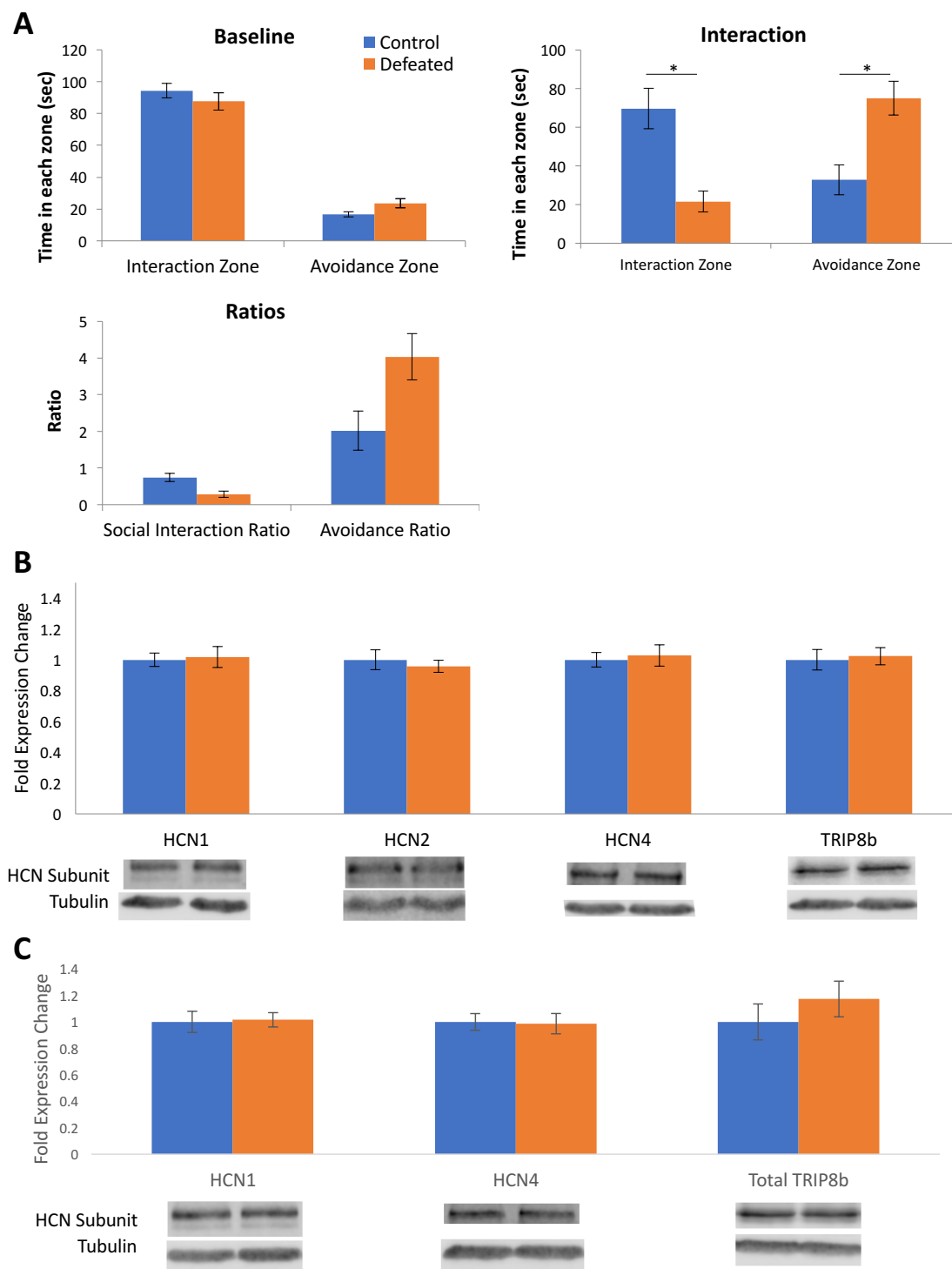
Figure 4: HCN channel expression does not change in the vHC or dHC 28 days after CSD. A) After 10 days of CSD and 28 days of rest, defeated mice showed significantly less time in the interaction zone and more time in the avoidance zone, yielding lower SIRs and ARs than undefeated controls. **B)** No change in HCN1, HCN2, HCN4, nor total TRIP8b was detected by western blot from dHC tissue 28 days after CSD. C) No change in HCN1, HCN4, nor total TRIP8b was detected by western blot from vHC tissue 28 days after CSD. Student's T-test; *p < 0.05; ncontrol = 12, ndefeated = 17.
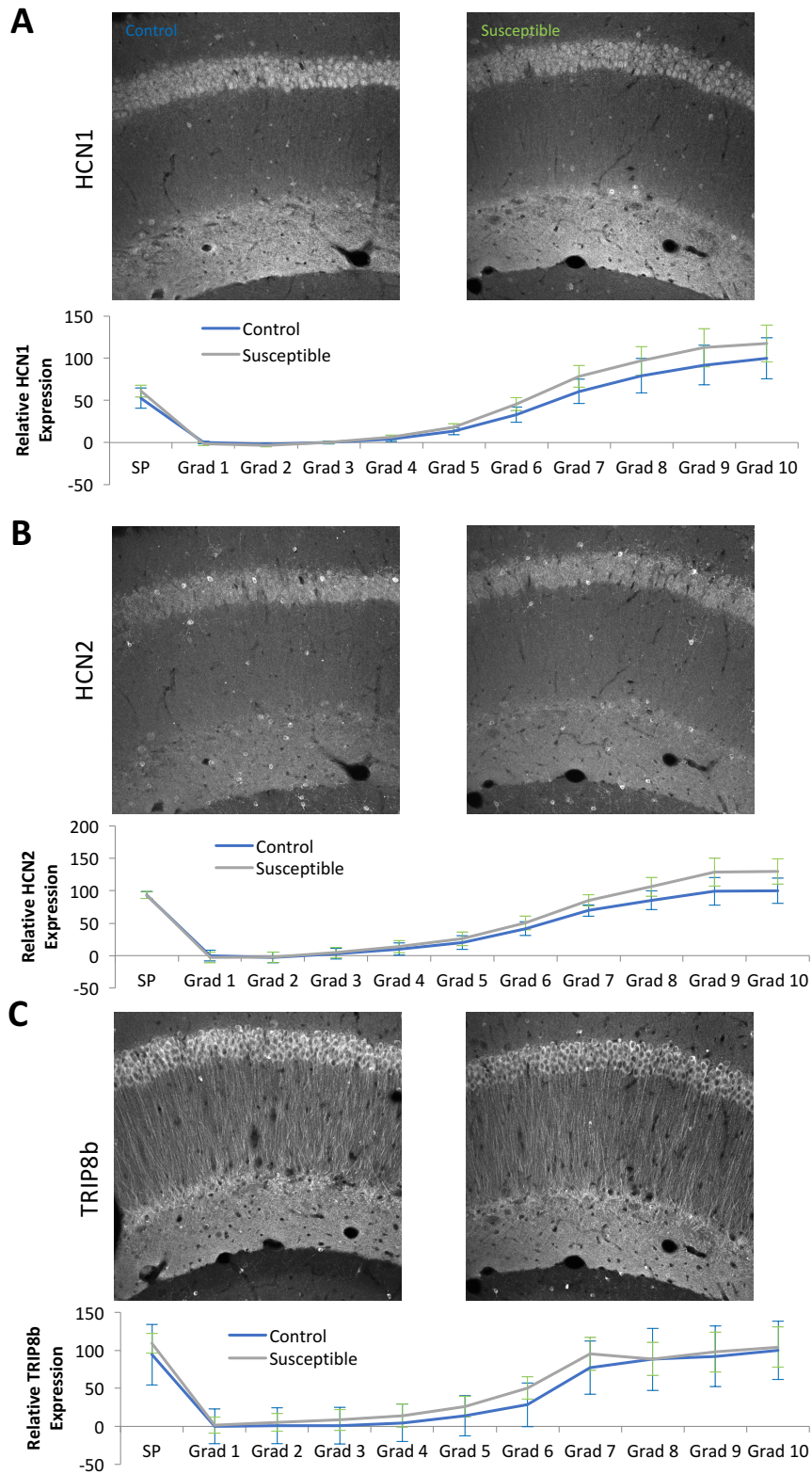
Figure 5: HCN channel localization is unchanged by CSD in the dorsal CA1. A) HCN1, **B)** HCN2, and **C)** TRIP8b localization was similar between control and defeated mice in dorsal CA1 pyramidal cells. n = 5

A

B

C
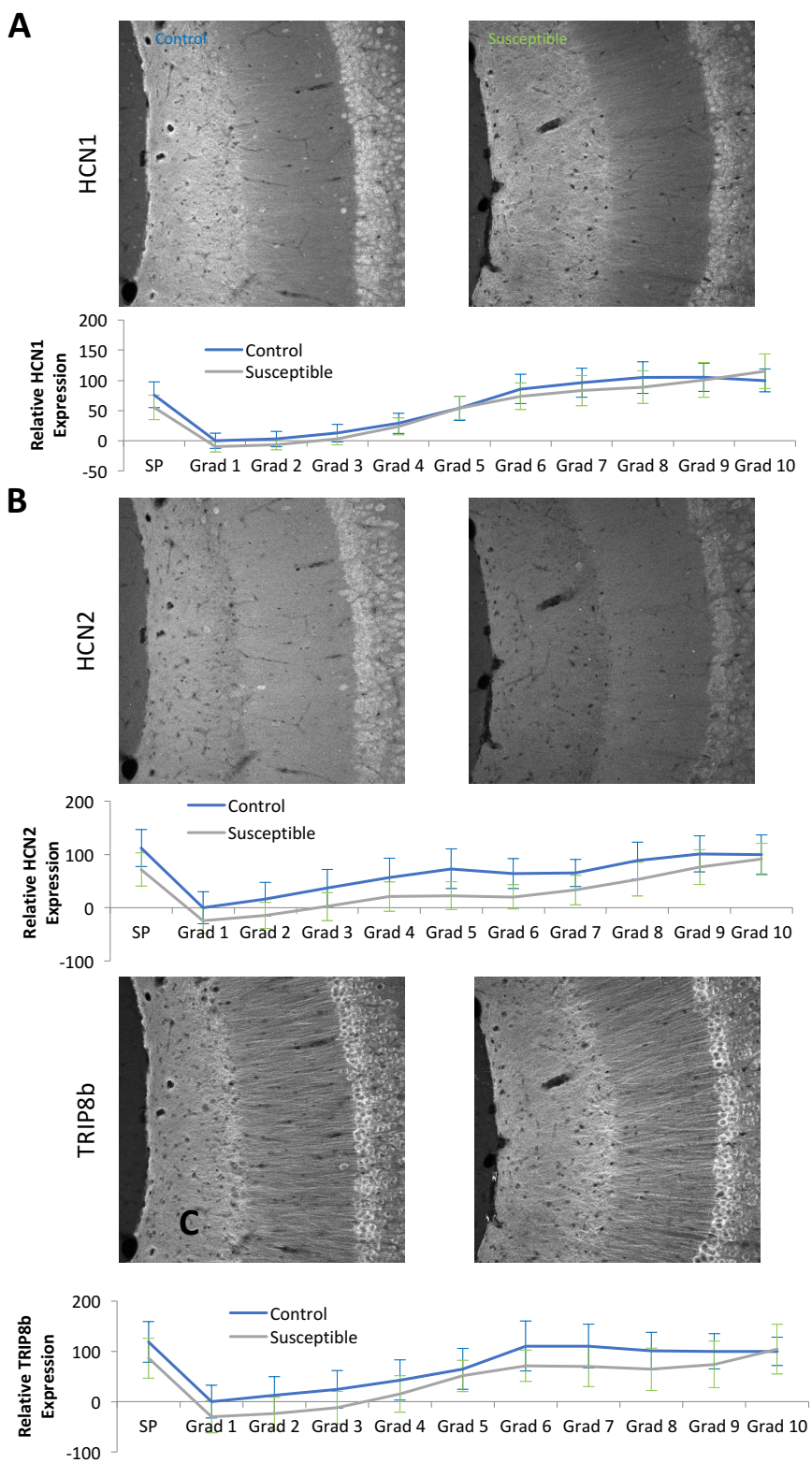
Figure 6: HCN channel localization is unchanged by CSD in the ventral CA1. A) HCN1, **B)** HCN2, and **C)** TRIP8b localization was similar between control and defeated mice in ventral CA1 pyramidal cells. n = 5.
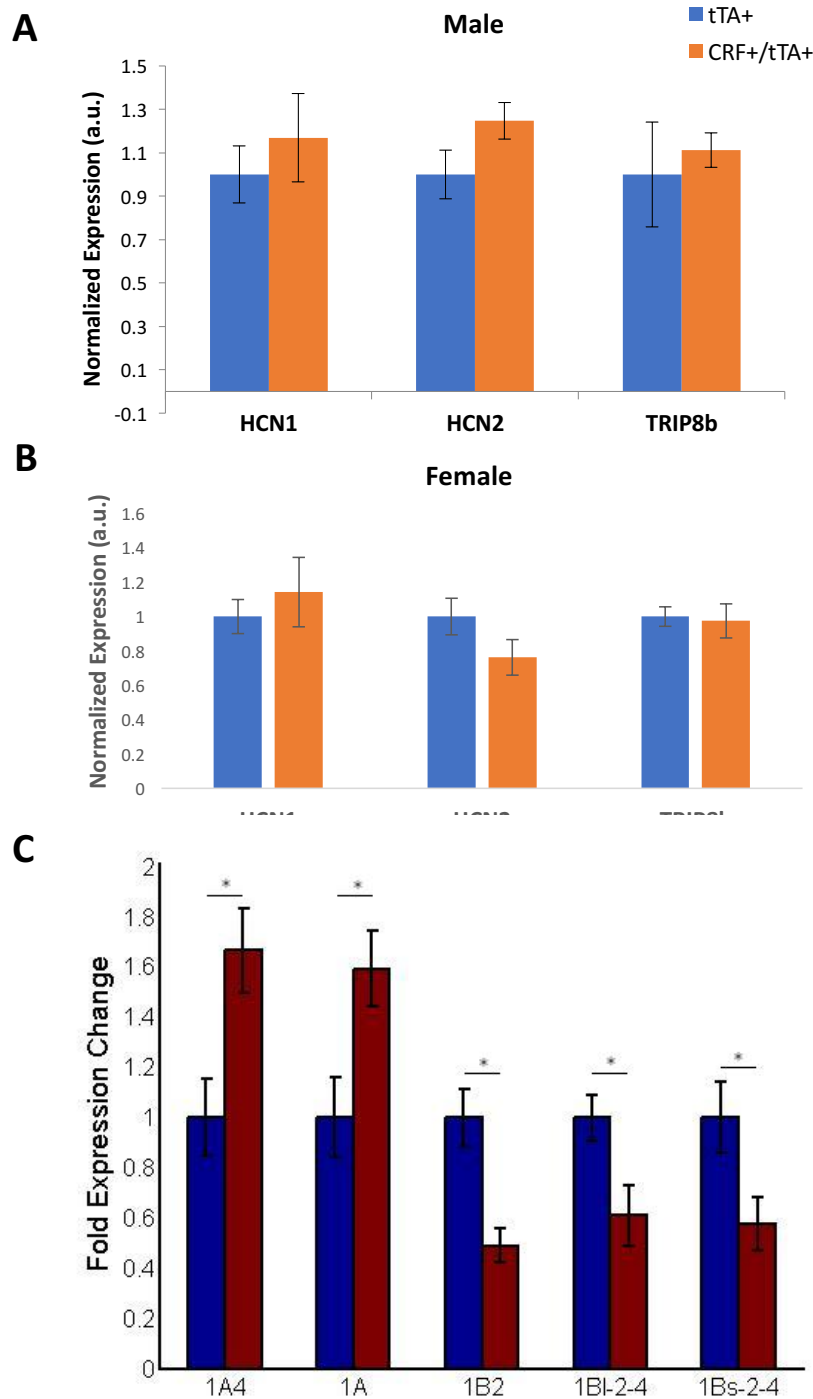
Figure 7: HCN channel expression is similar in ELS-like and control mice. A) tTA+/CRF+ (ELS-like) and tTA+ (control) male and female mice were euthanized at 3 months, and the CA1 region was isolated for qRT-PCR and western blot analysis. Male ELS-like mice showed similar HCN1, HCN2, and TRIP8b protein expression to controls. **B)** Female ELS-like mice showed similar HCN1, HCN2, and TRIP8b expression to controls. **C)** A significant increase in three Trip8b spliceforms driven by the 1a promoter and a significant decrease in two Trip8b spliceforms driven by the 1b promoter were detected in ELS-like male mice compared to controls. Student's T-test; *p < 0.05; Male nControl = 5, nELS-like = 7, Female nControl = 10, nELS-like = 6.
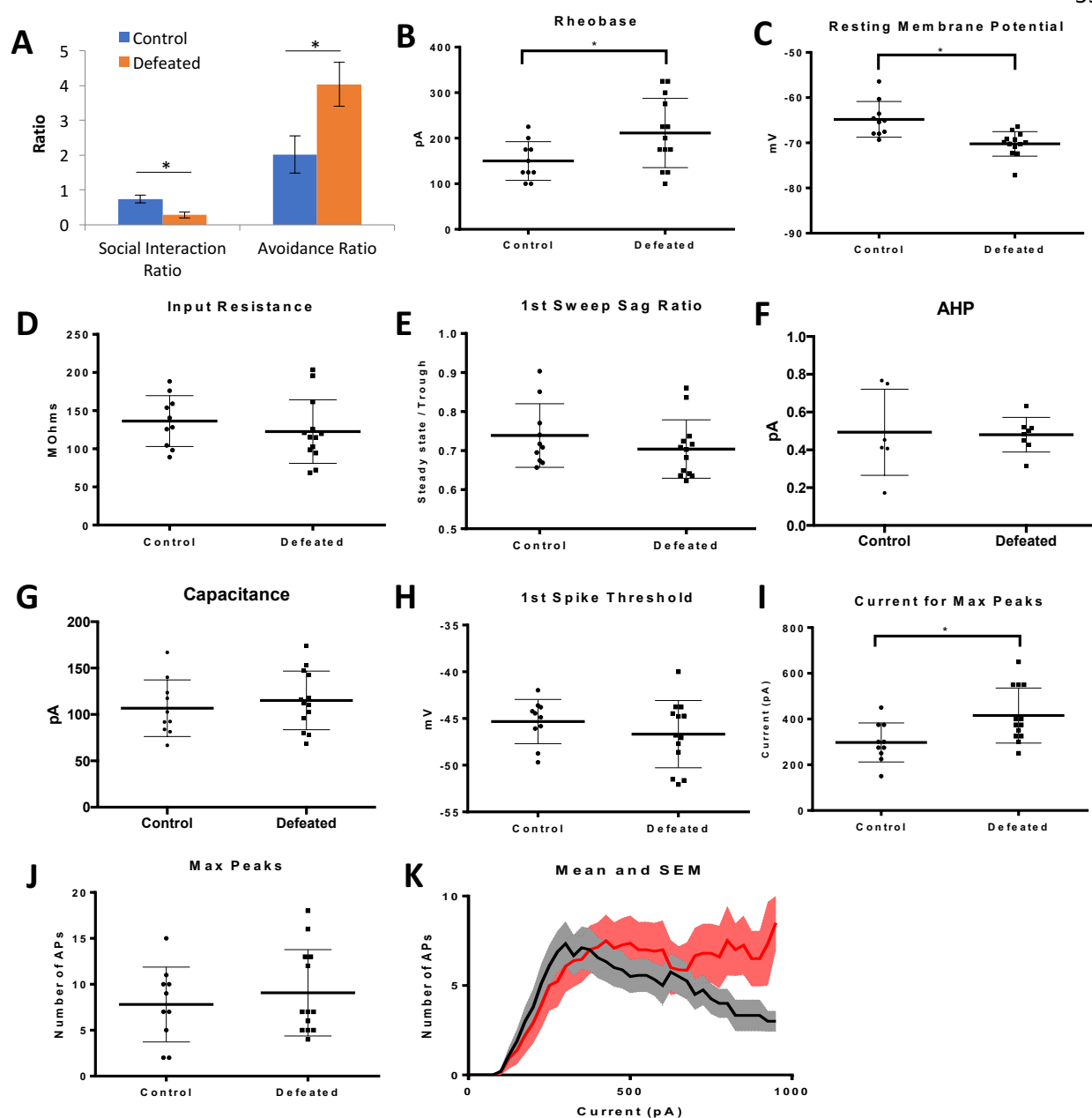
Figure 8: CA1 pyramidal cells are hypoexcitable in an Ih-independent manner after CSD. A) After 10 days of CSD, defeated mice showed significantly lower SIRs and ARs than undefeated controls. **B)** The rheobase was increased in defeated mice compared to controls. **C)** The Resting Membrane Potential (RMP) was decreased in defeated mice compared to controls. **D)** Input resistance, **E)** sag ratio, **F)** afterhyperpolarization (AHP), **G)** membrane capacitance, **H)** and action potential threshold was similar between control and defeated mice. **I)** The amount of current needed to facilitate the maximum amount of action potential firing was increased in defeated mice compared to controls. **J)** The maximum number of action potentials was similar between defeated and control mice. **K)** Average action potential firing per amount of current injected was analyzed in CA1 pyramidal cells from control and defeated mice. A depolarization block, noted by a decrease in the number of action potentials elicited at higher current injections, was evident in CA1 cells from control mice after the maximum number of action potentials were induced. A similar depolarization block was not detected in CA1 cells from defeated mice. Student's T-test; *p < 0.05; ncontrol = 10, ndefeated = 13.
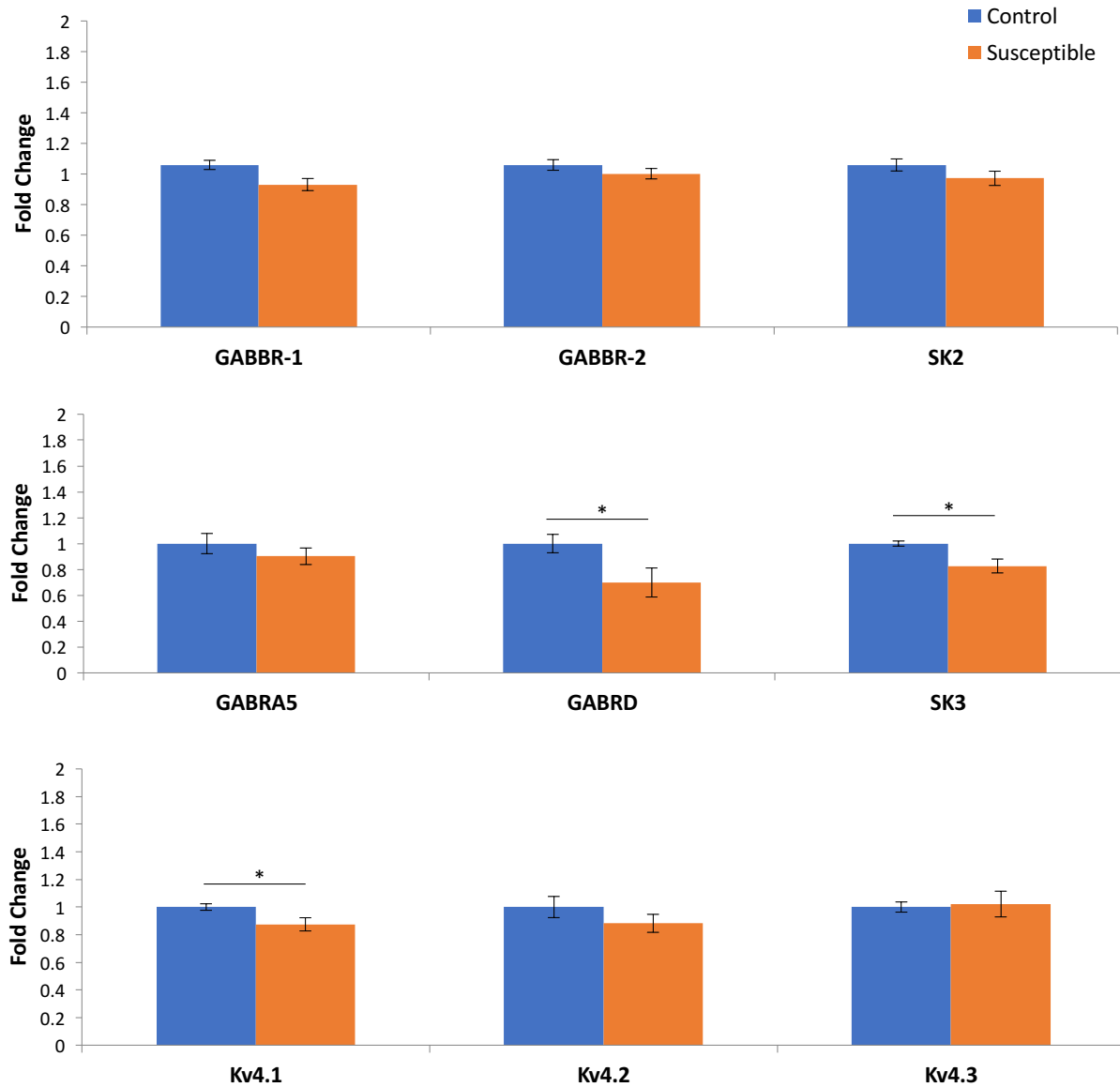
Figure 9: Transcription of potential ion channels mediated the CA1 hypoexcitable phenotype are largely unchanged. After CSD, CA1 tissue was isolated and mRNA was reverse transcribed for later qPCR quantification. While slight changes in the transcription of *Gabrd, Sk3,* and *Kv4.1* were noticed, they were regulated in the opposite manner as would be expected to explain the electrophysiological results. Student's T-test; *p < 0.05; ncontrol = 8, ndefeated = 13.
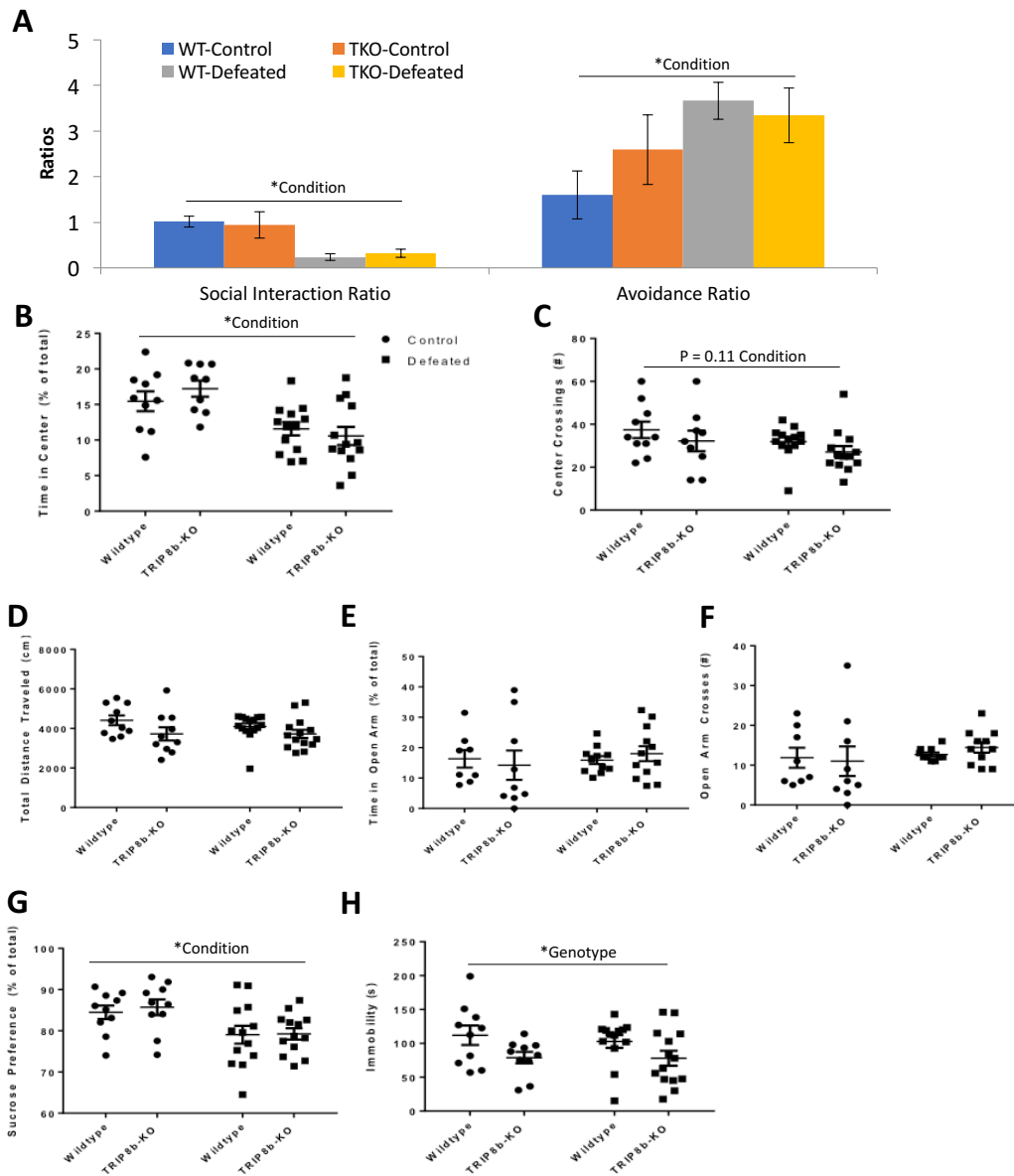
Figure 10: TRIP8b-KO mice are not protected from CSD stress. A) TRIP8b wildtype (*Trip8b*+/+) and KO (*Trip8b*-/-) mice underwent CSD for 10 days. Compared to controls, TRIP8b wildtype and KO mice displayed decreased SIR and increased AR, as evidenced by two-way ANOVA revealing an effect of condition but not genotype or a condition x genotype interaction. **B)** TRIP8b wildtype and KO mice displayed decreased center time in the OFT, as two-way ANOVA revealed an effect of condition but not genotype or a condition x genotype interaction. **C)** A trend towards decreased center crossings was seen for both TRIP8b wildtype and KO mice, as two-way ANOVA revealed a trend towards an effect of condition (p = 0.11) but not genotype or a condition x genotype interaction. **D)** TRIP8b wildtype and KO mice showed similar locomotor activity in the OFT. **E)** TRIP8b wildtype and KO mice showed similar behavior on the ZM in terms of time spent in the open arms and **F)** crossings into the open arms. **G)** TRIP8b and wildtype mice showed significantly less preference for sucrose, as two-way ANOVA revealed an effect of condition but not genotype or a condition x genotype interaction. **H)** Regardless of stress condition, TRIP8b KO mice showed decreased immobility compared to wildtype mice during the FST, as two-way ANOVA revealed an effect of genotype but not condition or a condition x genotype interaction. Two-Way ANOVA. *p < 0.05; both TRIP8b WT and KO mice ncontrol = 10, ndefeated = 14.
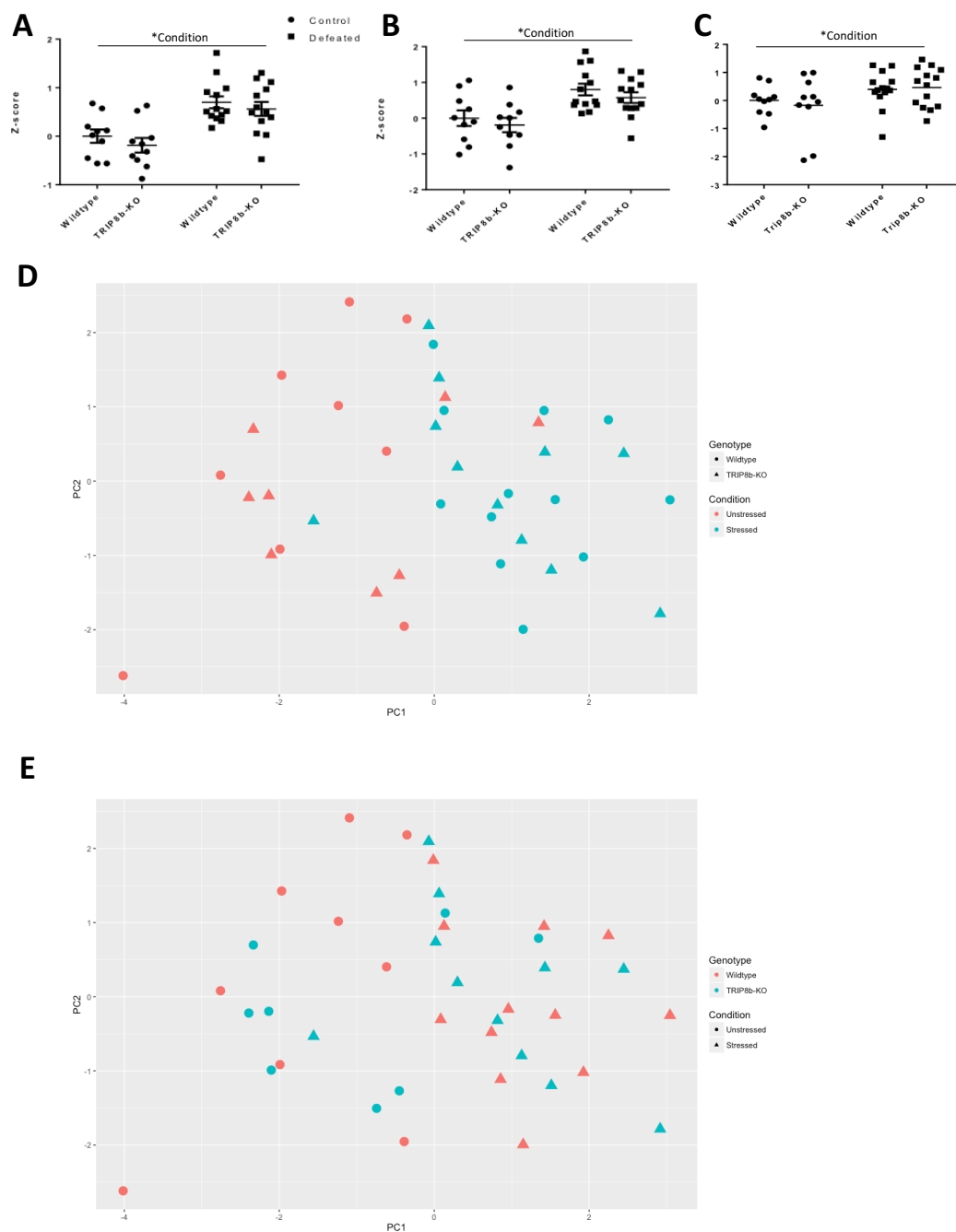
Figure 11: Z-score normalization and PCA confirm effects of stress on TRIP8b wildtype and KO mice. A) The Behavior Induced by Chronic Stress (BICS) index was compiled through z-score normalization of the primary endpoints for each assay and averaging the five assays together (detailed in methods). The BICS demonstrated that while stress greatly influenced the behavior of these mice, there were no significant differences in behavior between TRIP8b wildtype and KO mice, as two-way ANOVA revealed an effect of condition but not genotype or a condition x genotype interaction. **B)** The anxiety and **C)** depression subscales showed similar results to the BICS. **D,E)** PCA demonstrated two clusters of mice across the first principal component that corresponded to the stress condition of the mice. In the left panel, the color of the points corresponds to the stress condition and the shape of the points corresponds to the genotype. On the right, these designations are switched. Two-Way ANOVA. *p < 0.05; ncontrol = 10, ndefeated = 14.
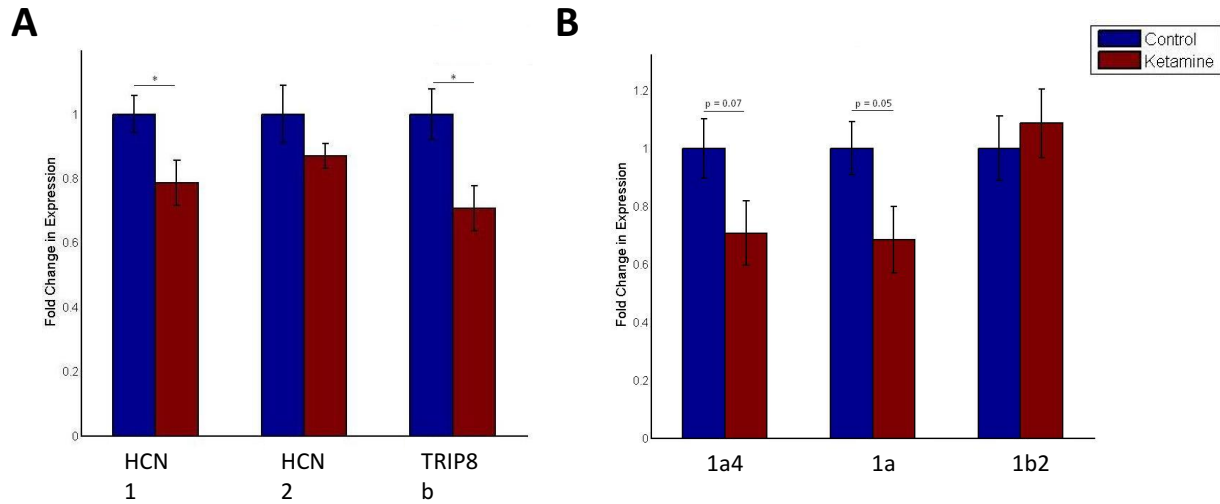
Figure 12: Ketamine causes a reduction in *Hcn1* and *Trip8b* transcription two hours after injection.
A) Male and female wildtype mice were injected with ketamine (10mg/kg i.p.), euthanized two hours later, and the CA1 was isolated for qRT-PCR analysis. While *Hcn2* mRNA remained unchanged, both *Hcn1* and *Trip8b* mRNA were reduced in ketamine-treated mice compared to saline controls. **B)** Trends (p = 0.07; p = 0.05) towards reduced *Trip8b(1a)* and *Trip8b(1a4)* but not *Trip8b(1b2)* were observed in the CA1 of ketamine-treated mice compared to controls. Student's T-test; *p < 0.05; n = 9

Expression of HCN channels and TRIP8b protein do not change after Chronic Social Defeat			
Region Analyzed	**Day after Social Defeat**	**Control/group (n)**	**Susceptible/group (n)**
Ventral Hippocampus	1	10	17
Dorsal Hippocampus	1	10	17
Ventral Hippocampus	28	12	17
Dorsal Hippocampus	28	12	17
CA1	1	8	13
Amygdala	1	8	13
medial Prefrontal Cortex	1	8	13

Table 1: Summary of experiments assaying HCN channel expression after CSD

Parameter	Result	If Ih Increased
Resting Membrane Potential	Hyperpolarized	Depolarized
Input Resistance	No Change	Decreased
Sag Ratio	No Change	Increased
Rheobase	Increased	Increased?
Capacitance	No Change	No Change
Spike Threshold	No Change	No Change
Temporal Summation	No Change	Decreased
Max Peaks	No Change	No Change
Depolarization Block	Not Present	No Change

Table 2: Summary of patch clamp experiments. The "Result" column corresponds to the actual electrophysiological outcomes after CSD while the "If Ih increased" column describes what would happen if the hypoexcitability was due to an increase in Ih.

Principle Component Analysis

	PC1	PC2	PC3	PC4	PC5
Standard deviation	1.66	1.2	1.14	1.03	0.84
Proportion of Variance	0.38	0.20	0.18	0.14	0.096
Cumulative Proportion	0.38	0.58	0.76	0.90	1.00
Condition (p-value)	**1.14e6***	1.00	0.98	1.00	0.99
Genotype (p-value)	1.00	1.00	0.87	1.00	0.14

Table 3: Principal Component Analysis (PCA) of BICS behavioral tests. The endpoints from the BICS behavioral battery were z-score normalized, and PCA analysis was run. Each principal component, along with the standard deviation of the values along that component and variance explained by that component, are shown. The Bonferroni-corrected p-value is displayed for comparisons between control and defeated (condition) and TRIP8b wildtype and KO (genotype) groups. While a significant difference in the values of control and defeated mice were found for the first principal component, no other significant differences were detected. Student's T-test with Bonferroni-corrections; *$p < 0.05$; ncontrol = 10, ndefeated = 14.

A

B

C
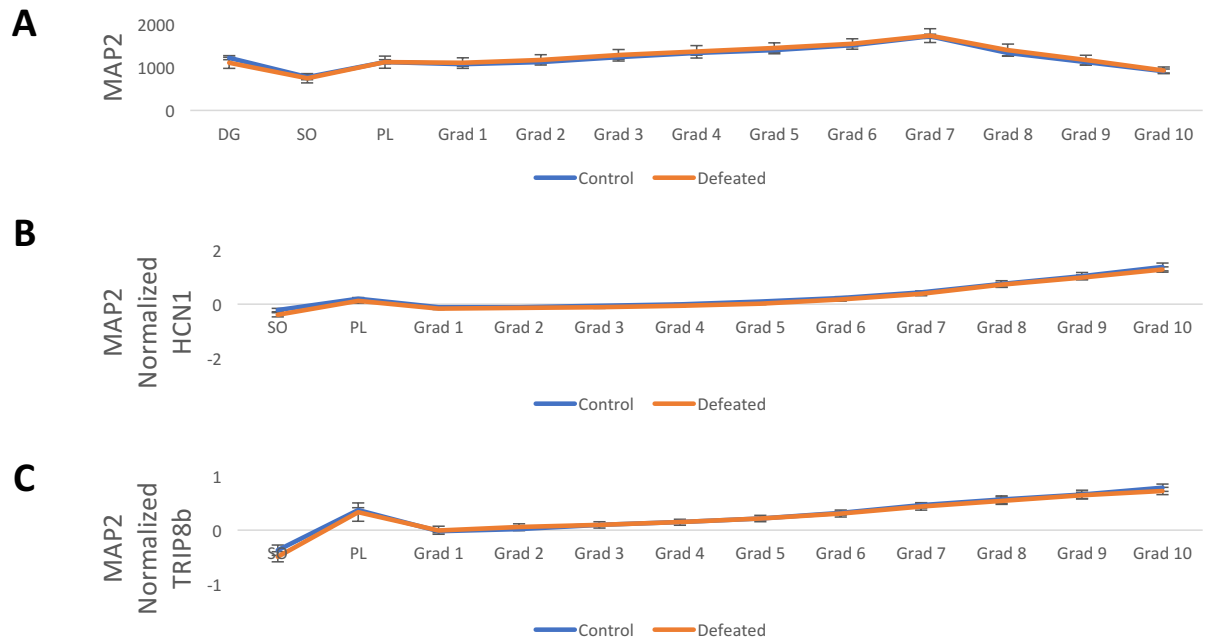
Supplementary Table 1: MAP2-corrected HCN1 and TRIP8b localization is unchanged in the dorsal CA1 after CSD. A separate cohort of mice underwent CSD, and HCN1 and TRIP8b expression in CA1 pyramidal cells was assessed. Using MAP2 as a marker of dendrites, no difference in CA1 dendritic morphology was detected (upper panel). In addition, when HCN1 (middle panel) and TRIP8b (lower panel) were corrected for MAP2 expression, no differences were detected between defeated and control mice. n = 5.

CHAPTER 3

HCN channels and acute stress

Abstract

Active coping is an adaptive stress response that improves outcomes in medical and neuropsychiatric diseases. To date, most research into coping style has focused on neurotransmitter activity and little is known about the intrinsic excitability of neurons in the associated brain regions that facilitate coping. Previous studies have shown that HCN channels regulate neuronal excitability in pyramidal cells and that HCN channel current (I_h) in the dorsal hippocampus (dHC) increases with chronic mild stress. Reduction of I_h in the dHC leads to antidepressant-like behavior, and this region has been implicated in the regulation of coping style. We hypothesized that the antidepressant-like behavior achieved with dHC knockdown of I_h is accompanied by increases in active coping. In this chapter, we found that global loss of TRIP8b, a necessary subunit for proper HCN channel localization in pyramidal cells, led to active coping behavior in numerous assays specific to coping style. We next developed a novel genetic approach to reduce HCN channel expression with a dominant negative TRIP8b isoform. This approach led to a robust reduction in I_h in the dHC and an increase in active coping. Together, these results represent the first demonstration that intrinsic dHC excitability through voltage-gated ion channels influences coping style.

Introduction

By 2030, Major Depressive Disorder (MDD) will be 1 of 3 leading causes of disease burden worldwide, with a lifetime incidence of about 10-15%[7,8,160,161] and a tremendous economic impact [reviewed in 2]. The mounting evidence of abnormal connectivity within cortico-limbic circuitry in MDD has led the field towards understanding the morphological, molecular, and electrophysiological changes behind these circuit dysfunctions[11,13-15]. Of these changes, molecular regulators of neuronal excitability are likely to influence MDD.

One important regulator of neuronal activity is the hyperpolarization-activated cyclic nucleotide-gated (HCN) channel[68-72]. HCN channels mediate a non-inactivating cationic current (I_h) that is active at the resting membrane potential in CA1 pyramidal neurons. Because of its effect on membrane resistance, I_h is critical for controlling neuronal excitability and regulating synaptic inputs[69,138,140,141,177,178]. In order to accomplish this function, HCN channels are expressed at significantly higher levels in the distal dendrites of CA1 pyramidal neurons[74]. This distribution of HCN channels is controlled by an auxiliary subunit, tetratricopeptide repeat-containing Rab8b-interacting protein (TRIP8b), and loss of this localizing protein ablates HCN channel distal dendritic enrichment[74,179].

Recently, our lab and others have shown that knock-out (KO) of the major pore-forming HCN channel subunits (HCN1 or HCN2) or TRIP8b leads to an antidepressant-like phenotype in mice on the Forced Swim Test (FST) and Tail Suspension Test (TST)[74,76,137]. Kim and colleagues[180] showed that HCN1 in the dorsal hippocampus (dHC) but not ventral (vHC) is increased with chronic mild stress and that shRNA knockdown of HCN1 in the dHC but not vHC leads to a reduction in anhedonia-like behavior and an increase in antidepressant-like behavior. Importantly, our lab has demonstrated that specific loss of distal dendritic HCN improves performance on both the FST and TST and that rescue of this enrichment specifically in the dHC is sufficient to reverse this antidepressant-like phenotype[137].

Though the effect of HCN channel loss in the dHC on antidepressant-like behavior is robust, it remains unclear why the dHC and not the vHC is implicated. Anatomical and functional studies have confirmed that the vHC uniquely influences emotional regulation through connections with limbic system brain regions, such as the amygdala and hypothalamus, while the dHC tends to be involved in memory and spatial navigation, with little direct connectivity to other brain regions implicated in MDD

symptomology[46,181-183]. However, the dHC has also been implicated in regulating coping behaviors[124], which are known to greatly influence MDD severity and treatment[108,110,111].

Though previous studies have emphasized individual differences in susceptibility and resilience to developing pathological behaviors under chronic stress (i.e. depression-like behaviors)[184], far fewer have assayed how individual animals adapt and respond to acute stressors. An individual's tendency towards certain responses to acute stress is often described as coping style, and two overarching categories are often described in both the human and rodent literature: active and passive coping[108,109]. Active coping, also described in patients as problem-centered or approach coping, is described as an individual's ability to directly address stressors and modulate emotional reactions in a way that mitigates the stressor's intensity[108]. In rodents, active coping behaviors similarly reduce the impact of acute stressors through directly addressing them, such as rodents' tendencies to reduce the stressfulness of an electrified probe by burying it as opposed to passively avoiding it[109,124]. Importantly, patients with strong active coping tendencies show better resistance to psychiatric illness and more favorable outcomes during treatment of chronic illnesses of all types, and though limited, studies have shown that active coping behaviors in rodents are correlated with decreased depression-like behaviors after chronic stress[185,186]. And while neurotransmitters have often been investigated as determinants of coping behaviors, no studies have looked at the intrinsic excitability of key neurons in brain regions involved in active coping.

Given the prior unexpected findings that reducing dHC I_h leads to antidepressant-like behavior and evidence that the dHC influences coping behavior , we hypothesized that loss of I_h in the dHC could lead to antidepressant-like changes as a component of a more broad increase in active coping. To test this, we subjected $Trip8b^{+/+}$ and $Trip8b^{-/-}$ mice to a number of coping assays, including the Two-Way Active Avoidance Test (2w-AA), the Resident-Intruder Test (RIT), Shock Probe Burying Test (SPBT), and the Repeated Forced Swim Test (rFST). We further developed a novel gene therapy approach to reduce I_h in wild type mice through expression of a dominant negative TRIP8b isoform and investigated if reducing I_h specifically in the dHC would promote active coping behaviors.

Material and Methods

Animals

Global *Trip8b*^{-/-} mice creation and genotyping have been previously described[74]. Although we have previously referred to these animals by the name of the gene encoding TRIP8b protein (*Pex5l*), we have elected to refer to them as *Trip8b* in this manuscript for clarity. Male 8 to 16 week-old *Trip8b*^{+/+} and *Trip8b*^{-/-} mice were used for all studies, as many of the coping assays, especially those measuring aggression, are not ethnologically appropriate for female mice. For electrophysiology and virus experiments, wildtype C57Bl/6J mice were obtained from Jackson Laboratories (Bar Harbor, Mn) at 8 weeks-old. Mice were maintained on a 12:12 hour light:dark cycle, with food and water given *ad libitum.* All animal experiments were performed according to protocols approved by the Institutional Animal Care and Use Committees of Northwestern University.

Virus

The DNA plasmid for *pAAV-hsynapsin-Cre-IRES-eGFP* was kindly provided by Dr. Pavel Osten (Cold Spring Harbor Laboratory), as in our previous report[137]. The TRIP8b(1b-2) isoform was then subcloned into this vector, and AAV serotype 2/8 vectors were produced by the Gene Therapy Program of the University of Pennsylvania.

Stereotaxic Viral Injection

Injection of viral vectors were done as previously described[137]. Briefly, mice were anesthetized with inhalational isoflurane and mounted on a stereotaxic instrument (Stoelting, Wood Dale, IL). A midline incision was made at the scalp, and a small craniotomy was performed with a dental drill. 1μl of 3×10^{12} vector genome (vg)/ml of AAV was injected into the dorsal CA1 (2.3 mm A/P, ±1.3 mm M/L, -1.7 D/V) of C57BL/6J mice at a rate of 0.3 μl/min via a 5 μl Hamilton syringe. After the injection, the needle was left in place for 5 minutes to allow the virus to diffuse before removing the needle at a rate of 1 mm/min. A minimum of 4 weeks was allowed to pass between injection and experimentation in order for maximal viral expression.

Immunohistochemistry.

As described in Chapter 2.

Electrophysiology

As described in Chapter 2.

Western Blotting

Western blotting was performed as previously described[80,137]. Primary antibodies used were: custom rabbit anti-HCN1, rabbit anti-HCN2, and guinea pig anti-TRIP8b, rabbit anti-MAP2 (Millipore Temecular, CA), and mouse anti-tubulin (Millipore Temecular, CA). Primary antibodies were diluted in blocking solution containing 5% milk and 0.1% Tween-20 in TBS (TBS-T). Band intensities were quantified using ImageStudio (Li-Cor, Lincoln, NE) software and normalized to the anti-tubulin signal for each sample.

Behavioral Testing

Before each behavioral task, the mice were acclimated to the behavioral testing room for at least 1 hr. All tests were performed in an isolated room under quiet conditions, and all behavioral experiments took place during the light part of that cycle. For experiments with multiple trials over many days, each trial occurred within 2 hours of the same time each day. For serial behavioral tasks, at least 4 days were allowed for the mice to recover before the next test started. All behavioral testing apparatuses were cleaned with 70% ethanol between trials. All experimenters were blinded to the subjects' groups during testing and analysis.

Open Field Test (OFT)

As described in Chapter 2.

Zero Maze (ZM)

As described in Chapter 2.

Morris Water Maze (MWM)

The MWM was done similarly to our previous publication[74], with minor deviations. The MWM consisted of tests in three phases: 4 days of visible platform training, 5 days of hidden platform training, and a probe trial which occurred before the hidden platform trials on the last 3 days of hidden platform testing (3 trials total over 3 days). The MWM consisted of a 120 cm diameter circular pool filled with 24°C ± 1°C water that was made opaque with white, non-toxic paint. Around the arena, different shaped cues corresponding to the 4 cardinal directions were prominently displayed during the hidden platform and probe trials. Each day of training consisted of 4 trials per mouse per day with >60s inter-trial intervals. Probe trials were single trials when performed. Mice were placed in one of four starting locations facing the pool wall and allowed to swim freely until finding a 10 x 10 cm platform submerged in water by ~1 cm (hidden and probe) with a cutoff of 60 s. During the visible platform trials, the platform had four 1 cc syringes on the corner of the platform and was just at water level. If the mouse failed to find the platform within 60 s, the experimenter guided the mouse to the platform location. For each trial, the mouse was allowed to remain on the platform for 20s before the experimenter returned the mouse to its homecage. All behavior was tracked with overhead cameras and analysis was done using Actimetrics WaterMaze. Average latency to reach the platform and distance traveled to the platform were the final endpoints for the hidden trials while average time spent in each quadrant represented the final endpoint for the probe trial.

Two-Way Active Avoidance (2w-AA)

The mice are tested in a two-way shuttlebox (Habitest; Coulbourne) equipped with an electrified grid floor and infrared sensors in each chamber. The 2w-AA consisted of 5 trials, each occurring daily, with each trial containing 30 active avoidance challenges per subject. The set-up for each trial was as follows: The arena was dimly lit, and the mouse was placed on the same side of the arena each day with the guillotine door open, allowing for free exploration. Each mouse was given 3 minutes to acclimate and explore the arena before the guillotine door closed, and the first challenge began. Each challenge began with the guillotine door raising and presentation of a 4kHz tone (65dB) and a 15W cue light on both sides of the arena. If the moues transitioned to the adjacent chamber within 8s, the challenge was counted as an "Avoidance," and the tone and cue light turned off, followed by an inter-trial interval (ITI) of 20-40s with

the guillotine door closed. If the mouse failed to move within 8s of the cue onset, a 0.3mA scrambled shock was delivered for 5s. If the moue transitioned to the adjacent chamber within this time, the trial was counted as an "Escape," and the tone and cue turned off, followed by the ITI. If the mouse fails to move within 5s, the cue and shock were both stopped, and the trial was counted as a "Failure." An ITI began before the next trial. The average counts of "Avoidance" were the main endpoints for this assay, as "Failures" were exceedingly rare.

Active Coping Index (ACI)

Three behavioral tasks to specifically assess active coping[109] were administered to a single cohort of mice. These three tests are rarely or never used to describe depression-like behavior, specifically. The tests went in increasing order of stressfulness, starting with the Resident Intruder Test (RIT), Shock Probe Burying Test (SPBT), and Repeated Forced Swim Test (rFST). 2 weeks before testing, each mouse was housed individually and allowed to acclimate to their surroundings. At 1 week before testing, a wildtype female mouse was added to reduce the effects of isolation stress. This housing paradigm ensured sufficient territoriality of the subjects for the resident intruder test and was maintained throughout the three assays.

Resident Intruder Test (RIT)

The RIT was performed similar to previous publications[187]. Briefly, at 15 min prior to testing, the female was removed, and a clear plexiglass cage top replaced the normal food hopper to allow for clear visualization of the mice by a video recorder placed overhead. A 10 min trial began when a 6-8wk old male intruder was placed in the cage, and the resultant behavior was recorded. After the trial, the intruder was removed, food hopper replaced, and female put back in the cage. Videos were documented for numerous behaviors: Aggressive Behaviors (Lateral Threat, Upright, Clinch/Bite, Keep Down, Chase), Social Behaviors (Social Exploration, Ano-Genital Sniff, Social Grooming, Mounting), Exploratory Behaviors (Sniffing, Rearing, Cage Exploration), Defensive/Submissive Behaviors (Being Groomed, Fleeing, On Back, Submissive Freeze, Defensive Sideways, Defensive Upright) and other

(Inactivity/Resting, Grooming, Digging). Aggressive behavior and attack latency were the main endpoints of this assay (averaged over daily trials for 3 days).

Shock Probe Burying Task (SPBT)

The SPBT was performed similar to previous publications[188]. Briefly, all trials took place in a 13 x 11 x 17cm plexiglass arena with about 3cm of standard cage bedding (clean wood shavings). The arena was placed in an isolation cubicle (Coulbourne), and behavior was monitored by overhead video camera remotely. A 3 trial test was administered to each mouse over 3 days. During the first day, the mouse underwent an Acclimation Trial of 15 min, where they were placed in the arena without a shock probe and could explore freely. The second day, an Acquisition Trial was administered, where the subject was placed in the arena with a shock probe (4cm x 1cm cylinder; 0.5mA). The probe was controlled manually by the experimenter and remained off unless the experimenter pushed a trigger. The probe was only electrified when the mouse made clear contact with the probe. The mouse explored the arena until it touched the probe with both paws and then was given its first shock. The resultant behavior was documented for the next 15 min of the trial, and the mouse was then returned to its homecage. There was no difference in the number of shocks received between groups (data not shown). On the third day, a Recall Trial was administered, where the subject was placed in the SPBT chamber with the shock probe, but it was never electrified. The mouse's behavior was documented for 15 min from the moment it entered the arena. Behaviors observed included burying, immobility (no ambulation with only occasional side to side, scanning movements of the head), ambulation, prod exploration (snout pointed towards the probe and sniffing), grooming, and rearing. The times spent burying and immobile as well as the latency to bury were the major endpoints for this assay during the Acquisition and Recall Trials. A "Change in Response" value was computed to determine if the mice showed differences in memory between the Acquisition and Recall Trial. The Change in Response was calculated by subtracting the total time spent freezing and burying in the Recall Trial from the total amount of time freezing and burying in the Acquisition Trial and dividing by the total time spent freezing and burying in the Acquisition Trial to get a ratio of the difference between trials normalized to the original amount of freezing and burying in the original trial.

Repeated Forced Swim Test (rFST)

The rFST was performed similar to previous publications[189]. Briefly, each trial consisted of a 6 min immersion in a 4L beaker of tap water at a temperature of 24 +/- 1°C, and a daily trial was administered for three days. An observer recorded the amount of time the mouse remained immobile (no purposeful movements other than those necessary to remain afloat) during each trial during two time periods: the first two minutes and the last four minutes. For the "classical" FST measurements, the last four minutes of the first trial were scored for total time spent immobile. For the rFST, the full 6 minutes of each trial were scored over all three trials, and the average time spent immobile across trials was the main endpoint of this assay.

Z-score normalization

A large source of irreproducibility within behavioral neuroscience likely comes from the use of a Single Point In Time assay (SPIT). In addition to needing more subjects to uncover significant findings, SPIT is more susceptible to being influenced by unforeseen environmental factors and random chance. The z-score normalization method is used to reduce variability among many similar behavioral assays to get a more accurate account of a single behavioral domain, as described previously[172]. Similar to the RDoCs introduced by the NIMH[190,191], this method aims to better describe how individual performances on multiple, similar behavioral tasks constitute overall behavior in a single domain – in this case, active coping. In addition, assays with multiple endpoints that measure different aspects of a particular behavior can be averaged together to give a z-score for the assay, such as was done for attack latency and time spent in offensive aggression for the RIT. In order to achieve an "index" for active coping, each individual assay's endpoints were converted into a z-score based on the normal distribution of the wildtype population. In essence, this converts all the data within an assay into a single value with a single "unit" of measurement based on the relative performance of each individual to the average performance of the control group. This not only greatly reduces individual test variability but also reveals a more rigorously defined assessment of how an individual mouse tends to behave. The following formula was used to compute z-scores:

$$Z = (x_{subject} - \mu_{control})/\sigma_{control}$$

Where $x_{subject}$ = individual endpoint value, $\mu_{control}$ = control population average and $\sigma_{control}$ = standard deviation. Control refers to either the *Trip8b*$^{+/+}$ or AAV-GFP populations.

To prevent weighting one assay more than another, multiple endpoints within the same assay were first z-score normalized and then averaged together, yielding a single composite z-score per assay. To make sure all z-scores were consistent, each endpoint's z-score was normalized so that a score > 0 depicted a tendency towards more active coping and a score < 0 depicted a tendency towards more passive coping. For instance, as a low latency for aggression is indicative of increased active coping, and the untransformed z-score for aggression demonstrates that negative scores had the lowest latencies (i.e. most aggression), the sign was flipped for this endpoint before the average for the assay was taken. A description of the combined endpoints within each assay to create the assay-specific indices are as follows: The Aggression Index consisted of average attack latency and average % time of offensive aggression. The SPBT Index consisted of the % time burying, % time freezing, and the latency to bury from both the Acquisition and Recall Trials (6 endpoints in total). The rFST index was solely comprised of the average immobility times across the three trials. The final ACI was then derived from the average of the assay indices.

Electron Microscopy

The distribution of HCN1 channel protein was examined using serial section, pre-embedding, silver-intensified, ultrasmall immunogold electron microscopy as described previously (PESIUSIGEM; Lörincz et al., 2002; Dougherty et al., 2013). Briefly, mice receiving GFP injections (n=2) or injections of 1b (n=2) were perfused with room temperature 0.9% saline, followed by acidic sodium acetate-buffered 2% paraformaldehyde/1% glutaraldehyde (pH = 6.0), then basic sodium borate-buffered 2% paraformaldehyde/1% glutaraldehyde (pH = 9.0). Slices (70 μm) were taken of the dorsal hippocampus,

rinsed in Tris-buffered saline (TBS), exposed to 1% $NaBH_4$, rinsed in TBS, blocked, and then incubated in anti-HCN1 antibody (Shin et al., 2008). After rinsing in TBS, slices were blocked again and incubated in ultrasmall immunogold particles (Aurion, Electron Microscopy Sciences), followed by rinsing in TBS, fixation of immunogold particles in 2% glutaraldehyde in phosphate-buffered saline (PBS), silver enhancement using the R-Gent SE-EM Enhancement Kit (Aurion), then osmication, and curing in Araldite 502. Polymerized slivers of CA1 were then dissected from slices, re-embedded, and rotated orthogonally to the plane of sectioning. Arrays of serial ultrathin sections (65 nm, as estimated using Small's Method of Minimal Folds) were then collected using a Leica UC6 ultramicrotome and a diamond knife, followed by counterstaining in 5% aqueous uranyl acetate and Reynold's lead citrate. Images were obtained at 7,500x or 10,000x magnification using a JEOL 1200EX transmission electron microscope or a Sigma HD VP scanning electron microscope in scanning-transmission (STEM) mode (Zeiss), respectively. The total number of dendrites analyzed in the PESIUSIGEM experiments was 36 and 93 dendrites with membrane-immunopositive signal for HCN1 in pSR and SLM, respectively.

Statistics

All statistical calculations were performed using GraphPad 6 and MATLAB. All behavioral data that followed a normal distribution had outliers removed if they were > 2 standard deviations away from the population mean to avoid Type II errors[166]. For pairwise comparisons, a two-tailed student's T-test was performed. For comparisons with two factors, a Two-Way ANOVA was used, and a Repeated Measures ANOVA was implemented when one of the factors was within subject (i.e. trials). Sidhak's *post-hoc* test was used as needed for pairwise comparisons following significant ANOVA results. Significance was denoted with an asterisk, representing a p-value < 0.05, and all values were reported as mean±S.E.M.

Results

Trip8b^{-/-} mice show increased active coping in the Two-Way Active Avoidance Test (2w-AA)

Loss of HCN channel distal dendritic enrichment through elimination or suppression of endogenous TRIP8b expression has been shown to increase antidepressant-like behavior in rodents[74,137]. To determine

whether loss of this distal dendritic enrichment affects active coping, we subjected *Trip8b$^{-/-}$* mice and *Trip8b$^{+/+}$* to 2w-AA, a well-validated test of active coping. In this test, mice are placed in a two-chambered shock arena with a door allowing shuttling between the two chambers. During an AA trial, the door lifts and a light and tone cue are presented, encouraging the mouse to shuttle to the other chamber. If this mouse fails to move, a low-intensity shock is delivered. Mice that are naturally more active copers will show more avoidances to the cue than passive copers, which refrain from moving until the shock is administered[109]. Consistent with our hypothesis, we found that *Trip8b$^{-/-}$* mice showed more avoidances on the first day of testing than their *Trip8b$^{+/+}$* counterparts **(Figure 1A,B)**. In addition, we observed that both *Trip8b$^{-/-}$* and *Trip8b$^{+/+}$* mice were able to learn to increase their avoidances over the following days of the trial, ultimately leading to >90% successful avoidance rate in both groups. This suggests that while *Trip8b$^{-/-}$* mice show an inherently increased propensity for active coping, both groups are able to successfully learn to cope actively.

Trip8b$^{-/-}$ mice show increased active coping on a behavioral battery that specifically tests coping style

2w-AA directly assays active coping, but it remains unknown if *Trip8b$^{-/-}$* mice show other signs of increased active coping in assays with more complex possible responses. For instance, while the 2w-AA favors active coping and punishes passive coping, the Shock Probe Burying Test (SPBT) measures active and passive coping behaviors without reinforcement of one or the other[124]. Further, improved performance on the 2w-AA may demonstrate that *Trip8b$^{-/-}$* mice learn to actively cope more quickly within the first trial, which could reflect a difference in memory acquisition as opposed to coping style. Therefore, the Repeated Forced Swim Test (rFST), which reinforces passive coping behavior over multiple trials, was used to determine if *Trip8b$^{-/-}$* mice show complementary deficits in passive coping while also testing if *Trip8b$^{-/-}$* mice have improved memory, as reflected in the rate of acquisition of passive coping as compared to wildtype mice. Because the 2w-AA is a simple behavioral task, we also evaluated aggressiveness in the Resident-Intruder Test (RIT) to determine if *Trip8b$^{-/-}$* mice show increased active coping behavior in a task where behavior is influenced by complex stimuli and other behavioral variables[109].

In order to further phenotype the *Trip8b*[^-/-] mice and avoid erroneous conclusions based on Single Point In Time (SPIT) assays, we administered these assays to a naive cohort of *Trip8b*[^+/+] and *Trip8b*[^-/-] mice in sequential order from least to most stressful: RIT, SPBT, and then rFST **(Figure 1C)**. In order to reduce ambiguity between multiple endpoints of coping within each assay, all of the salient endpoints were converted into a z-score based on the normal distribution of the *Trip8b*[^+/+] behavior (detailed description of analysis in methods) to give an "Index" for each assay[172].

Over three daily trials in the RIT, Trip8b-/- mice showed shorter attack latencies, increased time spent in offensive aggressive behavior, and an overall higher Aggression Index score **(Figure 1D; Supplementary Figure 1)**. Importantly, neither *Trip8b*[^+/+] nor *Trip8b*[^-/-] mice showed signs of 'violent aggression,' as there were no signs of excessive wounding, and rare wounding was mainly on the rump and restricted from sensitive areas (face, neck, genitals, etc). A full description of behaviors during this test are available in the supplementary materials **(Supplemental Table 1)**.

The week following RIT, *Trip8b*[^+/+] and *Trip8b*[^-/-] mice were tested on the SPBT, where *Trip8b*[^-/-] mice displayed less freezing, more burying, and a shorter latency to bury in the Acquisition Trial but no significant changes in the Recall Trial compared to *Trip8b*[^+/+] mice **(Supplementary Figure 2, Supplementary Table 2)**. An "SBPT Index" for each trial was again compiled using z-score normalization **(Supplementary Figure 2)**, while a composite SPBT Index achieved through the average of both trials confirmed that *Trip8b*[^-/-] mice demonstrated more active coping behavior overall in the SPBT **(Figure 1E)**. A "Change in Response" ratio was computed as the difference between the total time spent burying and freezing in the Acquisition and Recall Trial divided by the total time spent burying and freezing in the Acquisition Trial and demonstrated that both groups had similar changes in responses to the environment between trials, suggesting that differences in memory were not responsible for the differences in behavior **(Supplementary Figure 2)**.

Lastly, the rFST was administered to both groups one week following the SPBT. Similar to the classic FST, mice were placed in water for 6 minutes, and their total time spent immobile was recorded. However, this FST procedure was repeated on a second and third day to assess acquisition of passive coping-like behavior as the mouse became familiar with the task. By scoring the last four minutes of the first day's trial, we confirmed prior observations that the *Trip8b*[^-/-] mice spend significantly less time

immobile than *Trip8b*$^{+/+}$ counterparts on the "classic" FST **(Supplementary Figure 3)**. In addition, *Trip8b*$^{-/-}$

mice continued to spend less time immobile compared to *Trip8b*$^{+/+}$ controls across all three full rFST trials

(Supplementary Figure 3). Both groups spent significantly more time immobile on Trial 3 compared to

Trial 1, indicating that while *Trip8b*$^{-/-}$ mice showed a propensity towards more active coping, they were still

able to adapt to their environment via acquisition of passive coping in later trials. An average score of the

full time spent immobile in each of the three trials was z-score normalized into a "rFST Index", which

further confirmed that *Trip8b*$^{-/-}$ mice showed a decreased propensity for passive coping in the rFST

(Figure 1F).

The behavior on these three coping assays can be altered by a number of environmental stimuli

and can also be influenced by mental processes other than coping style, thus introducing high

variability[172]. To better understand *Trip8b*$^{-/-}$ mice's coping style overall, we combined the three indices

from the RIT, SPBT, and rFST to create an "Active Coping Index" (ACI) that was equally influenced by all

three tests. As predicted, Trip8b-/- mice demonstrated higher scores on the ACI than their *Trip8b*$^{+/+}$

counterparts (**Figrue 1G**). Importantly, *Trip8b*$^{-/-}$ mice show similar locomotor and anxiety-like activity

behavior compared to *Trip8b*$^{+/+}$ mice **(Supplementary Figure 4)**, and our previous publications have also

demonstrated that neither group shows differences in memory[74,137]. Thus, global HCN channel reduction

through *Trip8b*$^{-/-}$ leads specifically to increased active coping.

A novel gene therapy approach reduces HCN channels in the dHC

Previous studies have shown that the antidepressant-like behavior seen in HCN-KO mice

depends on downregulation of I$_h$ specifically in the dHC but not vHC[137,180]. Therefore,

we developed a novel gene therapy approach **(Figure 2A)** to target neurons using ectopic expression of

TRIP8b-(1b2), a dominant negative TRIP8b spliceform found in glial cells[80,89], in an AAV8 vector, which

advantageously circumvents selectivity, toxicity, and inflammation issues associated with shRNAs and

lentiviruses[192,193]. In addition, we inserted an IRES-GFP after the dominant negative TRIP8b(1b-2)

spliceform to track infected cells. We named this approach AAV-(1b-2) and developed a negative control

vector without the TRIP8b(1b-2) spliceform, termed AAV-GFP, for comparison.

Using unilateral AAV-GFP and AAV-(1b-2) injections into the dorsal hippocampi of wildtype C57BL/6J mice, we were able to investigate how our gene therapy strategy impacted HCN channel expression and distribution. As expected, we found that HCN1, HCN2, and endogenous TRIP8b proteins were reduced significantly in the dHC of AAV-(1b-2) compared to AAV-GFP injected hemispheres via western blot (Figure 2B,C) and immunohistochemistry **(Figure 2D,E)**. In addition, injection of AAV-(1b-2) but not AAV-GFP depleted HCN channel expression in distal dendrites of dHC pyramidal cells, which has previously been shown to influence antidepressant-like behavior[137].

In addition, we performed whole cell patch clamp electrophysiology experiments on acutely sliced AAV-GFP and AAV-(1b-2) injected dorsal CA1 pyramidal cells. Similar to our protein analysis, we demonstrated a large reduction in the sag ratio **(Figure 2F,G)** and I_h amplitude **(Figure 2H,I)** in AAV-(1b-2) injected cells compared to AAV-GFP injected controls. Similar to previous manipulations that reduce I_h in this cell type[74,76], we confirmed an increase in the excitability of AAV-(1b-2) injected cells compared to AAV-GFP injected controls **(Figure 2J)**. Overall, this suggests that our novel gene therapy approach increases the excitability of the dHC through reduction of HCN channel protein.

AAV-(1b-2) targets HCN channels to lysosomes

Our biochemical and electrophysiological experiments have indicated that our novel gene therapy AAV-(1b-2) reduces HCN channel expression and current, though the mechanism of this downregulation remains unknown. Therefore, we performed electron microscopy (EM) of serial sections from AAV-GFP and AAV-(1b-2) injected dHCs to evaluate the subcellular localization of HCN channels in CA1 pyramidal cells **(Figure 3)**.

Similar to HCN1 localization in wild-type animals, HCN1 immunoreactivity in AAV-GFP injected dHCs was strongest along the dendritic trunks, especially within the stratum lacunosum moleculare (SLM) that primarily encompasses the distal dendrites of CA1 pyramidal cells. Consistent with biochemical findings, HCN1 particles at the plasma membrane was markedly reduced in AAV-1b2 injected dHCs. This loss of HCN1 immunoreactivity was especially apparent in the SLM. Interestingly, in AAV-(1b-2) injected dHCs we observed a dramatic increase in HCN1 immunoreactivity within endosomes that approximated lysosomes. This subcellular anatomy together with biochemical evidence of decreased protein levels

suggests that expression of the TRIP8b(1b-2) spliceform promotes endocytosis of HCN channels from the plasma membrane and redistribution to lysosomes for degradation.

AAV-(1b-2) in the dHC leads to an increase in active coping

As our AAV-(1b-2) gene therapy approach reduces I_h in the dHC, we next sought to determine whether this manipulation leads to increased active coping, similar to global *Trip8b*^{-/-}. We bilaterally injected AAV-GFP or AAV-(1b-2) into C57BL/6J mice, waited 4 weeks to ensure maximal protein expression in infected neurons, and then assayed these mice on our ACI behavioral battery **(Figure 4A)**. Though AAV-(1b-2) mice exhibited no differences in aggressiveness in the RIT, AAV-(1b-2) mice showed increased active coping and less passive coping in both trials of the SPBT and less passive coping in the rFST **(Figure 4B, C, D; Supplemental Figures 5, 6, 7 and Supplementary Tables 3 and 4)**. Combining all three behavioral tests into the ACI demonstrated that AAV-(1b-2) mice showed a more robust active coping response compared to AAV-GFP controls **(Figure 4E)**. As with the *Trip8b*^{-/-} mice, no differences in locomotor, anxiety-like, or memory-related behaviors were noted between AAV-(1b-2) and AAV-GFP injected mice **(Supplementary Figure 8)**. Overall, these results demonstrate that increased excitability of dHC pyramidal cells achieved through the reduction of HCN channels leads to active coping **(Figure 4F)**.

Discussion

To our knowledge, this is the first time that any voltage-gated ion channel has been implicated in coping style and is the first demonstration that increased intrinsic excitability in the dHC facilitates active coping behaviors. In addition, this work suggests that enhancing active coping responses to acute stressors might explain why loss of HCN channels in the dHC but not vHC leads to antidepressant-like behaviors. Additionally, we describe a novel viral-mediated approach for reducing neuronal HCN channels that uniquely circumvents issues with target specificity and inflammation that can be seen with other knockdown approaches.   Overall, these data indicate that reducing dHC HCN channels could hold promise as therapy for patients with severe and intractable diseases exacerbated by inadequate coping, such as MDD.

Loss of dHC HCN channels promotes active coping and diminishes passive coping

Numerous studies have implicated HCN channels in depression-like behavior in rodents[74,76,137,180]. In particular, loss of HCN1, HCN2, or TRIP8b in the dorsal CA1 of the hippocampus promotes antidepressant-like behavior[74,137]. Similarly, a recent study demonstrated an increase in HCN1 and in the dorsal but not ventral CA1 of rats that have undergone Chronic Mild Stress (CMS) with changes in anxiety-like, depression-like, and anhedonia behaviors. Further, selective loss of HCN1 in the dorsal but not ventral CA1 is able to protect rats from developing these behaviors after CMS[76,180]. Thus, it seems evident that HCN and TRIP8b are potential targets for new antidepressant treatments.

One striking feature of HCN's role in these behaviors is the dependence on dorsal but not ventral CA1 pyramidal cells. Numerous studies have demonstrated distinctions between the two poles of the hippocampus in terms of gene expression, limbic system connectivity, and stress-related behaviors[46]. Along these lines, most reward- and anxiety-related behaviors seem to depend on vHC function[181-183,194,195], with the dHC mediating some of the cognitive and memory deficits seen with maladaptation to chronic stress[29,51]. In light of these differences, we reasoned that the changes in antidepressant-like behavior that have previously been associated with loss of dHC I_h could reflect an overall increase in active coping.

In line with this reasoning, we demonstrated that *Trip8b*^{-/-} mice, which show a profound reduction in dHC I_h[74], preferentially engage in active coping with presentation of acutely stressful situations, as seen in the first day of the 2w-AA **(Figure 1)**. The 2w-AA is a direct task of active coping, where choosing this style of coping over freezing leads to the adaptive response of avoiding a shock. However, this task is rather unimodal and favors one style of coping *a priori*. Therefore, we expanded our description of *Trip8b*^{-/-} mice's coping style to more complex tasks. The SPBT is a neutral task in terms of coping, as either avoidant freezing (passive coping) or burying (active coping) are equally adaptive responses to the stressor. The persistent preference for active coping and decreased passive coping in this task demonstrates that *Trip8b*^{-/-} mice do not simply learn to actively cope more quickly but instead choose this strategy given equal options. In contrast, the rFST is a task that favors passive coping, as immobility leads to floating and preservation of energy[173]. *Trip8b*^{-/-} mice display decreased passive coping in this task, again demonstrating that their preference for active coping is not simply a matter of more quickly

adapting to a situation, which would have been reflected in more immobility time than wildtype controls on the subsequent days of the rFST. Finally, the RIT assessed coping style in a more ethnologically relevant, in-cage assay. Once again, *Trip8b^{-/-}* mice showed a preference for active coping by increased aggression without showing signs of pathologically violent aggression. All in all, these findings together support the assertion that *Trip8b^{-/-}* mice prefer active coping when challenged with an acute stressor. Of note, while many studies have evaluated neurotransmitter- and GPCR-related mechanisms[109], this is the first study to explore the role of voltage-gated ion channels in coping.

TRIP8b facilitates HCN channel expression and proper localization in many brain regions, therefore examining *Trip8b^{-/-}* mice precludes us from ruling out developmental sequelae or effects facilitated through other brain regions. To circumvent these issues, we developed a novel gene therapy approach to overexpress a dominant negative TRIP8b isoform, TRIP8b(1b-2), that led to robust downregulation of HCN channels **(Figure 2)**. While the majority of TRIP8b isoforms upregulate HCN channels and increase surface trafficking, TRIP8b(1b-2) is unique in its ability to reduce HCN expression[80]. *In vivo,* loss of all TRIP8b isoforms still leads to a net loss of HCN channel surface trafficking as TRIP8b(1b-2) is endogenously expressed at much lower levels than the other TRIP8b isoforms[88]. We further showed that overexpression of TRIP8b(1b-2) leads to reduced I_h through a mechanism of redistribution of the ch   annels to lysosomal compartments for degradation **(Figure 3)**. Although a prior study found no effect of lentiviral mediated overexpression of TRIP8b(1b-2) in CA1 pyramidal neurons[89], our use of a distinct virus (AAV vs lentivirus), promoter (synapsin vs CaMKII), and expressed protein (untagged TRIP8b(1b-2) vs a GFP-fusion protein) likely explains success in reducing HCN channel function in our present study. Importantly, our experiments with AAV-(1b-2) confirmed our hypothesis that loss of dHC HCN channels leads to more active coping **(Figure 4)** and highlighted the importance of this region for regulating coping style.

Therapeutic potential of AAV-mediated suppression of neuronal HCN channel function

Importantly for therapeutic development, pharmacological antagonism of HCN channels to treat neuropsychiatric disease may lead to off-target effects, as HCN channel are expressed in the heart and essential to normal cardiac function[196]. Fortunately, TRIP8b lacks cardiac expression[74,80,197], and thus

represents a novel target for disrupting HCN channel function without inducing arrythmias[198]. While other viral transduction approaches have been effective at reducing HCN channels, we believe that the approach taken here with AAV-(1b-2) is optimal for future translational development. First, TRIP8b does not interact with other voltage-gated ion channels, which should circumvent off-target effects that commonly occur with shRNA approaches. Second, shRNA strategies require the use of RNA polymerase III compatible promoters, making cell-type specific promoters unfeasible. Using our approach, TRIP8b(1b-2) can be restricted to a particular subset of cells through a suitable promoter. This is particularly relevant because HCN channels are also expressed in oligodendrocytes[89,167], thus non-selective downregulation of HCN channels could have unwanted effects on oligodendrocyte function. Finally, adult hippocampal HCN channels are primarily comprised of both HCN1 and HCN2[167]. Whereas an shRNA-mediated strategy can target a single subunit, AAV-(1b-2) downregulates both HCN1 and HCN2. Dominant negative suppression of HCN channels thus avoids the potential complication that HCN2 could compensate for loss of HCN1 mediated by shRNA knockdown.

Interpreting HCN Channels' role in psychiatric disease

As mentioned, previous studies have tied HCN channel activity in the dHC to depression-like behavior, but our current study further defines this role as influencing coping with acute psychosocial stressors. While active coping has been linked to better outcomes for patients with Major Depressive Disorder (MDD)[108,110,111], it has also been reported to benefit many other psychiatric diseases, including Bipolar Disorder[112], Schizophrenia[114], Substance Abuse and Alcoholism[115,116], and PTSD[113]. It is notable that active coping has also been shown to benefit patients with non-psychiatric disorders, including chronic illness[117], HIV[120], diabetes[119], post-stroke recovery[121], and cardiovascular disease[118]. By identifying HCN channel function in the dHC as a determinant of coping strategy, we reason that it could impact the course of disease in many chronic illnesses.

As increasing emphasis has been put on understanding neuropsychiatric disease susceptibility and resilience, researchers have demonstrated multiple differing electrophysiological, genetic, and epigenetic phenotypes that predispose rodents to being susceptible or resilient to developing certain maladaptive behaviors that are described as being similar to human neuropsychiatric diseases

(anhedonia, fear-extinction deficits, decreased social interactions, etc)[184]. Though multiple molecular

mechanisms have been ascribed to whether these disease-like behaviors manifest in rodents after stress,

few have associated protective or maladaptive behaviors with this progression to pathological behavior.

Two studies, however, have demonstrated evidence that similar associations between active coping in

rodents may be similar to humans: First, rats that displayed more defensive aggressive postures and had

longer latencies to submissive postures during social defeat had fewer deficits in social interaction and

less pathological neuroendocrine responses to stress[185]. Second, rat strains that have shown multiple

differences in behavior on assays specific to coping style showed marked differences in social interaction

behavior as adults when undergoing social defeat as adolescence. In particular, the strain with more

active coping showed fewer deficits in social interaction with both a dominant male and female compared

to the strain with passive coping tendencies[186]. Though few in number, these studies begin to

demonstrate that rodents also engage in stress-mitigating behaviors that lead to protection against

developing maladaptive behaviors, similar to humans.

In light of the broad clinical utility of increasing active coping, if mechanisms that influence coping

behavior in mice are shared by humans, HCN channels may be a novel therapeutic target to benefit

patients with a multitude of diseases in which active coping has been found to be beneficial.
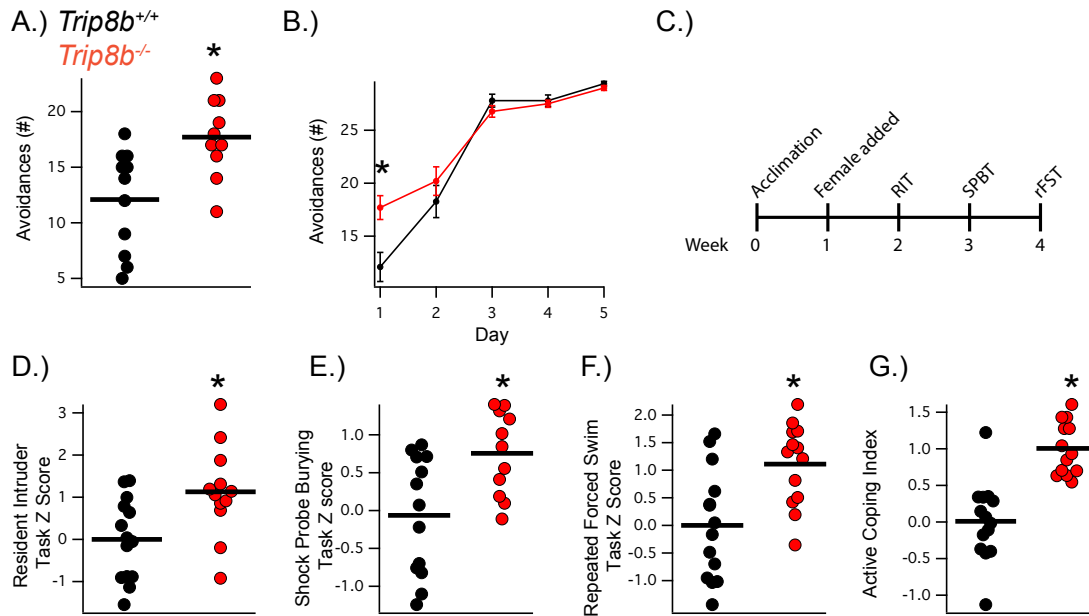
Figure 1: *Trip8b*^{-/-} mice display enhanced active coping. A) *Trip8b*^{-/-} mice show increased active coping through increased avoidances (t_{19} = 3.113, $p < 0.01$, n = 11,10) on the first day of the 2w-AA with **B)** similar learning of the 2w-AA compared to *Trip8b*^{+/+}. **C)** Timeline of ACI behavioral testing. **D)** *Trip8b*^{-/-} mice display more active coping on the SPBT (t_{22} = 2.914, $p < 0.01$, n = 13, 11), **E)** rFST (t_{25} = 3.256, $p < 0.01$, n =14, 13), and **F)** RIT (t_{24} = 2.819, $p < 0.01$, n = 14, 12). **G)** *Trip8b*^{-/-} mice display greater overall active coping on the ACI (t_{25} = 5.604, $p < 0.0001$, n = 14, 13).
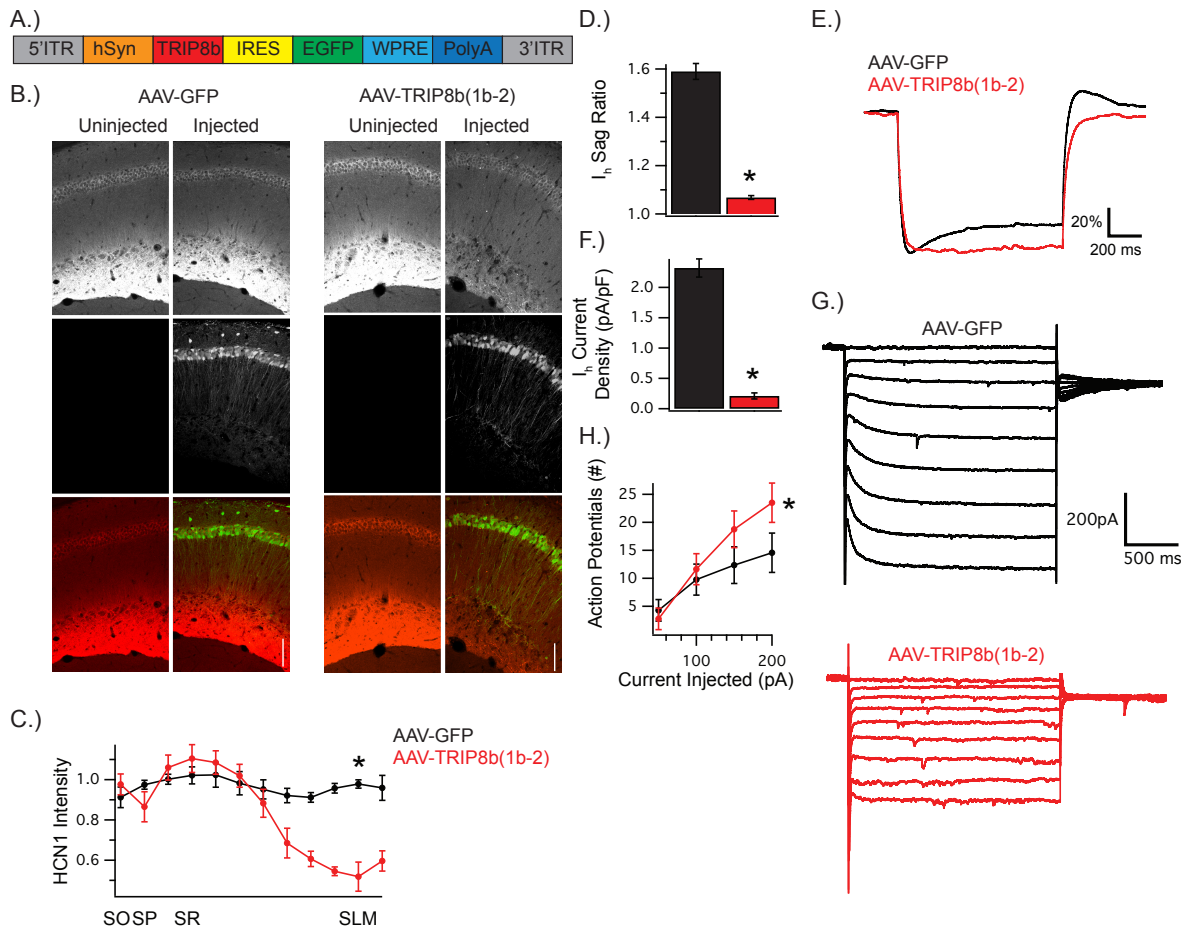
Figure 2: AAV-(1b-2) reduces HCN channels in the dHC and enhances active coping. A) Schematic of AAV-(1b-2). TRIP8b(1b-2) is driven by a human synapsin (hSyn) promoter with IRES-GFP to track infected cells. AAV-GFP expresses GFP through hSyn and lacks TRIP8b(1b-2). **B, C)** HCN1 is reduced in dCA1 cells, especially at the distal dendrites. **D,E)** dCA1 cells show reduced sag ratios and **F,G)** I_h amplitude, and **H)** increased excitability. **I)** AAV-(1b-2) mice show enhanced active coping compared to AAV-GFP mice on the ACI ($t_{11} = 4.586$, $p < 0.001$, n = 7, 6).
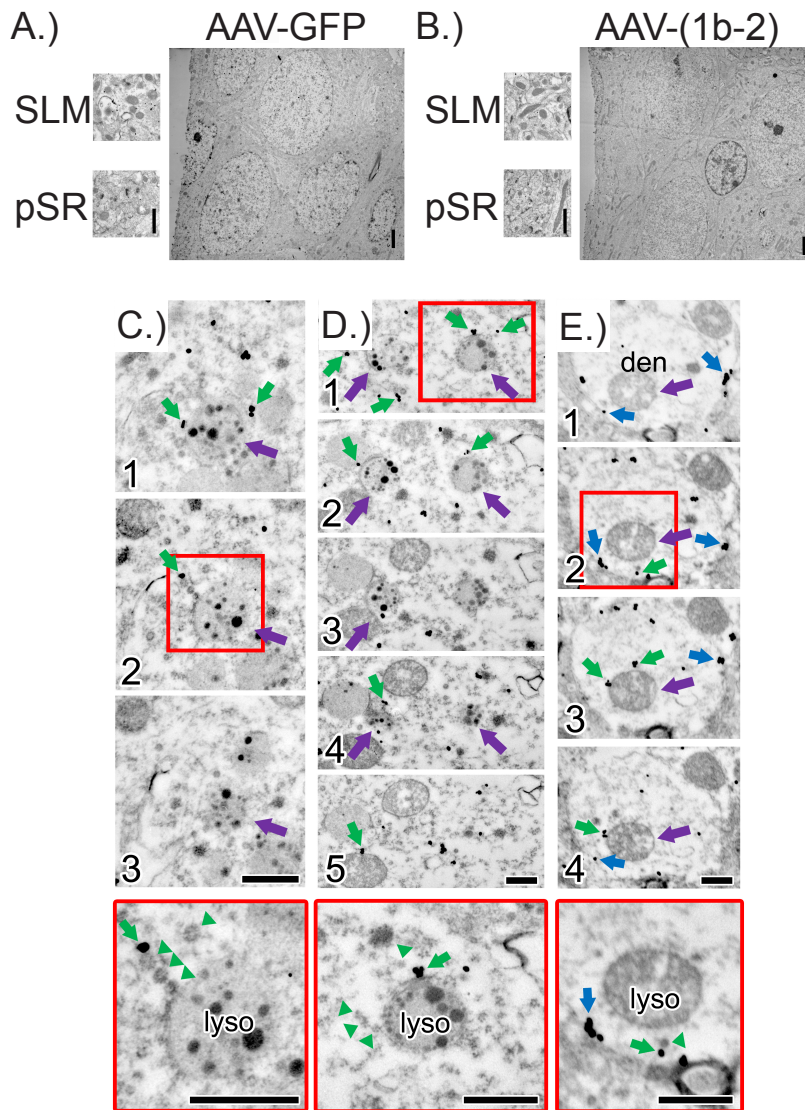
Figure 3: AAV-1b2 re-localizes HCN channels to lysosomes for degradation. A,B) Electron micrographs of dHC injected with either AAV-GFP or AAV-(1b-2). **C)** Electron micrographs of serial sections (1, 2, 3) through a lysosome near the soma (purple arrow) in close proximity to endosomes immunoreactive for HCN1 (immunogold particles; green arrows). Red box denotes approximate region shown at higher magnification in bottom panel. Note the ordered manner in which the endosomes are lined up near the lysosome (green arrowheads). **D)** Electron micrographs of serial sections (1, 2, 3, 4, 5) through two lysosomes near the soma (purple arrows) with endosomes immunoreactive for HCN1 (green arrows) nearby. **E)** Electron micrographs of serial sections (1, 2, 3, 4) through a spiny dendrite in the stratum lacunosum-moleculare. Despite a dramatic HCN1 decrease in the distal dendrites and the majority of HCN1 immunoreactivity localized to endosomes (green arrows) near lysosomes (purple arrows), occasional cell membrane-bound HCN1 was noted (blue arrows). Higher magnification images reveal orderly queuing near the lysosome (green arrowheads). Scale bars = 500nm
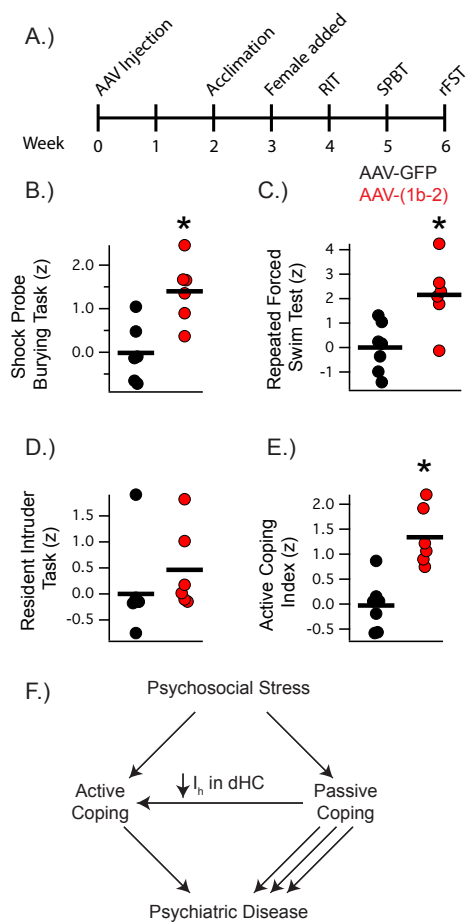
Figure 4: AAV-1b2 injection in the dHC leads to active coping. A) Timeline of viral injections and ACI behavioral assays. **B)** AAV-(1b-2) mice showed increased active coping in the SPBT (AAV-GFP: -0.01±0.27, AAV-(1b-2): 1.39±0.29, t_{10} = 3.510, p < 0.01, n = 6, 6). **C)** AAV-(1b-2) mice showed decreased average immobility time across the three rFST trials (AAV-GFP: 172.38±10.48s, AAV-(1b-2): 112.61±16.00s t_{11} = 3.212, p < 0.01, n= 7, 6). **D)** AAV-(1b-2) mice did not demonstrate statistically different z-scores from AAV-GFP mice (AAV-GFP: 0±0.40, AAV-(1b-2): 0.46±0.32, t_{10} = 0.8968, p > 0.05). **E)** AAV-(1b-2) mice show enhanced active coping compared to AAV-GFP mice on the ACI (t_{11} = 4.586, p < 0.001, n = 7, 6). **F)** Working model of how HCN Channel loss in the dorsal hippocampus leads to increased active coping. When an individual encounters acute psychosocial stress, they cope passively or actively. Those with Active Coping styles tend to be more resistant to developing most neuropsychiatric disorders and tend to do better with treatment than those who employ Passive Coping styles. Reduction of HCN channels and HCN channel current (I_h) specifically in the dorsal hippocampus facilitates Active Coping strategies, and thus explains how an increase in intrinsic dorsal but not ventral hippocampus excitability may lead to antidepressant-like effects in rodents.
Supplementary Figures

A.) *Trip8b*$^{+/+}$
Trip8b$^{-/-}$

B.)
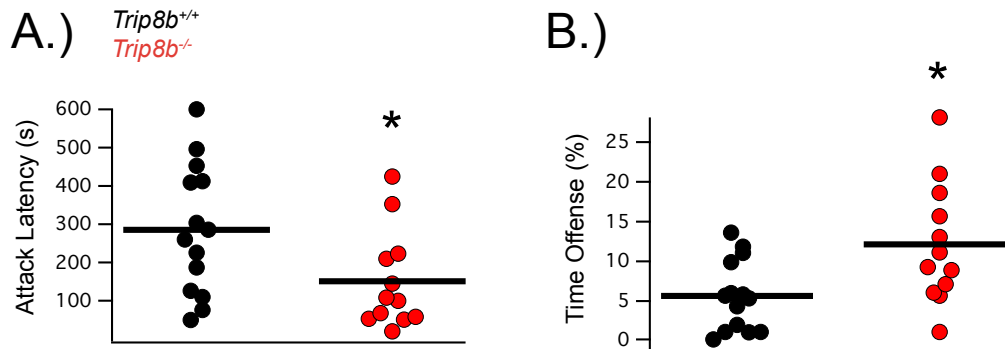
Supplementary Figure 1: *Trip8b*$^{-/-}$ **mice show increased active coping in the Resident Intruder Test (RIT).** (Related to Figure 1)
A) *Trip8b*$^{-/-}$ mice showed decreased attack latencies (*Trip8b*$^{+/+}$:285±45.24s, *Trip8b*$^{-/-}$: 150.91±37.01s, t_{24} = 2.248, $p < 0.05$) and **B)** increased time displaying offensive aggressive behavior (*Trip8b*$^{+/+}$:5.64±1.18%, *Trip8b*$^{-/-}$: 12.13±2.19%, t_{24} = 2.710, n= 14, 12, $p < 0.05$) compared to *Trip8b*$^{+/+}$.

Acquisition

Trip8b^{+/+}
Trip8b^{-/-}

Recall
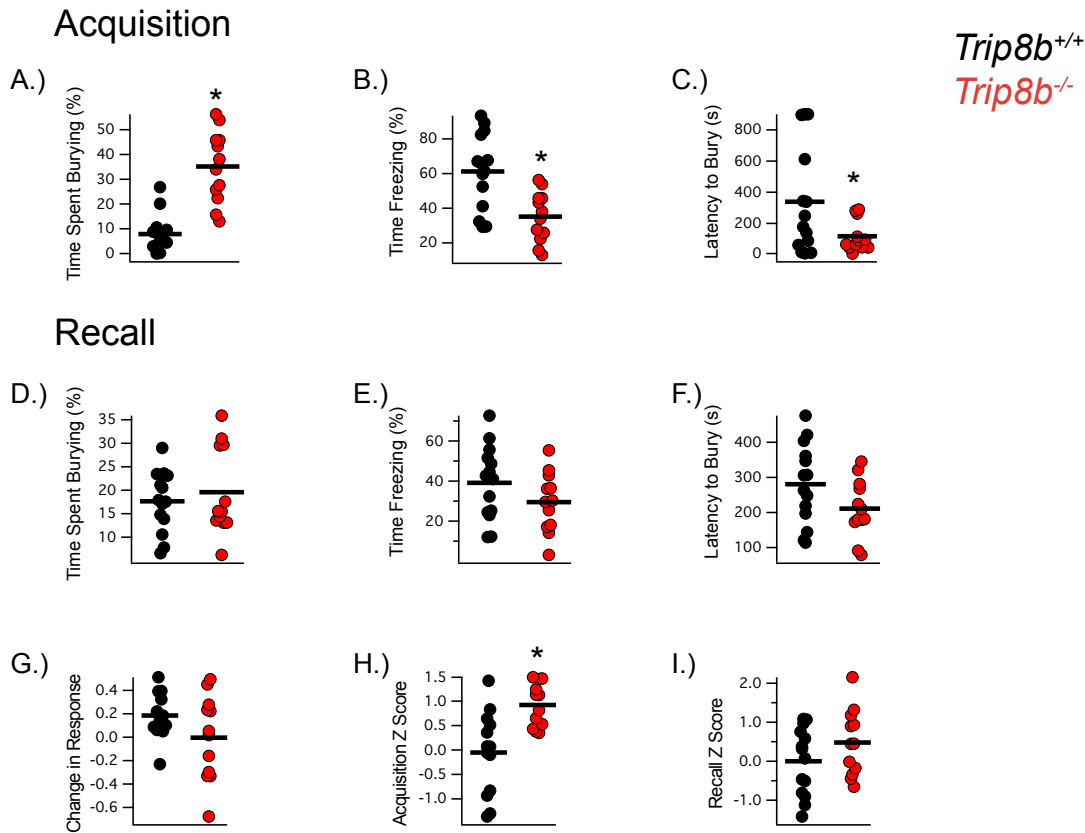
Supplementary Figure 2: *Trip8b^{-/-}* **mice show increased active and decreased passive coping in the Shock Probe Burying Task (SPBT).** (Related to Figure 1)

A) During the SPBT Acquisition Trial, the *Trip8b^{-/-}* mice showed increased time spent burying (*Trip8b^{+/+}*:7.85±2.19%, *Trip8b^{-/-}* : 14.31±2.04%, t_{24} = 2.155, p < 0.05, n = 14, 12), **B)** decreased time freezing (*Trip8b^{+/+}*:61.17±5.86%, *Trip8b^{-/-}* : 35.12±4.15%, t_{24} = 3.509, p < 0.01), **C)** and a decreased burying latency (*Trip8b^{+/+}*:339±92.2s, *Trip8b^{-/-}* : 117.75±29.03s, n = 14, 12 t_{24} = 2.139; p < 0.05) compared to *Trip8b^{+/+}* mice. **D)** On the SPBT Recall Trial, *Trip8b^{-/-}* mice did not show statistical differences in burying (*Trip8b^{+/+}*:17.63±1.72s, *Trip8b^{-/-}* : 19.58±2.69s, t_{24} = 0.6257, p = 0.54), **E)** freezing (*Trip8b^{+/+}*:39.09±4.89%, *Trip8b^{-/-}* : 29.48±4.28%,t_{24} = 1.454, p = 0.16), or **F)** burying latency (*Trip8b^{+/+}*:280.57±30.5s, *Trip8b^{-/-}* : 211.00±23.76s, t_{24} = 1.754, p = 0.09). **G)** To determine if mice had a difference in remembering the shock probe context, the Change In Response was measured by taking the total time spent freezing and burying in the Recall Trial, subtracting the total time freezing and burying in the Acquisition Trial, and dividing by the total freezing and burying during the Acquisition Trial. *Trip8b^{+/+}* and *Trip8b^{-/-}* mice had similar Changes in Response from the Acquisition trial (*Trip8b^{+/+}*:0.18±0.05, *Trip8b^{-/-}* : -0.00±0.1, t_{23} = 1.661; p > 0.05; n = 13, 12), suggesting that a difference memory was unlikely to influence behavior. **H)** Endpoints for the SPBT were z-score normalized based on the wildtype population statistics and averaged to give a final z-score for the Acquisition and Recall trials. *Trip8b^{-/-}* mice showed increased active coping during the SPBT Acquisition Trial (*Trip8b^{+/+}*:-0.05±0.23, *Trip8b^{-/-}* : 0.92±0.12,t_{23} = 3.251, p < 0.01, n= 12, 13) **I)** but no statistically significant increase in active coping behavior in the Recall Trial (*Trip8b^{+/+}*:0±0.23, *Trip8b^{-/-}* : 0.47±0.24,t_{24} = 1.426, p = 0.17, n = 14, 12)).
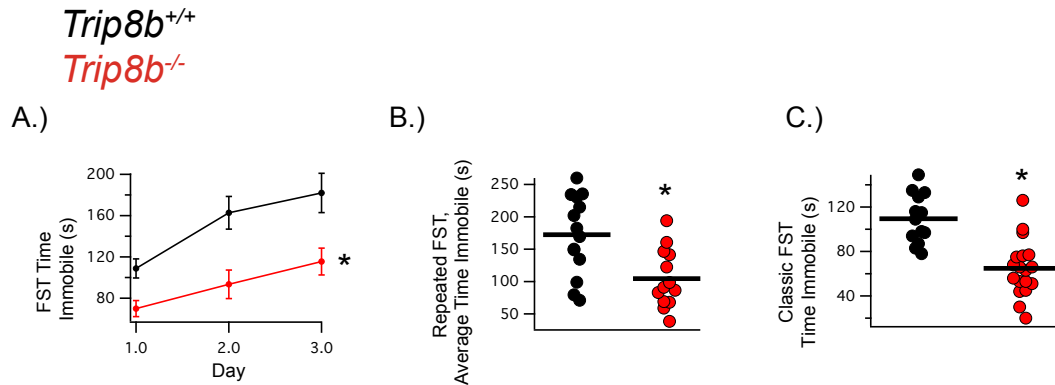
Supplementary Figure 3: *Trip8b*^{-/-} mice show decreased passive coping in the repeated Forced Swim Test (rFST). (Related to Figure 1)

A) *Trip8b*$^{+/+}$ and *Trip8b*$^{-/-}$ mice were both able to learn to increase their passive coping over the three trials (Repeated Measures Two-Way ANOVA; effect of trial $F(2,50) = 27.30$, $p < 0.0001$; effect of genotype $F(1,25) = 11.58$, $p < 0.01$; and no interaction, $p > 0.05$)). Sidhak's Test confirmed immobility differences between the first and third trial for *Trip8b*$^{+/+}$ ($p < 0.0001$) and *Trip8b*$^{-/-}$ mice ($p < 0.001$). **B)** *Trip8b*$^{-/-}$ mice showed decreased average immobility time across the three rFST trials ($t_{25} = 3.256$, $p < 0.01$, n = 14, 13). **C)** *Trip8b*$^{-/-}$ mice also showed decreased immobility ($t_{24} = 4.413$, $p < 0.001$, n = 13, 13) during the last 4 minutes of the first rFST trial, representing the common antidepressant screening test used in previous reports.
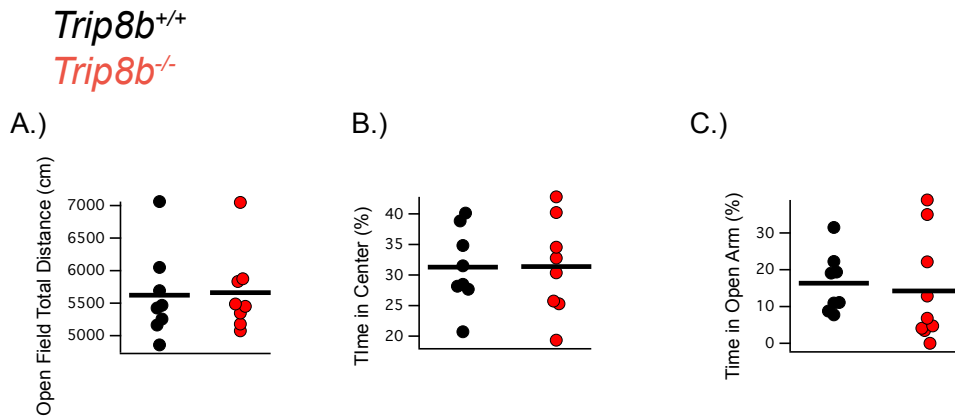
Supplementary Figure 4: *Trip8b^{-/-}* **mice perform similarly to** *Trip8b^{+/+}* **mice on tasks measuring memory, locomotion, or anxiety-like behavior.** (Related to Figure 1)
A) On the Open Field Test (OFT), *Trip8b^{+/+}* and *Trip8b^{-/-}* mice traveled similar distances in the arena (*Trip8b^{+/+}*:5621.29 ±240.91cm, *Trip8b^{-/-}* : 5661.81±221.57cm, t_{14} = 0.1238; p > 0.05). **B)** *Trip8b^{+/+}* and *Trip8b^{-/-}* mice also spent similar amounts of time in the center of the OFT arena (*Trip8b^{+/+}*:31.29±2.27%, *Trip8b^{-/-}* : 31.38±2.78%, t_{14} = 0.02502, p > 0.05, n = 8, 8) **C)** *Trip8b^{+/+}* and *Trip8b^{-/-}* mice spent similar amounts of time in the open arm of the Zero Maze (*Trip8b^{+/+}*:16.33±2.89%, *Trip8b^{-/-}* : 15.41±5.29%, t_{15} = 0.3636, p > 0.05, n= 8, 9). Note that our previous publication demonstrated that *Trip8b^{-/-}* mice show no differences from *Trip8b^{+/+}* on numerous hippocampus-dependent memory tasks[74].

A.)

B.)
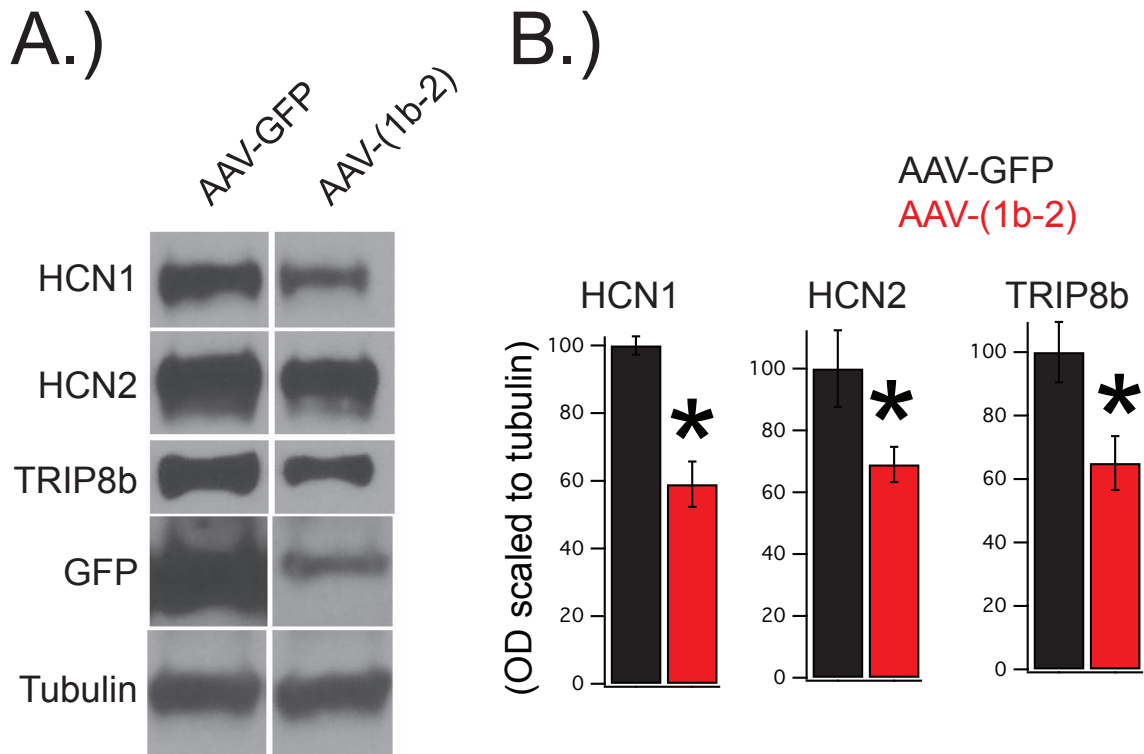
Supplementary Figure 5: AAV-(1b-2) injection leads to a reduction in HCN1, HCN2, and TRIP8b protein. (Related to Figure 2)
Wild type mice were bilaterally injected with either AAV-(1b-2) or AAV-GFP. Four weeks later the animals were deeply anesthetized and their hippocampi sub-dissected for western blot. **A.)** Representative images. **B.)** Quantification of the results from panel A.). Western blots from the hippocampus demonstrate a downregulation of HCN1 (AAV-GFP:$100\pm2.7\%$, AAV-(1b-2: $59\pm6.7\%$,n=9,12, t_{19}=4.93, p<0.01), HCN2 (AAV-GFP:$100\pm12.3\%$, AAV-(1b-2: $69\pm5.7\%$,n=8,11, t_{17}=2.45, p<0.05), and total TRIP8b (AAV-GFP:$100\pm9.5\%$, AAV-(1b-2: $65\pm8.5\%$,n=10,12, t_{20}=2.76, p<0.05) in the AAV-(1b-2) injected mice compared to the AAV-GFP controls.
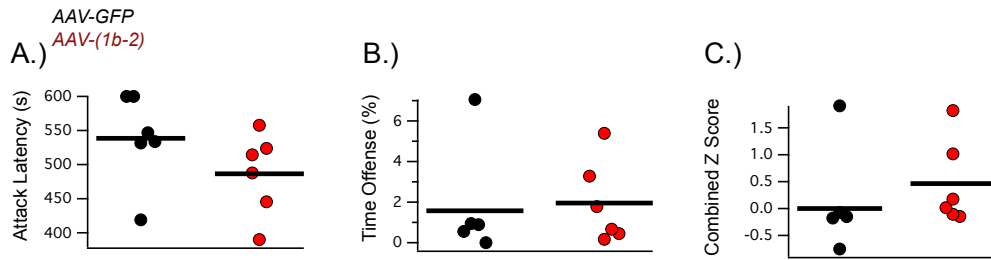
Supplementary Figure 6: AAV-(1b-2) mice did not show statistical differences from AAV-GFP mice on the Resident Intruder Test (RIT). (Related to Figure 4)
A) AAV-(1b-2) mice did not show a statistically significant difference in attack latency (AAV-GFP: 538.5±27.06s, AAV-(1b-2): 486.44±24.65s, t_{10} = 1.422, p > 0.05) or **B)** time displaying offensive aggression (AAV-GFP: 1.57±1.10%, AAV-(1b-2): 1.95±0.83% t_{10} = 0.2739, p > 0.05) compared to AAV-GFP mice.

Acquisition

AAV-GFP
AAV-TRIP8b(1b-2)

Recall
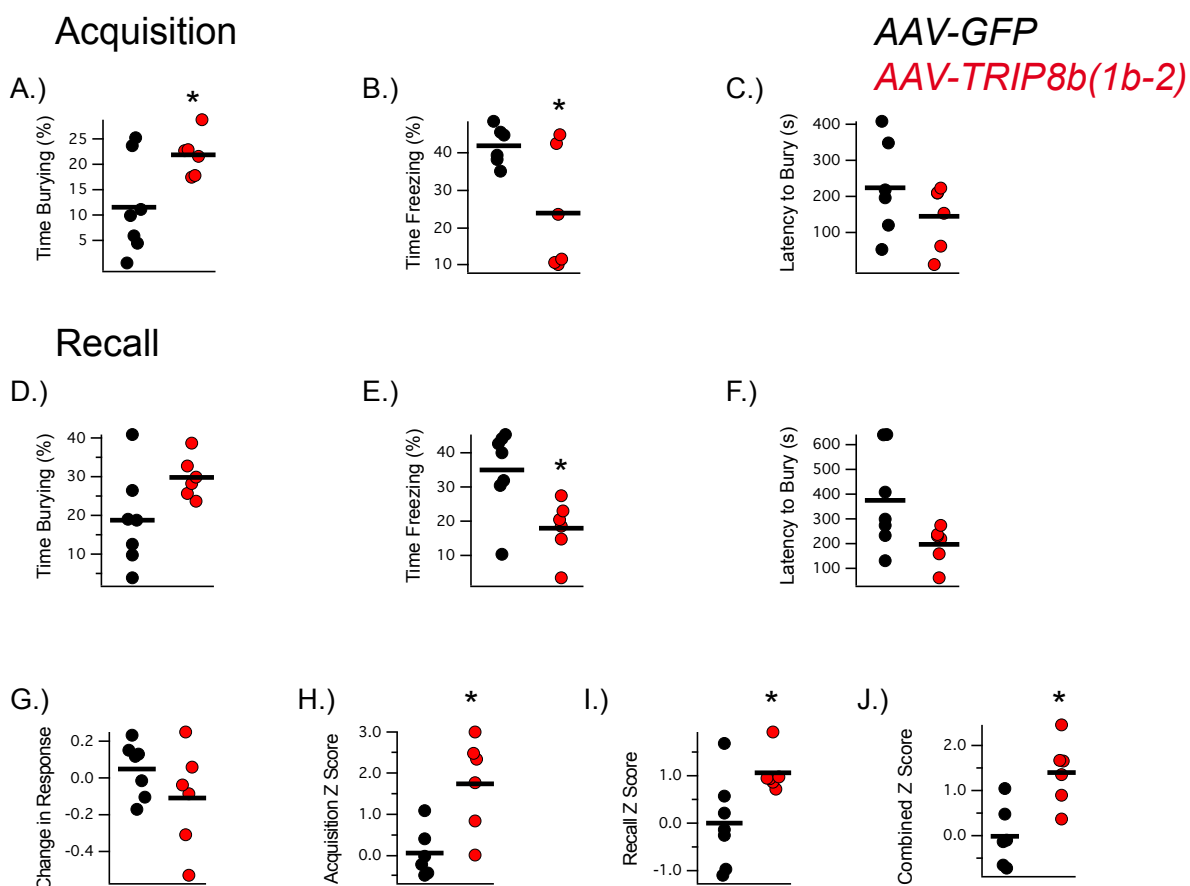
Supplementary Figure 7: AAV-(1b-2) mice show increased active and decreased passive coping in the Shock Probe Burying Task (SPBT). (Related to Figure 4)

A) Mice were bilaterally injected with AAV-GFP or AAV-(1b-2) and tested for active coping behavior at peak viral expression 4 weeks after surgery. During the SPBT Acquisition Trial, AAV-(1b-2) mice spent more time burying (AAV-GFP: 11.53±3.58%, AAV-(1b-2): 21.85±1.69%, t_{11} = 2.457, p < 0.05, n = 7, 6). **B)** less time freezing (AAV-GFP: 41.85±2.06%, AAV-(1b-2): 23.98±6.53%, t_{10} = 2.609, p < 0.05, n= 6, 6), **C)** and no statistically significant difference in latency to bury (AAV-GFP: 223.83±54.8s, AAV-(1b-2): 144.66±36.2s, t_{10} = 1.205, p > 0.05) compared to AAV-GFP mice. **D)** On the SPBT Recall Trial, AAV-(1b-2) displayed a trend towards more burying (AAV-GFP: 18.76±4.6%, AAV-(1b-2): 29.81±2.19%, t_{11} = 2.049, p = 0.06), **E)** a significant decrease in time spent freezing (AAV-GFP: 34.96±4.66%, AAV-(1b-2): 17.94±3.37%, t_{11} = 2.865, p < 0.05), **F)** and a trend towards a decreased latency to burying (AAV-GFP: 375.14±75.23s, AAV-(1b-2): 197.16±31.02s, t_{11} = 2.055, n=7,6, p = 0.06) compared to AAV-GFP mice. **G)** The Change in Response from the Acquisition to Recall Trial was similar between the two groups (AAV-GFP: 0.04±0.05, AAV-(1b-2): -0.10±0.11, t_{11} = 1.315, p > 0.05). **H)** Endpoints for the SPBT were z-score normalized based on the AAV-GFP population statistics and averaged to give a final z-score for the Acquisition and Recall trials. AAV-1b2 mice showed increased active coping during the Acquisition trial (AAV-GFP: 0.06±0.24, AAV-(1b-2): 1.73±0.45, t_{10} = 3.238, p < 0.01, n= 6, 6) and **I)** Recall Trials (AAV-GFP: 0.00±0.35, AAV-(1b-2): 1.06±0.17, t_{11} = 2.508, p < 0.05, n=7, 6) compared to AAV-GFP mice.
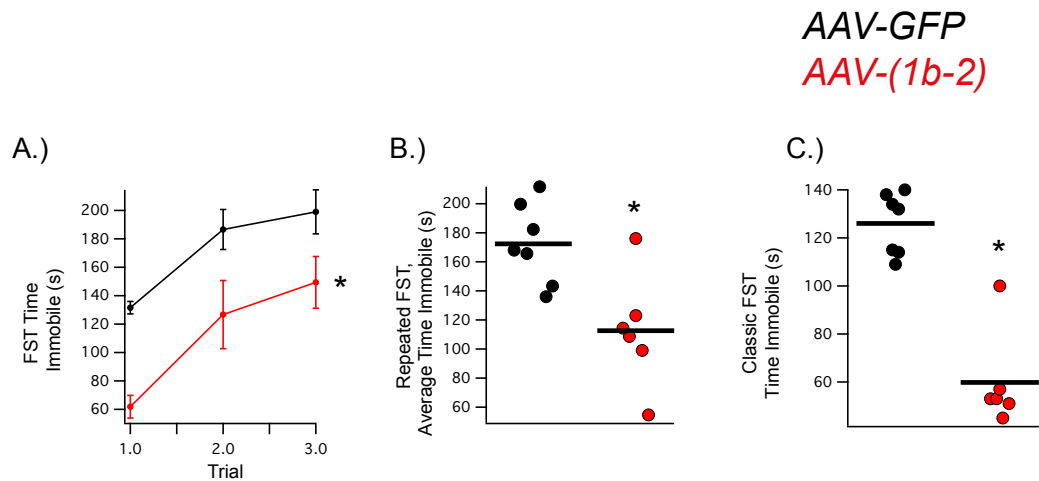
Supplementary Figure 8: AAV-(1b-2) mice show decreased passive coping in the repeated Forced Swim Test (rFST). (Related to Figure 4)
 A) AAV-GFP and AAV-(1b-2) mice were both able to learn to increase their passive coping over the three trials (Repeated Measures Two-Way ANOVA; effect of trial $F_{(2,22)} = 41.31$, $p < 0.0001$; effect of genotype $F_{(1,11)} = 10.32$, $p < 0.01$; and no interaction, $p > 0.05$; n= 7, 6)). Sidhak's Test confirmed immobility differences between the first and third trial for AAV-GFP ($p < 0.0001$) and AAV-(1b-2) ($p < 0.001$). **B)** AAV-(1b-2) mice showed decreased average immobility time across the three rFST trials (AAV-GFP: 172.38 ± 10.48s, AAV-(1b-2): 112.61 ± 16.00s $t_{11} = 3.212$, $p < 0.01$, n= 7, 6). **C)** AAV-(1b-2) mice also showed decreased immobility (AAV-GFP: 126.00 ± 4.86s, AAV-(1b-2): 59.83 ± 8.19s $t_{11} = 2.565$, $p < 0.05$, n= 7, 6) during the last 4 minutes of the first rFST trial, representing the common antidepressant screening test used in previous reports.
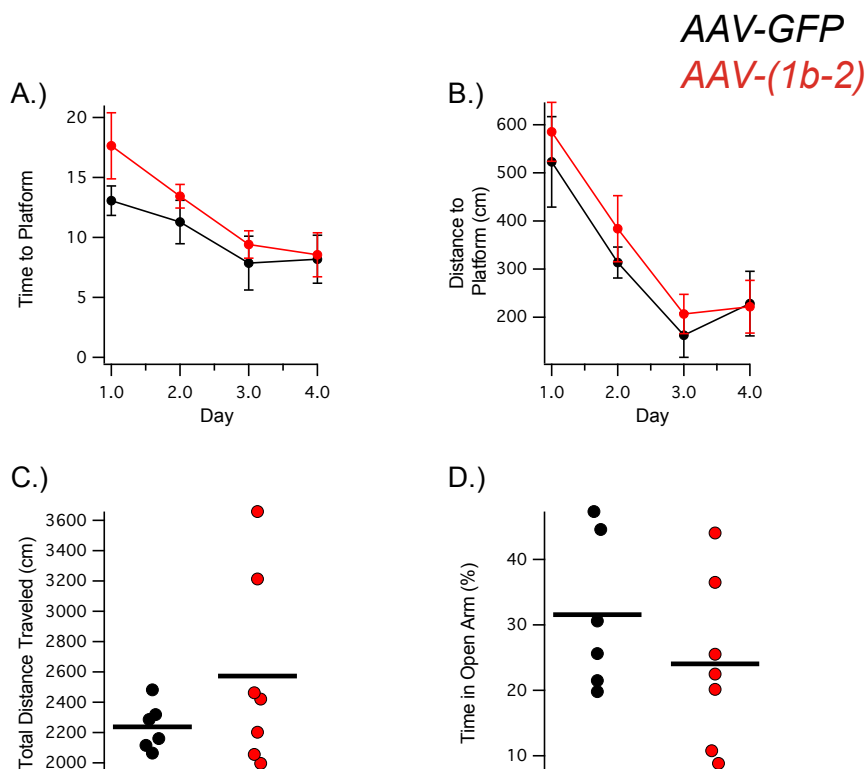
Supplementary Figure 9: AAV-(1b-2) mice perform similarly to AAV-GFP mice on tasks measuring memory, locomotion, or anxiety-like behavior (Related to Figure 4)
A) In the Morris Water Maze (MWM) hidden platform trials, Repeated Measures Two-Way ANOVA revealed an effect by trial for latency to reach the hidden platform but no effect for injection condition nor an interaction between trial x injection condition ($F_{Trial}(3,3) = 9.382$, $p = 0.0001$; $F_{Injection}(1,11) = 1.415$, $p > 0.05$; $F_{Interaction}(3,33) = 0.6612$, $p > 0.05$). **B)** Repeated Measures Two-Way ANOVA revealed an effect of trial for distance traveled to the hidden platform but no effects for injection condition or interaction ($F_{Trial}(3,33) = 16.89$, $p < 0.0001$; $F_{Injection}(1,11) = 0.7347$, $p > 0.05$; $F_{Interaction}(3,33) = 0.1822$, $p > 0.05$). During MWM probe trial, Two-way ANOVA yield a significant effect for Quadrant but not for Injection Condition nor an Interaction ($F_{Quadrant}(3,44) = 51.60$, $p < 0.0001$, $F_{Injection}(1,44) = 8.373 \times 10^{-8}$, $p > 0.05$, $F_{Interaction}(3,44) = 1.272$, $p > 0.05$).**C)** In the Open Field Test, AAV-(1b-2) and AAV-GFP mice traveled similar distances (AAV-GFP: 2237 ± 63.11cm, AAV-(1b-2): 2572 ± 237.16cm, n=6,7, t_{11}=-1.267, $p > 0.05$) and spent similar amounts of time in the center of the arena (AAV-GFP: $14.84\pm3.16\%$, AAV-(1b-2): $12.74\pm2.07\%$, n=6,7, t_{11}=-0.57, $p > 0.05$). **D)** AAV-GFP and AAV-(1b-2) mice spent similar amounts of time in the open arms of the Zero Maze (AAV-GFP: $31.55\pm4.80\%$, AAV-(1b-2): $24.02\pm4.83\%$, n=6,7, t_{11}=1.09, $p > 0.05$).

Supplementary Tables

Offensive Aggressive Behavior

	Lateral Threat	Upright	Clinch/Bite	Keep Down	Chase
Trip8b [+/+]	1.1 (0.4)	0.8 (0.3)	1.6 (0.4)	1.7 (0.4)	0.5 (0.2)
Trip8b [-/-]	3.3 (1.0)	0.9 (0.3)	3.7 (0.8)	3.2 (0.8)	1.0 (0.4)

Social Behavior

	Social Explore	AG Sniff	Social Groom	Mount
Trip8b [+/+]	19.6 (1.8)	9.1 (1.2)	7.0 (1.6)	0.2 (0.2)
Trip8b [-/-]	13.4 (1.7)	8.1 (1.8)	7.4 (2.2)	0.2 (0.1)

Exploratory Behavior

	Sniff	Rearing	Cage Exploration
Trip8b [+/+]	15.3 (1.6)	3.8 (0.9)	26.8 (3.2)
Trip8b [-/-]	10.6 (1.3)	4.5 (1.0)	30.2 (3.8)

Defensive/Submissive Behaviors

	On Back	Submissive Freeze	Being Groomed	Defensive Upright	Flee	Defensive Sideways
Trip8b [+/+]	0 (0)	0 (0)	0.9 (0.3)	0 (0)	1.3 (0.5)	0 (0)
Trip8b [-/-]	0 (0)	0 (0)	0.3 (0.2)	0 (0)	0.8 (0.3)	0 (0)

Other Behaviors

	Inactivity/ Rest	Groom	Digging
Trip8b [+/+]	4.8 (1.3)	3.3 (0.4)	2.3 (0.9)
Trip8b [-/-]	3.3 (1.0)	4.8 (1.0)	4.2 (1.7)

Behaviors by group

	Offensive Behavior	Social Behavior	Exploratory Behavior	Defensive/ Submissive Behaviors	Other Behaviors
Trip8b [+/+]	5.6 (1.2)	35.9 (3.9)	45.9 (3.0)	2.2 (0.7)	10.4 (1.0)
Trip8b [-/-]	12.1 (2.2)	29.1 (5.2)	45.3 (4.4)	1.2 (0.5)	12.3 (1.5)

Supplementary Table 1: Descriptive statistics for behaviors observed in the Resident Intruder Test for *Trip8b*^{+/+} and *Trip8b*^{-/-} animals (Related to Figure 1)
Values displayed represent percent of total time with standard error of the mean shown in parentheses.

Shock Probe Burying Test - Acquisition

	Burying	Freezing	Ambulation	Prod Exploring	Grooming	Rearing
Trip8b [+/+]	7.9 (2.4)	63.4 (6.4)	20.4 (4.4)	5.4 (0.6)	1.4 (0.5)	1.7 (0.6)
Trip8b [-/-]	15.3 (2.0)	35.1 (4.2)	35.9 (3.3)	6.9 (0.8)	4.9 (1.8)	1.9 (0.6)

Shock Probe Burying Test - Recall

	Burying	Freezing	Ambulation	Prod Exploring	Grooming	Rearing
Trip8b [+/+]	17.6 (1.8)	39.1 (5.3)	30.1 (2.8)	6.9 (0.7)	2.6 (0.7)	3.7 (1.0)
Trip8b [-/-]	19.6 (2.7)	29.5 (4.3)	33.9 (3.1)	7.1 (0.9)	5.7 (2.3)	4.2 (1.1)

Supplementary Table 2 Descriptive statistics for behaviors observed in the Shock Probe Burying Test for *Trip8b*^{+/+} and *Trip8b*^{-/-} animals (Related to Figure 1)
Values displayed represent percent of total time with standard error of the mean shown in parentheses.

Offensive Aggressive Behavior

	Lateral Threat	Upright	Clinch/Bite	Keep Down	Chase
AAV-GFP	0.2 (0.2)	0.3 (0.2)	0.6 (0.4)	0.2 (0.2)	0.2 (0.2)
AAV-(1b-2)	0.6 (0.4)	0.2 (0.1)	1.0 (0.3)	0.1 (0.1)	0.1 (0.0)

Social Behavior

	Social Explore	AG Sniff	Social Groom	Mount
AAV-GFP	21.1 (1.7)	9.0 (1.4)	14.5 (2.5)	0 (0)
AAV-(1b-2)	20.9 (2.1)	7.8 (2.0)	11.8 (1.2)	0 (0)

Exploratory Behavior

	Sniff	Rearing	Cage Explore
AAV-GFP	10.8 (1.9)	5.8 (1.3)	22.9 (3.9)
AAV-(1b-2)	11.8 (3.5)	7.0 (2.8)	24.2 (2.9)

Defensive/Submissive Behaviors

	On Back	Submissive Freeze	Being Groomed	Defensive Upright	Flee	Defensive Sideways
AAV-GFP	0.1 (0.1)	2.3 (1.2)	0.6 (0.3)	0.4 (0.3)	1.2 (0.5)	0.5 (0.2)
AAV-(1b-2)	0.1 (0.1)	1.5 (0.4)	1.1 (0.6)	0.5 (0.3)	1.3 (0.5)	0.6 (0.3)

Other Behaviors

	Inactivity/ Rest	Groom	Digging
AAV-GFP	2.7 (1.0)	3.0 (1.2)	3.7 (2.3)
AAV-(1b-2)	3.0 (0.9)	4.1 (1.5)	2.3 (0.6)

Behaviors by group

	Offensive Behavior	Social Behavior	Exploratory Behavior	Defensive/ Submissive Behaviors	Other Behaviors
AAV-GFP	1.6 (1.1)	44.6 (3.3)	39.5 (4.6)	5.0 (2.2)	9.3 (2.0)
AAV-(1b-2)	2.0 (1.0)	40.6 (3.3)	42.9 (3.8)	5.1 (1.6)	9.5 (2.1)

Supplementary Table 3: Descriptive statistics for behaviors observed in the Resident Intruder Test for AAV-GFP and AAV-(1b-2) treated animals (Related to Figure 4)
Values displayed represent percent of total time with standard error of the mean shown in parentheses.

Shock Probe Burying Test - Acquisition

	Burying	Freezing	Ambulation	Prod Exploring	Grooming	Rearing
AAV-GFP	13.4 (3.6)	41.9 (2.1)	30.6 (3.3)	7.3 (0.7)	3.2 (1.0)	3.4 (0.6)
AAV-(1b-2)	21.9 (1.7)	24.0 (6.5)	36.7 (4.6)	8.4 (1.5)	1.8 (0.9)	3.4 (1.2)

Shock Probe Burying Test - Recall

	Burying	Freezing	Ambulation	Prod Exploring	Grooming	Rearing
AAV-GFP	18.8 (4.6)	35.0 (4.7)	29.2 (1.6)	6.6 (1.0)	5.5 (1.1)	4.9 (1.1)
AAV-(1b-2)	29.8 (2.2)	17.9 (3.4)	34.4 (3.2)	6.7 (1.0)	4.5 (1.8)	5.4 (1.3)

Supplementary Table 4: Descriptive statistics for behaviors observed in the Shock Probe Burying Test for AAV-GFP and AAV-(1b-2) treated animals (Related to Figure 4)
Values displayed represent percent of total time with standard error of the mean shown in parentheses.

CHAPTER 4

HCN2 influences metabolism and feeding

Abstract

Hyperpolarization-activated Cyclic Nucleotide-gated (HCN) channels are important regulators of excitability in neural, cardiac, and other pacemaking cells, which are often altered in disease. In mice, loss of HCN2 specifically leads to cardiac dysrhythmias, persistent spike-wave discharges similar to absence epilepsy, ataxia, tremor, reduced neuropathic and inflammatory pain, antidepressant-like behavior, infertility, and severely restricted growth. While many of these phenotypes have putative tissue-specific mechanisms, the cause of the restricted growth in HCN2 knockout animals remains a mystery. Here, we characterize a novel, 3kb insertion mutation of HCN2 in the Tremor and Reduced Lifespan 2 (TRLS/2J) mouse that leads to complete loss of HCN2 protein, and we show that this mutation causes many phenotypes similar to other HCN2 ablation mice. We then demonstrate that while TRLS/2J mice have low blood glucose levels and impaired growth, dysfunction in hormonal secretion from the pancreas, pituitary, and thyroid are unlikely to lead to this phenotype. Instead, we find that homozygous TRLS/2J mice eat significantly less than their wildtype and heterozygous counterparts and show that delayed gastrointestinal (GI) transit time is associated with both the reduced growth and feeding seen in these mice. Lastly, we knockout HCN2 in parasympathetic neurons (*Chat*[+]) but find no signs of growth restriction in these mice. In summary, a novel mutation in HCN2 leads to impaired GI motility and likely causes the severe growth restriction seen in HCN2 ablation mice.

Introduction

Hyperpolarization-activated Cyclic Nucleotide gated (HCN) channels are ubiquitously expressed in neural and cardiac tissues primarily. These channels greatly influence the excitability of both pacemaking and non-pacemaking cells by conducting a depolarizing, hyperpolarization-activated inward current (I_h) that is present at the resting membrane potential[73,79]. HCN channels form both hetero- and homo-tetramers in a "dimer-of-dimers" configuration from four pore-forming subunits, HCN1-4[73,79]. Differing expression pattern, channel gating kinetics, and responsivity to modulators such as cyclic nucleotides distinguish the effects of each subunit on cellular and somatic processes[73,79].

In mice, knockout (KO) of HCN1, HCN2, or HCN4 result in dramatic phenotypes that are specific to the subunit removed. Homozygous HCN4-KO mice are embryonic lethal, dying *in utero* at E10.5 – 11.5 from cardiac-specific dysfunction[199]. By contrast, HCN1-KO mice show almost no gross anatomical abnormalities, and instead show impaired motor learning, a higher susceptibility to chemically-induced seizures, and an antidepressant-like phenotype[74,140,141]. The dramatic difference in phenotypes between these mice is likely due to the relative expression pattern of the deleted subunit, with HCN1 predominating in many regions of the brain but being sparsely expressed in the heart while HCN4 is the predominant isoform expressed in cardiac tissue but only expressed in select brain regions[139].

HCN2 is expressed at high levels in both the heart and nervous system, and the phenotypes that result from HCN2 deletion mirror these expression patterns. Though homozygous HCN2-KO mice are born in Mendelian ratios from heterozygous parents, they begin to display a severe phenotype noticeable between the second and third weeks of life[87,142]. This phenotype includes cardiac dysrhythmias, persistent absence epilepsy-like spike-wave discharges, ataxia, tremor, reduced neuropathic and inflammatory pain, antidepressant-like behavior, infertility, and severely restricted growth[74,87,142,143]. Of these numerous phenotypes, a few have been characterized on the cellular level. For instance, the reduced inflammatory and neuropathic pain is due to HCN2 loss in nociceptive DRG neurons[143], as shown through *Hcn2* ablation through the cre-lox system in *Nav1.8*^{+} cells[145]. In addition, the cardiac dysrhythmia, in the form of variable R-R interval bradycardia, is recapitulated with cardiac-specific KO of *Hcn2*[87].

While many of the phenotypes observed in HCN2-KO mice have been established through cell-specific ablations, the severe growth defect has yet to be recapitulated. Specifically, *Hcn2* has been

ablated in cardiomyocytes (*Mlc2a*^{+})[87], nociceptive neurons (*Nav1.8*[+])[145,146], glutamatergic forebrain neurons (*Nex*[+])[144], forebrain GABAergic neurons (*Dlx5/6*[+])[144], and oligodendrocyte lineage cells (*Cnp*[+], unpublished data) without causing the growth restriction seen in global HCN2-KO mice. In this chapter, we present the first detailed characterization of a spontaneous mutation in *Hcn2* found in Tremor and Reduced Lifespan 2 (TRLS/2J) mice. This mutation causes complete loss of HCN2 protein and phenotype consistent with other HCN2 ablation mice. In addition, we investigated the TRLS/2J mice's growth defect in detail, attempting to isolate a mechanism causing this phenotype.

Materials and Methods

Animals

TRLS/2J mice arose in a breeding colony of WB/ReJ-*Kit*[W]/J mice as being weak and of small size with early mortality. These mice were then backcrossed to C57BL/6J mice for 4 generations without seeing signs of the Kit[W] allele, indicated by a white ventral spot on a black fur coat[200]. TRLS/2J heterozygous mice (*Trls2*^{+/-}) were set up to breed at Northwestern University, resulting in wildtype (*Trls2*^{+/+}), *Trls2*^{+/-}, and homozygous TRLS/2J (*Trls2*^{-/-}) mice at the expected Mendelian ratios. Similar to other HCN2 ablation mice, both male and female *Trls2*^{-/-} mice were infertile. After sequencing *Hcn2* in the TRLS/2J mice, primers were developed for genotyping as follows: WT-F-5' GATGTTGCCTCACAGAGAATGC, Common-R-3' CCTCCCTTTGACTCTCTCCTCA, and MUT-F-5' GTTCTTTACTGGCATCGGCTACG. As shown in **Figure 1B**, the wildtype allele created a 473 bp band and the mutant allele created a 289 bp band. Upon weaning, TRLS/2J mice's diet of Teklad LM-485 Mouse/Rat Diet 7912 (Envigo; Madison, WI) was supplemented with Recovery DietGel (ClearH20; Westbrook, Me), which was changed at least twice weekly. Otherwise, mice had access to food and water *ad libitum*. Homozygous *Hcn2*-Flox (*Hcn2*[flx/flx]) mice on a C57BL/6J background were generously donated by Andreas Ludwig and mated with *Chat*[cre/-] mice on a C57BL/6J background, purchased from Jackson Laboratories (Bar Harbour, ME). The F1 generation of ChAT-cre^{+/-}/HCN2[flx/-] mice were bred with *Hcn2*[Flx/Flx] mice to produce *Hcn2*[Flx/Flx]/*Chat*[cre/-] and *Hcn2*[Flx/Flx]/*Chat*[cre/-] controls. These mice were not supplemented with diet gel, as they showed no signs of restricted growth. Male and female mice were used for all studies, and mice were age-matched. Mice

were maintained on a 14:10 hour light:dark cycle. All animal experiments were performed according to protocols approved by the Institutional Animal Care and Use Committee of Northwestern University.

HCN2 Gene Sequencing

Sanger sequencing was performed by Northwestern's Center for Genetic Medicine (CGM) using PCR products generated by lab-created primers (See Supplementary Table 1 for sequences). PCR products were gene purified with QIAquick Gel Extraction Kits (Qiagen; Germantown, MD) before being sent to CGM for sequencing. Sequence chromatograms were verified for quality using A Plasmid Editor (aPE; University of Utah; Salt Lake City, UT), and BLAST (NCBI; Bethesda, MD) was used to map experimentally-derived sequences to canonical sequences of the mammalian genome.

Western Blot

Western Blots were done as previously described in chapter 2. The antibody against C-terminal HCN2 was custom made while the N-terminal antibody was purchased from Alomone (Jeruselum, Israel).

Growth Curve

TRLS/2J mice had their weight and length measured starting at postnatal day 7 (P7). Weight was assessed using a portable scale with accuracy to one decimal place in grams, while length was measured with electronic calipers with accuracy to two decimal places in millimeters. Mice were weighed once daily until P21, where they were weaned into separate cages by sex and were then weighed every 7 days until P56. Mice used in growth studies were not used in any subsequent studies to avoid the effects of stress associated with these measurements.

Behavioral Testing

For all behavioral experiments, mice were acclimated to the testing room for 30 minutes in singly housed cages, and all tests were performed during the light phase of the dark/light cycle (6:00a to 8:00p). The testing room was sound-proofed, and between each trial of testing, all apparatuses were cleaned with 70% ethanol. The experimenter was blind to the genotypes of the mice to prevent bias.

Tail Suspension Test (TST)

Antidepressant-like behavior was assessed by the TST, as previously described[74]. Briefly, mice were suspended by their tails for 6 minutes. Immobility time, defined as time spent without movement of the fore- or hindlimbs, was measured by an observer blinded to genotype.

RotaRod

The rotarod test was performed as previously described[142]. Briefly, the RotaRod assay took place over 4 trials: two training trials and two test trials. During each trial, the mouse was placed on a rotating rod (Ugo Basile; Varese, Italy) accelerated from 4 to 40 rpm over a 5 min period, and the latency to fall off the rod was recorded. If the mouse did not fall within 5 min, the mouse was removed from the rod and given a latency to fall value of 300s. The two test trials were averaged together to give the final endpoint in this assay.

EEG

EEG was done as previously described[75] with the following modifications. Briefly, mice were anesthetized with isoflurane and placed in a stereotaxic frame. A prefabricated mouse headmount (Pinnacle Technologies; Lawrence, KS) was fastened onto the skull with super glue, and 4 small holes were created with a dental drill to allow placement of 4 screw electrodes (2 screws placed 1mm anterior to bregma and 2 screws placed 7mm posterior to bregma, each being 1.5mm lateral to the central sulcus). Dental acrylic was fashioned over the skull to add stability to the headmount, and the scalp was closed with sutures. Mice were allowed 7 days to recover and then were placed in the recording chambers for continuous, 24h, video-EEG recordings, collected with Sirenia Acquisition Software (Pinnacle) and band pass filtered at 1-25Hz. EEG/video analysis was performed offline using MATLAB/EEGLAB (Mathworks; Natick, MA) by manually scrolling through 10 s epochs of EEG data to detect epileptiform activity by an experienced observer blinded to each subject's genotype. Spike-wave discharges were identified as periods of the EEG exhibiting a distinct 3-8Hz spike-wave morphology, with amplitudes at least twice that of the baseline[197].

Tail vein blood and serum collection

Tail vein blood was collected in CB 300 Z microvette tubes (Nümbrecht, Germany) at two different time points, one hour after lights on and one hour after lights off. Collected tail vein blood was immediately put on ice and spun down at 4000rpm in an Eppendorf 5424 R Centrifuge (Hauppauge, NY), and the serum was collected and stored at -80C until being assayed.

Blood Glucose Measurements

A drop of tail vein blood was applied to a Freestyle Precision Neo glucose meter (Abbott; Alameda, CA) before each tail vein blood draw and again after the blood draw was completed. These two measurements were averaged together for each animal and represented the blood glucose concentration at that time point.

Pancreatic, pituitary, and thyroid hormone measurements

All hormone concentrations were assessed from serum collected at a one hour pre-lights off time point from trunk blood after decapitation. All hormone assessments were done with kits per the manufacturers' instructions. The following kits were used: Ultra Sensitive Mouse Insulin ELISA (Crystal Chem; Downer's Grove, IL), Mouse Pituitary Magnetic Bead Panel (EMD Millipore; Billerica, MA), and Rat Thyroid Hormone Magnetic Bead Panel (EMD Millipore). The insulin ELISA was read on a Spectra Max 190/plus 384 (Molecular Devices Corporation; Sunnyvale, California) and the pituitary and thyroid panels were read with a Luminex 200 (Northbrook, IL). All ELISA assays were run in duplicate for each serum sample, and technical replicates were averaged together to give the final endpoint per mouse.

Hemotoxylin and Eosin (H&E) Staining and Microscopy

Mice were euthanized and tissue was immediately collected, fixed in 10% formalin, and sent to the Northwestern Mouse and Histology Phenotyping Laboratory for processing and staining. Sections were cut to 4 μm thickness, mounted on slides, and stained with H&E. Pictures were obtained with a Zeiss Axioplan 2 and AxioVision Software (Jena, Germany).

Feeding Studies

Feedings studies were administered over three weeks, with a different diet provided during each week of testing. Each feeding trial took place over 72hrs, and was broken up into three 24hr periods. *Trls2*$^{+/+}$, *Trls2*$^{+/-}$, and *Trls2*$^{-/-}$ cage mates at 8-10 weeks of age were separated into single housing with the normal diet of rodent chow and diet gel (as described above) removed but water provided *ad libitum*. During the first feeding trial, each mouse was given ~20g of diet gel on the floor of the cage, and the weight of the gel was measured and recorded at the beginning of the 24hr period. At the end of each 24hr period, the amount of remaining diet gel was weighed and recorded, and new diet gel was again weighed, recorded, and put in the mouse's cage for the next 24hr period. After three 24hr periods (72hrs), the mice were placed into their original, group housing cages with their original diets of rodent chow and diet gel until the next testing period. The protocol for these trials were repeated each week, with moist, ground chow given during the second feeding trial and diet gel and solid rodent chow both given during the third and final trial ("choice" trial). The average amount of food eaten during each 24hr period was recorded, and each 24hr value was averaged together to yield the average amount eaten per 24hr period for each mouse.

Gastrointestinal Transit Time (GTT) Assay

Each mouse was singly housed 18 hrs prior to each trial in cages without food but with water *ad libitum*. At the start of each GTT trial, mice were gavaged with a methylcellulose gel, consisting of 1.5% sodium carboxymethyl cellulose (Sigma-Aldrich; St. Louis, MO) in water mixed with 6% carmine red (Sigma-Aldrich; St. Louis, MO). Immediately after each gavage period, the GTT time started and an investigator blind to genotype inspected each cage every 5min for presence of red feces, at which point they recorded the time. GTT was defined as the length of time it took for red feces to appear from when the mouse was first gavaged.

Statistics

All statistical calculations were performed using GraphPad 6. For comparisons of three groups with one factor, a One-Way ANOVA was used. For comparisons of three groups over time (within trial comparisons),

a Repeated Measures ANOVA was used. Tukey's *post-hoc* test was used for pairwise comparisons following significant ANOVA results. Significance was denoted with an asterisk, representing a p-value < 0.05, and all values were reported as mean±S.E.M.

Results

A 3kb insertion mutation leads to loss of HCN2 protein in TRLS/2J mice

TRLS/2J mice are born at normal Mendelian ratios and begin to develop a tremor and wasting between the second and third week of life. TRLS/2J mice displayed non-complementarity when bred with an HCN2 ablation mouse (BKS(Cg)-trls/J), suggesting that a similar ablation of HCN2 protein was present, and the affected allele was mapped to chromosome 10[200]. To characterize the mutation leading to this phenotype, we sequenced HCN2 and found a 3kb insertion in the coding sequence of exon 4 (**Figure 1 A**). This sequence is composed of genomic pieces of chromosomes 2 and 15 in the middle and is bookended by a small (9 bp) unidentified stretch of DNA on one side and unidentified DNA with many sequences similar to Mammalian apparent LTR Retrotransposons (MaLR) on the other. Based on this sequence information, we developed primers to genotype the mice (**Figure 1B**), and detection of the homozygous insertion allele always corresponded to the expected TRLS/2J phenotype. To determine the impact of this insertion, we performed western blots from hippocampal tissue with antibodies against the C- and N-terminus of HCN2, which confirmed a complete loss of protein (**Figure 1C**). These data suggest that the detected insertion in exon 4 of HCN2 is responsible for the TRLS/2J phenotype and results in loss of HCN2 protein.

TRLS/2J mice display similar phenotypes to other HCN2 ablation mutants

Weight and length was recorded daily from P7 until P21 and then weekly until P56 thereafter for *Trls2*^{+/+}, *Trls2*^{+/-}, and *Trls2*^{-/-} mice. Beginning in the third week of life, *Trls2*^{-/-} mice's growth rate slowed, revealing much lower weight and length measurements than their *Trls2*^{+/+} or *Trls2*^{+/-} siblings (**Figure 2A, B**). A significant tremor was observed in *Trls2*^{-/-} mice during this time period, and difficulty with ambulation in the homecage was observed. *Trls2*^{+/-} mice were indistinguishable from their *Trls2*^{+/+} siblings.

Starting at 8 weeks of life, age- and sex-matched $Trls2^{+/+}$, $Trls2^{+/-}$, and $Trls2^{-/-}$ mice were assessed for locomotor activity via RotaRod, antidepressant-like activity on the TST, and epileptic phenotypes during 24hr video-EEG monitoring. Similar to other HCN2 ablation mice, $Trls2^{-/-}$ mice showed a significantly decreased latency to fall from a rotating rod (**Figure 2C**), confirming their severe ataxia. In addition, $Trls2^{-/-}$ mice spent decreased time immobile on the TST (**Figure 2D**), representing increased antidepressant-like behavior. $Trls2^{+/+}$ and $Trls2^{+/-}$ mice performed similarly on both tests. This lack of immobility in $Trls2^{-/-}$ mice was not due to their natural tremor, as only clear movements of the hindlimbs and forelimbs would have been counted as mobility. While these mice did not seem to be hyperlocomotive, an Open Field Test was not employed as these mice showed great difficulty ambulating. In fact, when tested on a moving belt in the DigiGait apparatus, $Trls2^{-/-}$ mice were unable to ambulate faster than 3cm/s, while $Trls2^{+/+}$ and $Trls2^{+/-}$ ambulated easily at over 24cm/s (data not shown). $Trls2^{+/+}$ and $Trls2^{+/-}$ mice performed similarly on both tests.

TRLS/2J mice were then affixed with an EEG headset and were assayed in a home cage for 24 hours for detection of epileptiform activity. Again, consistent with other HCN2 ablation mice, $Trls2^{-/-}$ mice showed persistent spike-wave discharges consistent with absence epilepsy (**Figure 2E**). Interestingly, $Trls2^{+/-}$ mice showed some epileptiform activity, though the frequency of these spike-wave discharges was greatly reduced compared to $Trls2^{-/-}$ (data not shown). $Trls2^{+/+}$ mice showed no signs of epileptic activity. Similar to previous reports, the epileptiform activity in $Trls2^{-/-}$ mice was attenuated greatly by ethosuxamide (data not shown). Thus, $Trls2^{-/-}$ mice show similar deficits to other HCN2 ablation mice, further adding evidence that HCN2 influences multiple phenotypes.

TRLS/2J mice display metabolic dysfunction consistent with nutritional deficiency

HCN2 expression has been reported in many neural and non-neural organs, including the brain, spinal cord, peripheral nerves, heart, pituitary gland, pancreas, GI tract, and kidneys. To investigate what might cause the severe growth restriction in these mice, we assessed their non-fasting blood glucose levels at one hour after lights were turned on and one hour after they turned off. Though $Trls2^{+/+}$ and $Trls2^{+/-}$ mice showed similar glucose levels, $Trls2^{-/-}$ mice had reduced blood glucose concentrations (**Figure 3A**).

Because HCN2 has been shown to impact beta-cell function in the pancreas in a potassium-dependent manner[147], we measured the blood insulin levels of TLRS/2J mice at one hour after lights off. The low blood sugar at both time points suggested that a diabetic phenotype was unlikely. By contrast, if hyperinsulinemia was the cause of the restricted growth in these mice, we would expect higher than normal levels of serum insulin at this time point. However, while $Trls2^{+/+}$ and $Trls2^{+/-}$ mice displayed similar insulin levels, $Trls2^{-/-}$ mice showed significantly decreased insulin (**Figure 3B**), which was appropriately low due to their lower blood glucose status.

HCN2 is also expressed in the hypothalamus and pituitary gland, where HCN2 has been shown to be involved in prolactin exocytosis in lactotrophs[149], though it is also expressed in nearly every other hormone secreting cell as well[148]. Thus, we investigated whether pituitary hypofunction may lead to the low glucose levels and growth restriction in TRLS/2J mice. Through assaying serum levels of pituitary hormones, we found that while ACTH levels were similar between $Trls2^{+/+}$ and $Trls2^{-/-}$ mice (**Figure 3C**), both TSH and GH were elevated in $Trls2^{-/-}$ mice (**Figure 3D, E**). The increased GH is consistent with malnutrition[201], and while TSH is generally low to normal in malnutrition[202], the elevation of these hormones is inconsistent with hypopituitarism. The elevation in TSH led us to assay serum T3 and T4 levels. Compared to $Trls2^{+/+}$ mice, $Trls2^{-/-}$ mice showed decreased T3 and T4 (**Figure 3F**), suggesting an appropriate elevation of TSH to stimulate these low levels. Though these low thyroid levels are consistent with nutritional deficiency but also with congenital hypothyroidism, we performed H&E stains of $Trls2^{+/+}$ and $Trls2^{-/-}$ thyroids. In transgenic mouse models of congenital hypothyroidism, TSH is generally very high, and thyroid gland morphology is greatly altered. For instance, in *Titf1/Pax8* double mutants, follicles are observed to be mixed within zones of irregular and diffuse hyperplasia, with lengthened columnar cells[203]. In the Thyroid Peroxidase (*Tpo*) mutant and a *Duox2* mutation mouse, which lacks creation of hydrogen peroxide needed for TPO function, follicles are few in number and swollen, with many proliferating epithelial cells[204,205]. Finally, knockout of *Kcne2*, a potassium channel expressed in the thyroid, leads to congenital hypothyroidism typified by flattened thyrocytes[206]. In contrast to these cases, $Trls2^{+/+}$ and $Trls2^{-/-}$ mice had normal thyroid morphology without swollen colloidal cells, epithelial dysplasia, or hypoplastic follicles, suggesting appropriately active thyroid function (**Figure 3G**). In total,

these results suggest that the growth restriction in these mice is likely due to a nutritional deficiency instead of dysfunction in the hormonal pancreas, pituitary gland, or thyroid.

TRLS/2J mice show decreased feeding and slow gut motility

$Trls2^{-/-}$ mice will often die before 4 weeks of age if they are not supplemented with diet gel, though they have been observed to eat normal mouse chow. Therefore, to investigate the feeding of these mice more rigorously, we tracked the amount of food eaten by these mice over three different diets over three weeks. First, we fed $Trls2^{+/+}$, $Trls2^{+/-}$, and $Trls2^{-/-}$ mice diet gel for 3 days and measured the amount of diet gel eaten over each 24 hour period. The following week, we fed these mice moistened, ground chow, and the last week we gave them a choice between diet gel and intact mouse chow. Though $Trls2^{+/+}$ and $Trls2^{+/-}$ mice ate similar amounts of all three diets, $Trls2^{-/-}$ mice ate significantly less diet gel and moist chow (**Figure 4A, B**). During the choice diet, $Trls2^{-/-}$ mice ate similar amounts of diet gel to the $Trls2^{+/+}$ and $Trls2^{+/-}$ mice, but they ate significantly less of the normal chow, consistent with them eating less overall (**Figure 4C**). As all three diets were placed on the floor of the mouse's cage, it's unlikely that difficulty in ambulation caused the reduction in the amount of food eaten.

The Trls2$^{-/-}$ mice tended to show poor growth starting during the second and third week of life, and since the GI tract continues to develop in mice during this time[207,208], we determined if $Trls2^{-/-}$ mice had underdeveloped GI structures during adulthood. Though all the GI structures in $Trls2^{-/-}$ mice were observed to be smaller than $Trls2^{+/+}$, there were no major morphological anomalies identified in the stomach, duodenum, jejunum, ileum, cecum, or colon (**Supplementary Figures 1,2,3**). The small size of these organs was consistent with the overall smaller size of these mice in general, and similarly smaller structures were noted in the skin, which was grossly thinner than $Trls2^{+/+}$ mice and demonstrated reduced size on H&E (**Supplementary Figure 4**).

As early satiety and anorexia can be symptoms of a GI dysmotility, we assessed the TRLS/2J mice's GI Transit Time (GTT). After fasting $Trls2^{+/+}$, $Trls2^{+/-}$, and $Trls2^{-/-}$ mice for 18 hours with free access to water, we gavaged the mice with a 3% methylcellulose solution plus carmine red and measured the amount of time before the first red feces appeared. Interestingly, while $Trls2^{+/-}$ mice showed significantly faster GTTs than $Trls2^{+/+}$ mice, $Trls2^{-/-}$ mice showed significantly slower gut motility (**Figure 4D**). While not

necessarily increased in size compared to $Trls2^{+/+}$ mice, it was observed that $Trls2^{-/-}$ mice often had distended stomachs but otherwise unremarkable small and large intestines, grossly. Thus, it is likely that the slow gut motility may lead to early satiety in $Trls2^{-/-}$ mice, leading to decreased food intake and nutritional deficiency.

Parasympathetic HCN2 loss does not lead to reduced growth

Previously immunohistochemical analysis of the GI tract has suggested that HCN2 exists within acetylcholine-esterase (*Chat*) positive nerve terminals, suggesting that HCN2 may be involved in vagal innervation of the gut. As activation of the parasympathetic nervous system promotes gut motility[209], we reasoned that the loss of HCN2 in TRLS/2J mice may lead to GI dysmotility through impaired parasympathetic input to the gut. Thus, we bred HCN2-flox with ChAT-cre mice to produce mice with specific loss of HCN2 in parasympathetic nerves. However, at 3 weeks of age, these mice displayed no gross abnormalities, including normal motor function, lack of tremor, and normal growth. Thus, it is unlikely that parasympathetic HCN2 loss leads to the GI dysmotility or growth restriction observed in TRLS/2J mice.

Discussion

In this chapter, we identify the mutation in HCN2 that leads to small size in the TRLS/2J mouse line and phenotype these mice, showing they are similar to mice with other HCN2 mutations that cause complete loss of HCN2 protein. Through rigorous investigation of insulin, pituitary hormones, and thyroid hormones, we present a strong argument for nutritional deficiency but not primary pancreatic, pituitary, or thyroid dysfunction causing the small size in these mice. This nutritional deficiency is supported by evidence of reduced feeding in $Trls2^{-/-}$ mice. Finally, we show that altered GI motility is a plausible explanation for the growth deficits in these mice, as the GI tract of $Trls2^{-/-}$ mice are morphologically indistinguishable from $Trls2^{+/+}$ mice.

TRLS/2J mice show similar phenotypes to previous HCN2 ablation mice

HCN channels play a prominent role in both the heart and nervous system, and the individual expression and unique characteristics of each of the four pore-forming subunits (HCN1-4) impact health and disease in different ways[79]. In human patients, reported HCN2 mutations generally have mild impacts on channel function but result in epileptic syndromes starting in childhood. In mice where HCN2 protein is ablated either by transgenic approaches resulting in genetic recombination or spontaneous mutations, a distinct and syndromic phenotype occurs[87,142]. Specifically, HCN2 ablation leads to cardiac dysrhythmias, persistent spike-wave discharges similar to absence epilepsy, ataxia, tremor, reduced neuropathic and inflammatory pain, antidepressant-like behavior, infertility, and severely restricted growth[74,87,142,143]. Of these symptoms, many have been linked to specific tissues or neural circuitry. The arrhythmias are due to cardiac HCN2 loss[87], the epileptiform discharges due to thalamocortical circuits[197], reduced pain phenotypes to nociceptive DRG neurons[145], and antidepressant-like behavior due to loss of HCN2 in the hippocampus[74]. However, some symptoms of HCN2 ablation have yet to be discovered, such as the cause of the persistent growth restriction.

In the experiments presented here, we add further support that HCN2 ablation leads to a distinct syndrome, verifying that ataxia, tremor, epilepsy, antidepressant-like behavior, infertility, and growth restriction are all part of the HCN2 ablation syndrome. In addition, while some epileptiform activity persists in *Trls2*$^{+/-}$ mice, no differences in growth, motor skills, coordination, nor antidepressant-like behavior were noted, suggesting that the remaining (~50%) HCN2 does not cause significant pathology in these domains. This is consistent with patient studies describing HCN2 mutations that subtly increase or decrease channel function and gating and cause specific epileptic syndromes[210-212]. Interestingly, there have been no reported mutations resulting in complete loss of HCN2, and one may speculate that this is due to the development of severe disease and early mortality, as seen in *Trls2*$^{-/-}$ mice.

Growth restriction in TRLS/2J mice is unlikely to be due to hormonal dysfunction

Though HCN channels are generally studied in the heart and brain, these channels have been found to be expressed and regulate function in other tissues, including the kidneys[156-158], pancreas[147], pituitary[148,149], carotid bodies[155], and GI tract[150-154]. In particular, studies have found a functional role for HCN2 in hormone secreting tissues, especially the pancreas and pituitary[147,149]. In the β-cells of the

pancreas, overexpressing HCN2 increased insulin secretion in response to glucose, though a dominant

negative isoform of HCN only reduced insulin secretion during hypokalemic conditions[147]. In the pituitary,

HCN2 was found in many pituitary cells, and I_h was detectable in gonadotrophs, thyrotrophs,

somatotrophs, and lactotrophs as well as other cell types that were not as readily identified[148]. In addition,

functional studies demonstrated that HCN2 plays a prominent regulatory role of exocytosis of prolactin in

cultured lactotrophs[149]. For these reasons, we investigated whether hormonal dysregulation might be the

cause of growth restriction in the TRLS/2J mice.

While we demonstrated that there are significant differences in hormones between $Trls2^{+/+}$ and

$Trls2^{-/-}$ mice, these changes were more consistent with malnutrition than frank dysregulation of hormone

secretion. For instance, while blood glucose levels were found to be decreased in $Trls2^{-/-}$ mice, insulin

was appropriately low. If the low blood glucose were insulin-dependent, we would have expected to see

high insulin levels by contrast. Alternatively, if insulin was inappropriately low, blood glucose would

expected to be increased. Thus, it is unlikely that β-cell dysfunction leads to growth restriction in TRLS/2J

mice. Similarly, while GH and TSH were elevated, ACTH was similar between groups. First, this suggests

that neither hyper- nor hypopituitarism was likely. Second, if mice were growth restricted due to primary

pituitary dysfunction, we would have expected both GH and TSH to be low. Thus, it seemed unlikely that

primary pituitary dysfunction led to the restricted growth in these mice.

Finally, because TSH was elevated, and thyroid hormone has been shown to alter HCN2

transcription in the heart[213], we assayed serum T3 and T4 levels. While a decrease in these levels was

found, this would again be unlikely to lead to growth restriction. For one, hypothyroidism after the

neonatal period is often associated with weight gain, not loss, and the mice did not begin losing weight

until just before weaning. By contrast, mice with congenital hypothyroidism are small from birth, and the

difference in size is apparent much earlier[203-205]. In addition, T3 and T4 levels were not completely absent

and TSH was appropriately elevated, suggesting regulation along the pituitary-thyroid axis was mostly

intact. Again, reports from congenital hypothyroidism mice have shown more greatly elevated TSH, nearly

20-100 times higher than the less than 2-fold increase seen here[203-205]. Still, we also investigated the

structure of the thyroid in $Trls2^{+/+}$ and $Trls2^{-/-}$ mice, but observed similar and normal morphology of the

thyroid gland in both mice, in stark contrast to mice with congenital hypothyroidism[203-205], even when due

to ion channel dysfunction[206]. Thus, thyroid dysfunction is unlikely to lead to the growth restriction in these mice.

Though we can't exclude more subtle changes in hormone dynamics, such as changes in the pulsatile release of certain pituitary hormones, we believe that these more subtle changes would be unlikely to lead to the severe growth restriction observed in these mice[214]. In addition, while we did not assay cortisol directly, the similar levels of ACTH between the mice suggests dysfunction along the HPA axis to be unlikely. In summary, we believe that the growth restriction observed in HCN2 ablation animals is unlikely to be due to primary dysfunction in hormone secreting tissues.

Growth restriction in TRLS/2J mice is likely due to malnutrition secondary to GI dysmotility

The low glucose and mixed hormonal panel was consistent with malnutrition as the cause of the poor growth in TRLS/2J mice. In addition, the growth curves of these mice suggested that these mice grow normally until the second or third week of life, where they then fail to gain weight and length appropriately. During this period in murine development, two important events tend to occur. First, mice tend to start eating solid food in addition to mother's milk and the intestines mature and form clear villi[207,208]. Because we observed that TRLS/2J mice die early without Recovery Diet Gel or moist chow, we hypothesized that TRLS/2J mice may be malnourished due to an inability to eat a solid diet. To test this, we put the mice through three different diet paradigms: diet gel only, moist and ground chow, and a choice between a solid food pellet and diet gel. The results confirmed our hypothesis that $Trls2^{-/-}$ mice eat less than their $Trls2^{+/+}$ and $Trls2^{+/-}$ littermates, regardless of diet, and have an increasingly difficult time eating solid chow and so prefer softer diet gel when possible. Because $Trsl2^{-/-}$ mice clearly ate all the food types, we believe it's unlikely that the growth restriction was due to ambulatory dysfunction or voluntary motor deficits.

Upon necropsy, we noticed that $Trls2^{-/-}$ mice often had distended stomachs but relatively normal small intestines and colon, grossly. In addition, H&E stains of stomach, intestinal, and colonic segments showed no significant differences between $Trls2^{+/+}$ and $Trsl2^{-/-}$ mice. Therefore, we reasoned that slow gut motility and potentially early satiety may lead to the anorexia and poor growth of $Trls2^{-/-}$ mice. Accordingly, we tracked the time it took for a colored, fibrous gel to make it through the entire

gastrointestinal tract in the GTT assay. As expected, we found that $Trls2^{-/-}$ mice had a significantly longer GTT than $Trls2^{+/+}$. Surprisingly, however, we found that $Trls2^{+/-}$ mice had a faster GTT than $Trls2^{+/+}$. This suggested that at least two different regulators of gut motility may be at play.

The presence of HCN channels in the GI tract has been observed by many groups. While most of these groups have found I_h or HCN2 specifically in Interstitial Cells of Cajal (ICCs), the endogenous pacemaking cells of the gut, or other Enteric Nervous System (ENS) neurons[151-153], one study reported that HCN2 was localized to ChAT^{+} cells and not ICCs[159]. These ChAT^{+} cells are likely to be acetylcholine secreting, parasympathetic neurons, which may increase gut motility both through direct innervation of smooth muscles and ICCs. It's possible that the degree of HCN2 loss may affect these two mechanisms divergently. For instance, while one mechanism may be insensitive to partial loss of the channel, the other may be significantly affected. In addition, when full loss of HCN2 is achieved, one system may be so strongly affected as to cancel the influence of the other. This would be especially true if one system influences the other, as might occur with parasympathetic modulation of ICCs. One may speculate that this division of HCN2 function may lead to the increased gut motility seen in the $Trls2^{+/-}$ and the decreased gut motility seen in $Trls2^{-/-}$ mice. Thus, we reasoned that loss of HCN2 in these cells may lead to the decreased gut motility and growth restriction of TRLS/2J mice. However, creation of a ChAT[+] cell-specific HCN2-KO mouse did not lead to reduced size, and thus suggests that intrinsic ENS dysfunction is more likely to lead to the growth restriction observed in these mice. However, future experiments directly testing this hypothesis are necessary.

Decreased gut motility can be an incredibly distressing symptom that manifests during the courses of many diseases. While primary dysmotility disorders, such as Chronic Intestinal Pseudo-obstruction (CIP) and Hirchsprung's diease[215], can lead to anorexia and weight loss, secondary gut dysmotility is common in numerous other diseases, including diabetes[216,217], Parkinson's Disease[218,219], and severe illness resulting in ICU admittance[220]. The impact of GI motility in these diseases can be quite severe, as many patients with gasteroparesis lose >10% of their body weight and 40% of those with gasteroparesis are resistant to pharmacotherapy[221]. It's interesting to note that HCN channel expression has been shown to be altered in patients with Hirchsprung's Disease[222] and rodent models of diabetes[223] and Parkinson's Disease[224], though no firm association between HCN dysfunction and the gastric

dysmotility observed in these diseases has yet been uncovered. Still, the evidence presented here suggests that HCN2 may have an important role in regulating GI motility, and future investigations of HCN2 in terms of GI motility may uncover new mechanisms for disease pathogenesis and hopefully new treatments for patients with symptoms of slowed GI motility.
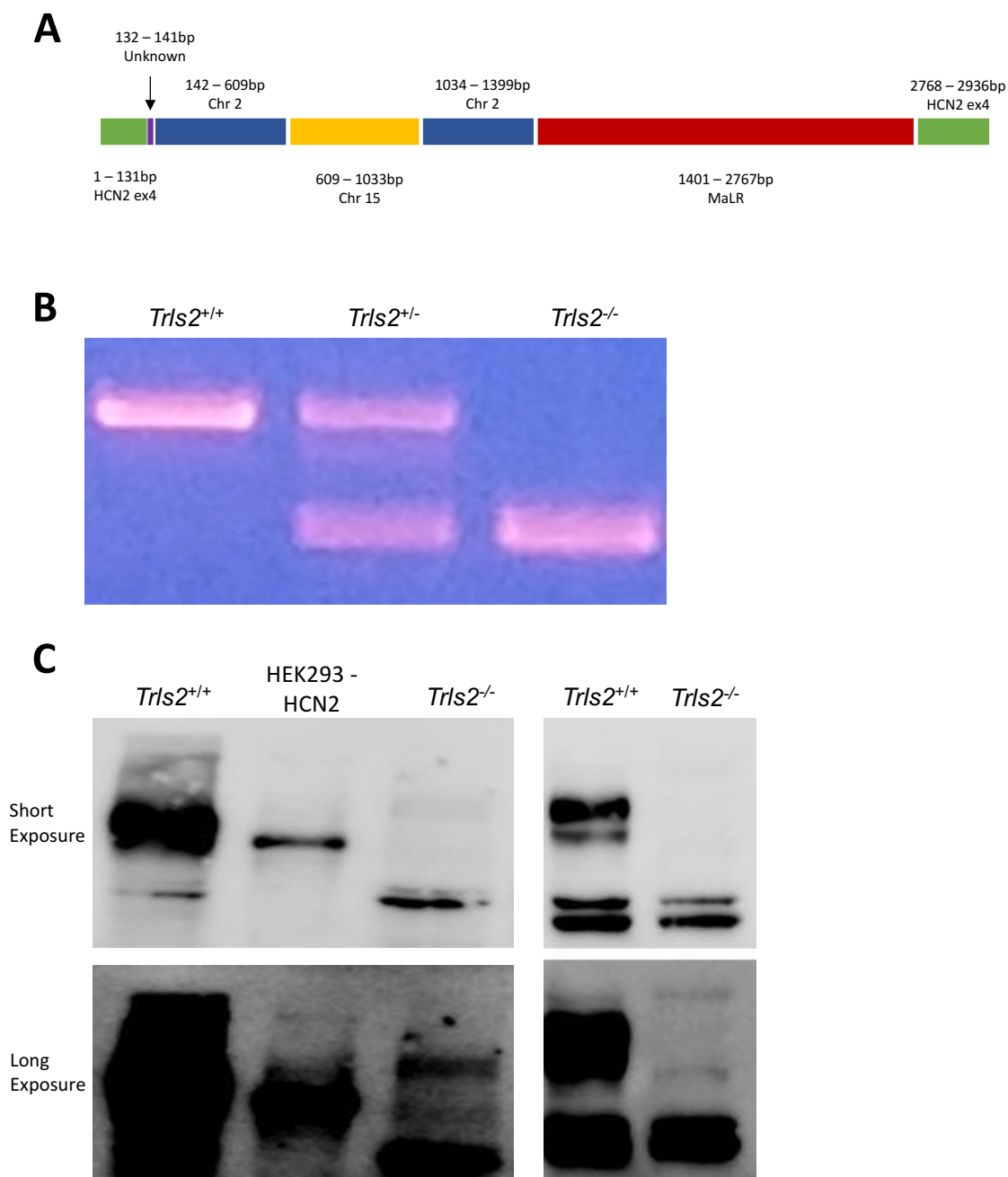
A

132 – 141bp
Unknown

142 – 609bp
Chr 2

1034 – 1399bp
Chr 2

2768 – 2936bp
HCN2 ex4

1 – 131bp
HCN2 ex4

609 – 1033bp
Chr 15

1401 – 2767bp
MaLR

B

Trls2+/+   Trls2+/-   Trls2-/-

C

Trls2+/+   HEK293 - HCN2   Trls2-/-   Trls2+/+   Trls2-/-

Short Exposure

Long Exposure

Figure 1: Insertion in exon 4 of Hcn2 causes loss of protein in TRLS/2J mice. A) Sanger sequencing revealed a ~2.5kb insertion into exon 4 of HCN2. This mutation started with an unknown, 9bp sequence followed by genomic DNA from Chromosome (Chr) 2, genomic DNA from Chr 15, another distinct genomic sequence from Chr 2, and then a large Mammalian apparent LTR Retrotransposon (MaLR) sequence. **B)** Primers were made to genotype TRLS/2J mice based on the mutation sequence and could detect the wildtype allele (473bp) and the TRLS/2J allele (289bp). An example of this genotyping is shown from TRLS2+/+, TRLS2+/-, and TRLS2-/- mice. **C)** N-terminal (left panels) and C-terminal (right panel) antibodies against HCN2 revealed complete loss of protein in TRLS2-/- mice. The upper panels were taken with a short exposure while the lower panels were taken with a longer exposure to confirm that no protein band was present. Two non-specific bands are located in both Trls2+/+ and Trls2-/- mice.
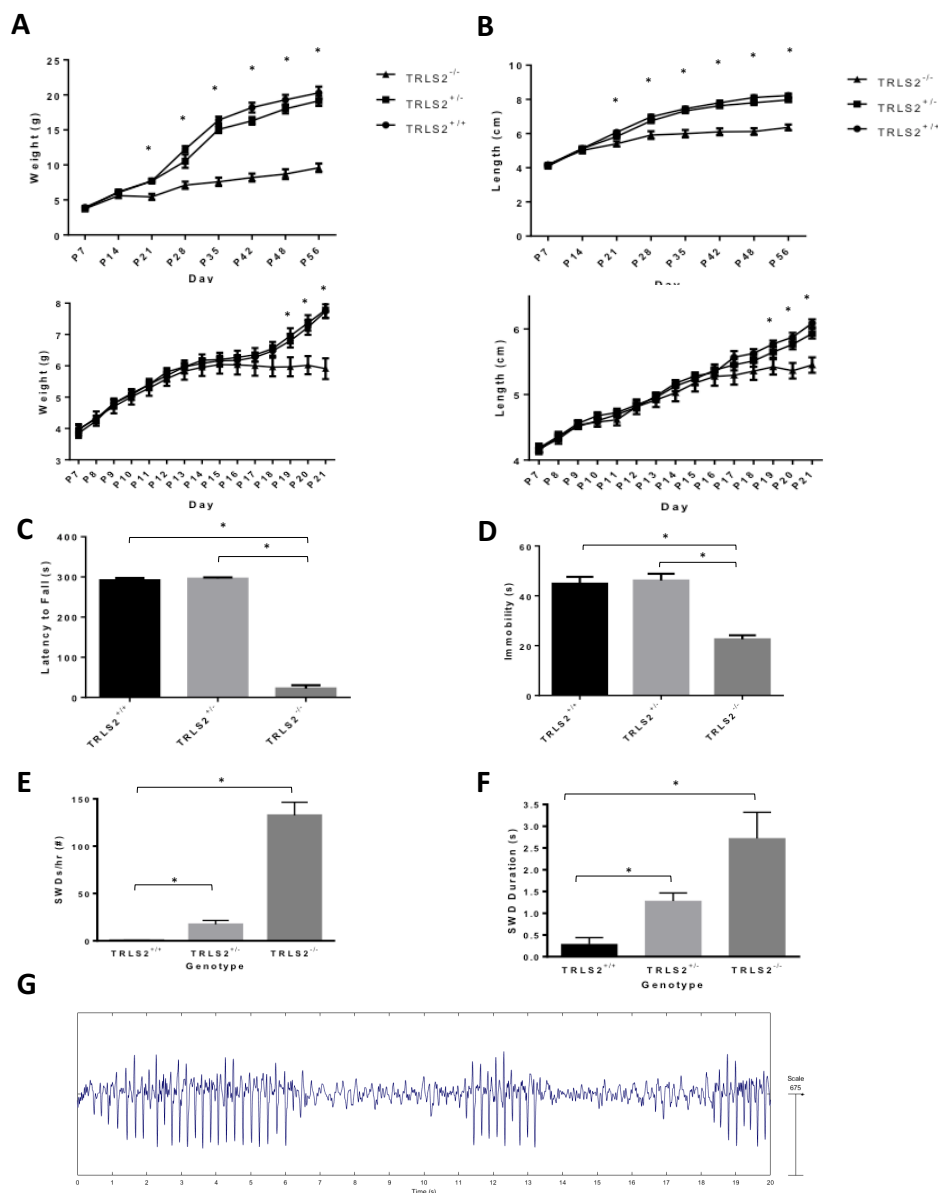
Figure 2: TRLS/2J mice show similar phenotypes to other HCN2 ablation mice. A) Weights and **B)** lengths of *Trls2+/+*, *Trls2+/-*, and *Trls2-/-* mice were obtained daily from P7 to P21 (right graphs) and weekly until P56 thereafter (left panel). *Trls2-/-* mice began to fall of the growth curve between P14 and P21. (Repeated Measures Two-Way ANOVA. Weekly Weight: $F_{Time}(7,196) = 385.9$, $p < 0.0001$; $F_{Genotype}(2,28) = 65.39$, $p < 0.0001$, $F_{Interaction}(14,196) = 33.42$, $p < 0.0001$. Weekly Length: $F_{Time}(7,196) = 676.9$, $p < 0.0001$; $F_{Genotype}(2,28) = 36.58$, $p < 0.0001$; $F_{Interaction}(14,196) = 27.09$, $p < 0.0001$. Pre-weaning Weight: $F_{Time}(14,532) = 352.7$, $p < 0.0001$; $F_{Interaction}(28,532) = 12.75$, $p < 0.0001$. Pre-weaning Length: $F_{Time}(14,560) = 468.5$, $p < 0.0001$; $F_{Interaction}(28,560) = 5.815$). Tukey's Post Hoc Test was used to detect individual differences between groups. An * denotes $p < 0.05$ between *Trls2+/+* and *Trls2-/-* as well as between *Trls2+/-* and *Trls2-/-*. An denotes $p < 0.05$ between *Trls2+/+* and *Trls2+/-*. **C)** *Trls2-/-* mice showed significantly shorter latencies to fall on the RotaRod (One-Way ANOVA. $F(2,29) = 543.4$, $p < 0.0001$; Tukey's Post Hoc Test $p < 0.05$). **D)** *Trls2-/-* mice showed significantly reduced immobility on the Tail Suspension Test (One-Way ANOVA. $F(2,29) = 12.46$, $p < 0.0001$; Tukey's Post Hoc Test $p < 0.05$). E) Representative spike-wave discharges from *Trls2-/-* mouse. Significance ($p < 0.05$) is denoted with an *, and error bars represent Standard Error of the Mean. (n+/+ = 10-13, n+/- = 12-19, n-/- = 5-10)
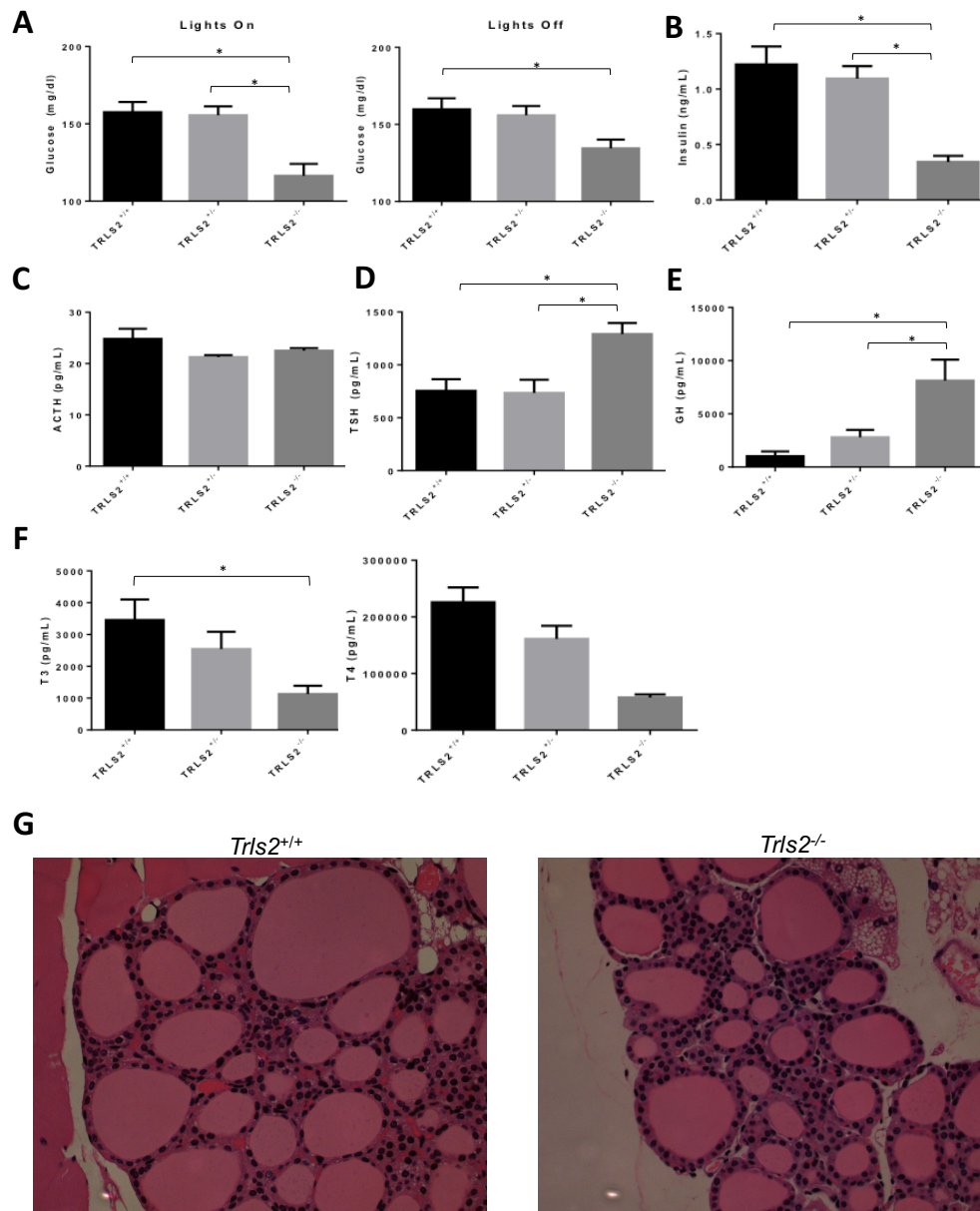
Figure 3: *Trls2-/-* mice demonstrate appropriate hormone responses to low blood glucose. A) Blood glucose was assessed at two time points in *Trls2+/+*, *Trls2+/-*, and *Trls2-/-* mice, one hour after lights on (top graph) and an hour after lights off (bottom graph). *Trls2-/-* mice show significantly lower blood glucose at both time points (One-Way ANOVA. Lights On: $F_{(2,33)} = 11.79$, $p < 0.0001$. Lights Off: $F_{(2,33)} = 4.626$, $p < 0.05$. Tukey's Post Hoc Test $p < 0.05$). **B)** *Trls2-/-* mice have significantly less serum insulin at one hour after lights off (One-Way ANOVA. $F_{(2,30)} = 13.72$, $p < 0.0001$. Tukey's Post Hoc Test $p < 0.05$). **C)** Serum ACTH levels are similar between *Trls2+/+*, *Trls2+/-*, and *Trls2-/-* mice. **D)** Serum TSH (One-Way ANOVA. $F_{(2,33)} = 7.739$, $p < 0.01$. Tukey's Post Hoc Test $p < 0.05$). and **E)** GH (One-Way ANOVA. $F_{(2,31)} = 9.103$, $p < 0.001$. Tukey's Post Hoc Test $p < 0.05$) are increased *Trls2-/-* mice. **F)** T3 (top graph; One-Way ANOVA. $F_{(2,28)} = 5.699$, $p < 0.01$. Tukey's Post Hoc Test $p < 0.05$) and T4 (bottom graph; One-Way ANOVA. $F_{(2,32)} = 17.96$, $p < 0.0001$. Tukey's Post Hoc Test $p < 0.05$) are decreased in *Trls2-/-* mice. **G)** H&E sections (40x) of thyroid gland morphology is similar between TRLS2+/+ and TRLS2-/-, without signs of swollen colloidal cells or hypothyroidism. Significance ($p < 0.05$) is denoted with an *, and error bars represent Standard Error of the Mean. (n+/+ = 10-12, n+/- = 10-12, n-/- = 10-12)
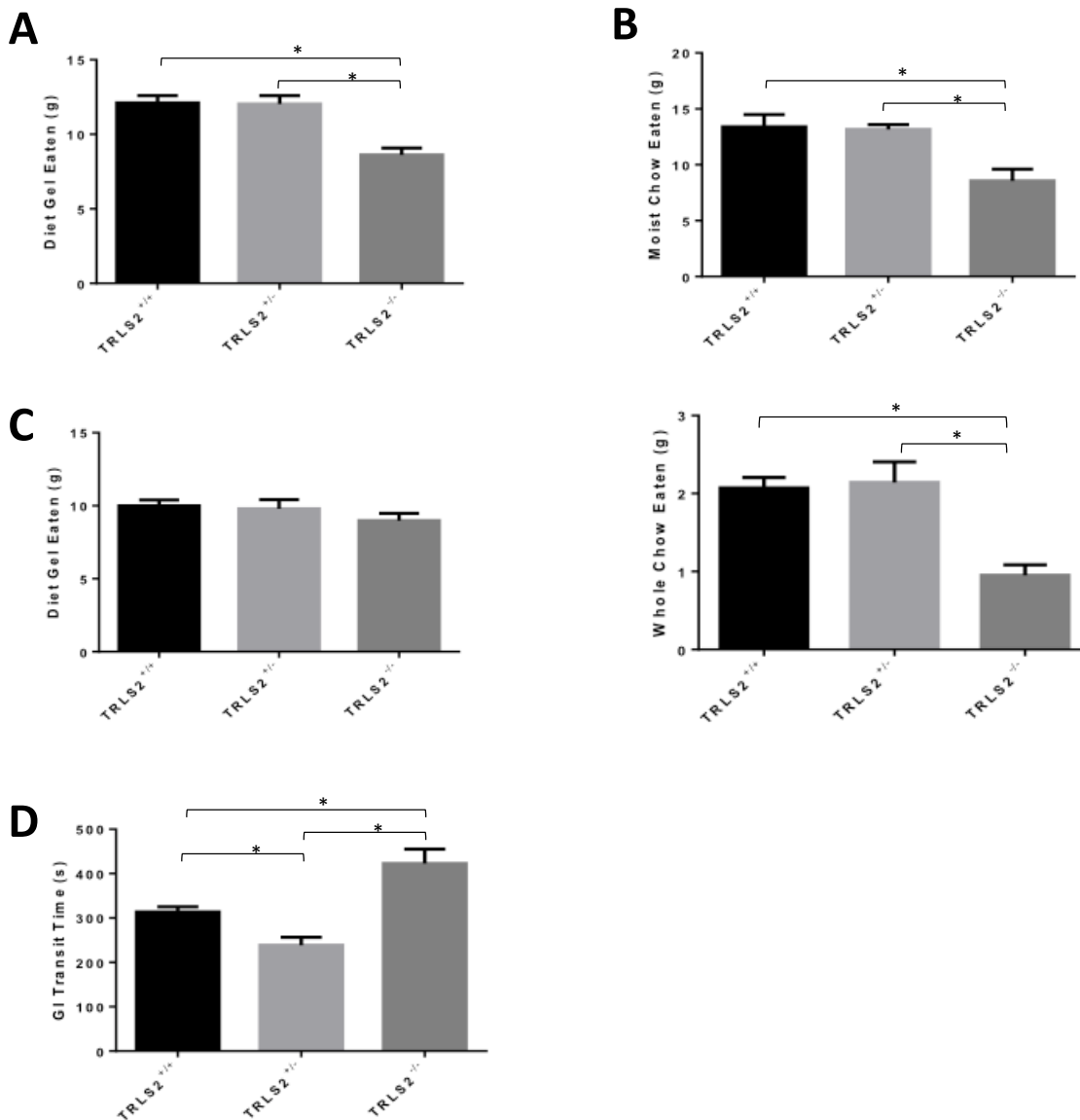
Figure 4: TRLS2-/- mice feed less and have slow GI tract motility. A) *Trls2+/+*, *Trls2+/-*, and *Trls2-/-* mice were given diet gel and water, and the amount of diet gel eaten was tracked during three consecutive 24 hour periods. The average amount of diet gel eaten by *Trls2-/-* mice was significantly less than *Trls2+/+* and *Trls2+/-* mice (One-Way ANOVA. $F_{(2,31)} = 9.013$, $p < 0.001$. Tukey's Post Hoc Test $p < 0.05$). **B)** *Trls2-/-* mice eat less moist chow (One-Way ANOVA. $F_{(2,20)} = 8.749$, $p < 0.01$. Tukey's Post Hoc Test $p < 0.05$). **C)** When given a choice between diet gel and intact chow, *Trls2-/-* mice eat similar amounts of diet gel to *Trls2+/+* and *Trls2+/-* mice but eat significantly less chow (One-Way ANOVA. $F_{(2,21)} = 11.65$, $p < 0.001$. Tukey's Post Hoc Test $p < 0.05$). **D)** Mice were gavaged with a red methylcellulose gel and the time for red feces to appear was noted for each mouse. While *Trls2+/-* demonstrated faster GI transit times (GTT) than *Trls2+/+*, *Trls2-/-* had much slower transit times than either *Trls2+/+* or *Trls2+/-* (One-Way ANOVA. $F_{(2,35)} = 19.35$, $p < 0.0001$. Tukey's Post Hoc Test $p < 0.05$). Significance ($p < 0.05$) is denoted with an *, and error bars represent Standard Error of the Mean. (n+/+ = 9-15, n+/- = 8-13, n-/- = 7-10)

A

Trls2+/+
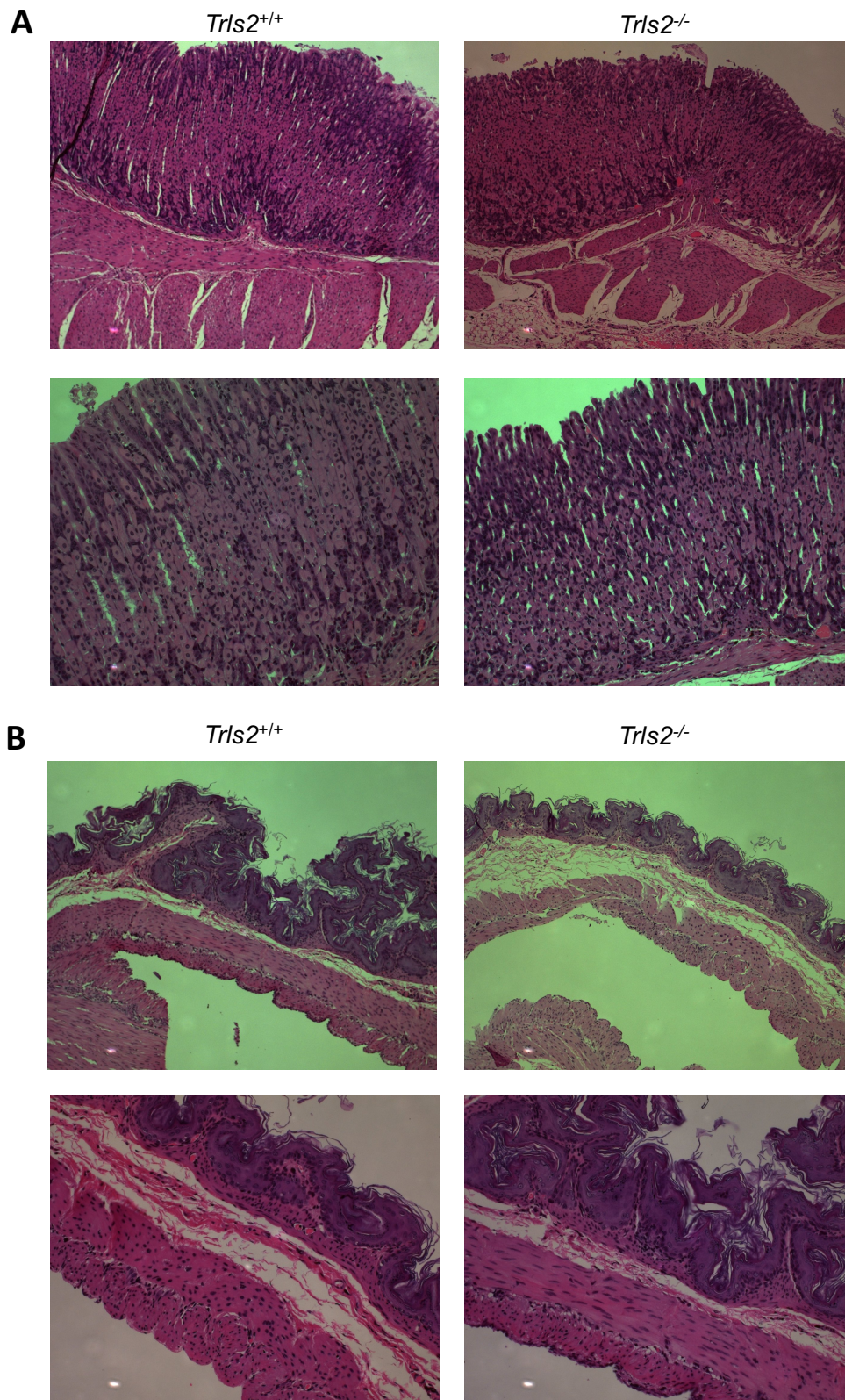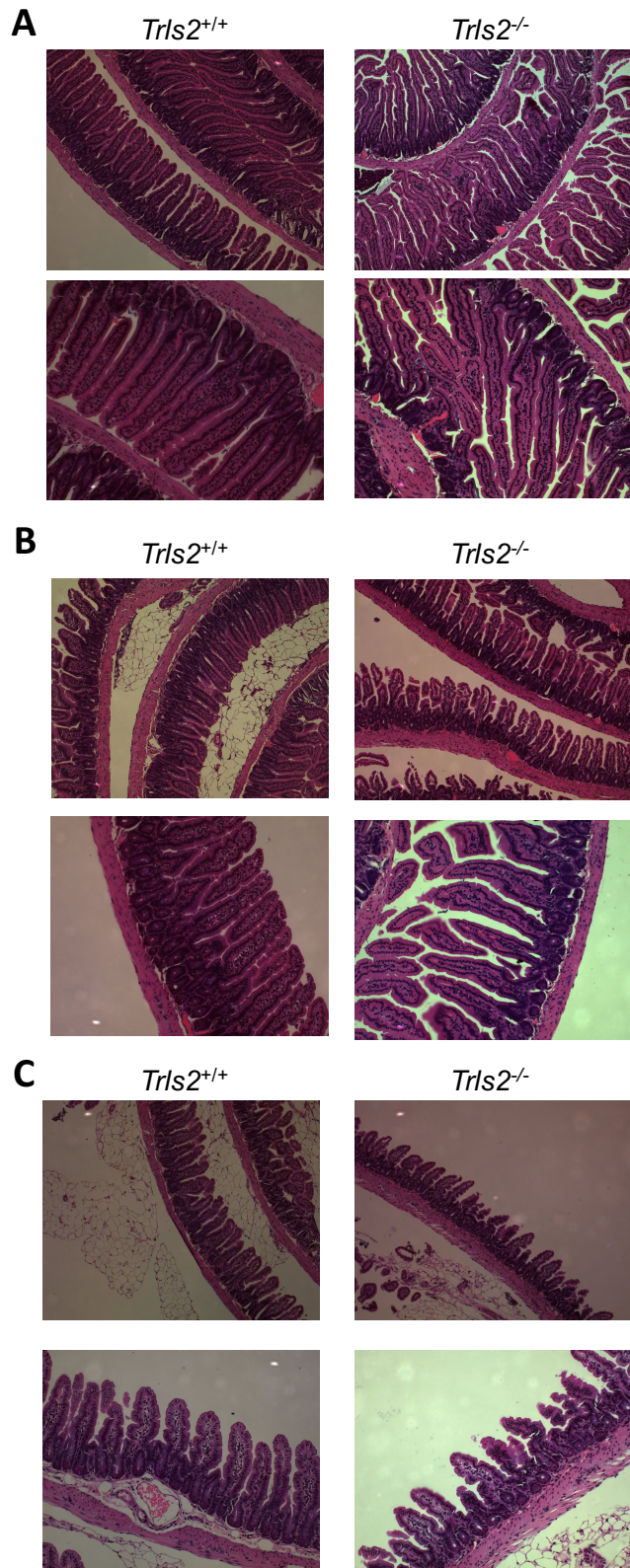
Trls2-/-

B

Trls2+/+

Trls2-/-

Supplementary Figure 1: *Trls2+/+* and *Trls2-/-* mice have similar gastric morphology. A) H&E sections (10x top panels; 20x bottom panels) of glandular and **B)** distal stomach.

Supplementary Figure 2: _Trls2+/+_ and _Trls2-/-_ mice have similar morphology of small intestines.
H&E sections (10x top panels; 20x bottom panels) of duodenum, B) jejunum, and C) Ileum.

A

Trls2+/+   Trls2-/-

B

Trls2+/+   Trls2-/-
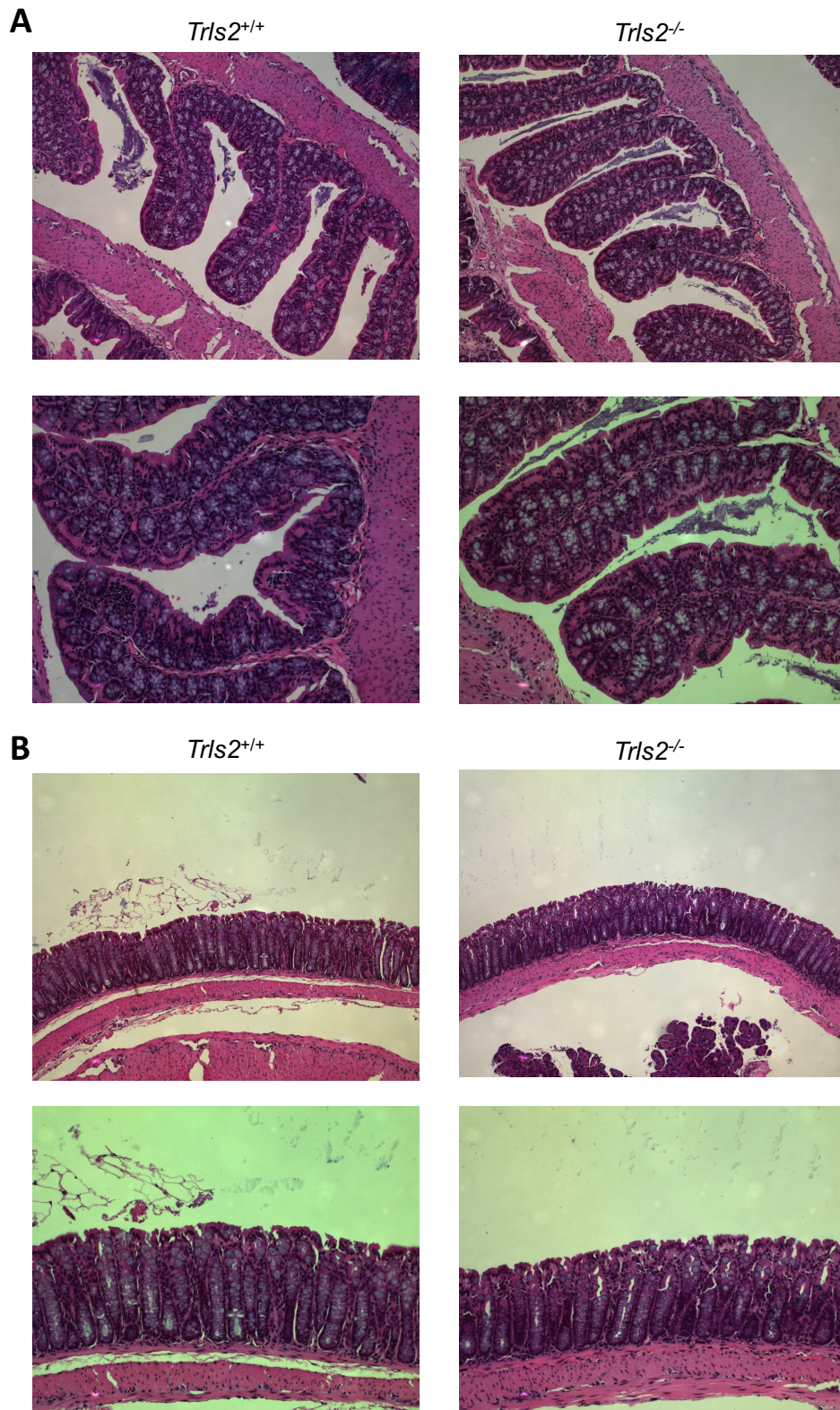
Supplementary Figure 3: *Trls2+/+* and *Trls2-/-* mice have similar morphology of the large intestines. A) H&E sections (10x top panels; 20x bottom panels) of cecum and **B)** distal colon.

Trls2+/+   *Trls2-/-*
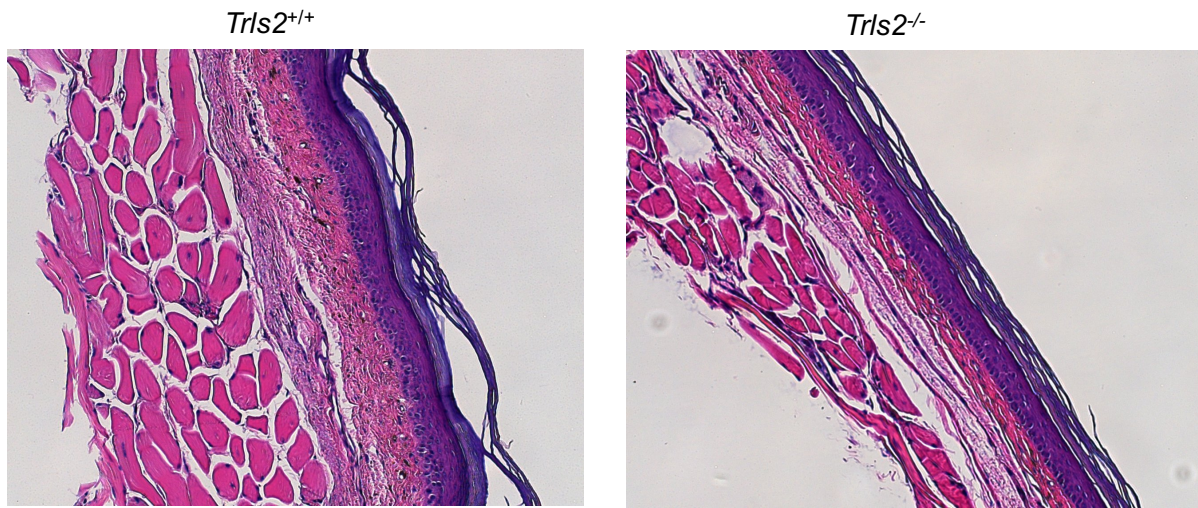
Supplementary Figure 4: *Trls2+/+* and *Trls2-/-* mice have similar skin morphology. A) H&E sections (10x top panels; 20x bottom panels) of foot pads.

HCN2 Exon Primers

Primer	Sequence
1F	GCTTGCTGGCCAGAGCCTCAGTT
2F	AAGGCCAAGAGCTGTGAGCA
3F	TGGGACTCTCATGGTCACACG
5F	GTGGCATTAGGGTGGACCTG
4F	GATGTTGCCTCACAGAGAATGC
6-7F	GAGTTACCAAGCCAGTCACTGAG
8F	CATGGCTTTGGTGTGGATGACG
1R	CCGAGGTCACCATCCGGGACGT
2R	ATGCTTGGTCCTCTCCCTGC
3R	GGCACAAGGGCAAATGGGAG
4R	CCTCCCTTTGACTCTCTCCTCA
5R	GGCTAAAACTCCCCAAGTCCTGTG
6-7R	ATGCCATGCCATGCCTCTACTT
8R	CGTCATCCACACCAAAGCCATG

Insertion Mutation Primers

Primer	Sequence
3kb-1 F	GTTCTTTACTGGCATCGGCTACG
3kb-2 F	CCTTCCGGTCTTGCTCATG
3kb-2 R	CTCTGGTGTGTGAAATTTCAGAGG
3kb-3 F	CAGCTCCTCTATGTACTTGCTCTC
3kb-3 R	GGACTTGGTAATGTGTAAGGGTCAC
3kb-4F	AAGGGACTTGACACGGATACAAC
3kb-4R	AGCATATGTAAAGACTGTGGGACTT

Supplementary Table 1: Primer used for Sanger Sequencing of HCN2 and Insertion Mutation.

CHAPTER 5

Summary, discussion, and future directions

Summary

In the three preceding chapters, mouse models of acute and chronic stress were employed to better understand how HCN channels change during stress and how loss of HCN channels leads to changes in various stress-responsive behaviors. It was demonstrated that HCN channel protein, localization, and function does not change with Chronic Social Defeat (CSD) stress nor in a transgenic mouse model of Early Life Stress (ELS). *Trip8b*$^{-/-}$ mice were not protected from CSD in terms of most stress-induced behaviors. Despite these paucity of finding with chronic stress, it was demonstrated that *Trip8b*$^{-/-}$ mice do have distinctly adaptive reactions to acute stress, demonstrating a propensity towards active coping in numerous assays that specifically test these behaviors. In addition, a novel gene therapy strategy, AAV-1B2, was shown to reduce HCN channels specifically in the dorsal CA1 through lysosome mediated degradation and increased the intrinsic excitability of this region. Importantly, this increase in intrinsic excitability through HCN channel loss in the dorsal hippocampus (dHC) was sufficient to cause similar active coping behaviors as seen in *Trip8b*$^{-/-}$ mice. Together, these results suggest that HCN channel function may be uniquely tied to coping style, which may be adaptive for numerous psychiatric disorders but may also still be subverted by extreme and chronic psychosocial stress.

In addition to these findings regarding stress, a novel mutation in HCN2 was characterized and confirmed that ablation of this protein led to a distinct phenotype including absence epilepsy-like EEG abnormalities, ataxia, antidepressant-like behavior, and severe growth restriction. It was further shown that while persistent differences exist in metabolically relevant hormones of the pancreas, pituitary, and thyroid, these changes were consistent with malnutrition and low blood glucose. Finally, data was presented which suggests that loss of HCN2 leads to impaired GI tract motility through dysfunction in the Enteric Nervous System (ENS) and that this slow motility may lead to early satiety, anorexia, and growth restriction in these mice.

Discussion and Future Directions

Conflicting results with chronic stress leave the question of HCN channel function in MDD open

The results presented in this thesis concerning HCN channel expression and function after CSD are clear, but a recent report describing chronic stress in rats is quite divergent from what is presented here[180]. The contrast between these two reports is surprising enough to warrant a closer comparison of both methods and results, presented below.

In Kim et. al. (2017)[180], 7-8 week old (P49 – P56) adult Sprague Dawley rats were subjected to Chronic Unpredictable Stress (CUS) for two weeks and, preceding CUS, showed anhedonia on the Sucrose Preference Test (SPT), anxiety-like behavior in the Open Field Test (OFT), and increased immobility in the Forced Swim Test (FST). They then show that HCN1 is increased in the dorsal but not ventral CA1 perisomatic region, though a non-significant trend may be apparent in the mid but not distal SLM. They then characterize the CUS cells electrophysiologically and find a decrease in input resistance, an increase in the current needed to elicit an action potential, an increase in the resonance frequency, and an increase in I_h when stepping from -30mV to -140mV only at the soma but not at the dendrites. These changes were not seen in the ventral CA1. They then showed that reduction of HCN1 via lentiviral shRNA protected against CUS-induced aberrant behaviors and that blocking the SERCA pump in CA1 pyramidal cells, which was previously shown to increase perisomatic I_h strongly while affecting dendritic I_h to an almost negligible amount, lead to anxiety-like behavior in the OFT.

While there are some obvious differences between the studies, such as in the stress paradigms used, rodent models, and methods of reducing HCN channels, a few more subtle distinctions deserve discussion. The most important of these differences is the odd subcellular localization of increased perisomatic HCN channels versus those in the distal dendrites. Our lab had previously shown that distal dendritic HCN channels were necessary for the antidepressant-like behaviors in mice[137], which is clearly divergent from these results. While the differences in anti-HCN1 antibodies used may account for some of the differences, the somatic and dendritic recordings are very clear. While the differences in species used between the two experiments may explain these differences, it seems likely that a non-dendritic mechanism for I_h results from the chronic stress.

Another point of interest is in the representation of I_h in the Kim 2017 report. While they do show a change in I_h directly in voltage clamp after CUS, the rest of the paper does not measure I_h or the sag

ratio directly, instead relying on changes in input resistance and resonance as markers of I_h. Though this is a small point, it would seem more straightforward to express changes in I_h directly rather than indirect measures.

Lastly, the SPT was done differently, allowing only 12 hours in darkness for sucrose consumption, and while the water bottle placement was said to be counterbalanced before the test, the placement of the bottles was not switched during the test. While a minor point, the neophobia of the sucrose water during this short test may reflect a difference in active versus passive coping, as animals that prefer passive coping may not drink the sucrose as readily if given only a short period of time to consume it, assuming the neophobia leads to avoidant behavior.

Still, the thoroughness of this study and reproducibility of its findings within the study are praiseworthy, and it seems likely that chronic stress in some form does impact I_h. The obvious, and probably most important, next step would be to determine if HCN channel increases are present in the hippocampi of untreated MDD patients, though to date no human or animal study of MDD has reported significant changes in HCN on the genome, transcriptome, or proteome levels. In contrast, specific changes in potassium channels have been noted after CSD in the ventral hippocampi of both resilient and susceptible animals (Bagot 2016).

HCN channels, coping, and human disease

When the distal dendritic distribution of HCN channels in the dHC was reduced by loss of TRIP8b or through AAV-1B2 injections, these mice displayed prominent active coping behaviors in a number of situations. First, *Trip8b$^{-/-}$* mice displayed active coping in both the Two-Way Avoidance Assay (2w-AA) and the Resident-Intruder Test (RIT), decreased passive coping in repeated FST (rFST), and both a decrease in passive and an increase in active coping on the Shock Probe Burying Test (SPBT). Similarly, AAV-1B2 injected mice showed decreased passive coping on the rFST and SPBT and increased active coping on the SPBT. However, the implication from these findings for human disease, especially for MDD pathogenesis, are unclear, though these results may help to explain a few of the mysteries surrounding the role of HCN channels in depression-like behavior in rodent models.

As mentioned in Chapter 3 and in the section above, the antidepressant-like effects of HCN1 knockdown in the Kim 2017 paper were restricted to the dHC, which canonically does not make direct connections to the limbic system and is rarely involved in MDD pathogenesis[46]. Thus, it may be possible that the changes in behavior seen in the Kim 2017 paper are facilitated by active coping behaviors. While active coping has been shown to prevent MDD pathogenesis and aid in its treatment[108,110,111], it's likely that persistent and extreme stress would override these protections, leading to pathological behaviors. In Chapter 2, the particular stress paradigm we employed was social in nature and very extreme, with the constant threat of attack present 24 hours a day through the perforated, plexiglass divider. Though speculative, it's possible that the extreme nature of the stressor used in Chapter 2 was sufficient to override the protection *Trip8b*^{-/-} mice may have had from HCN channel loss, thus resulting in depression-like behaviors. Anecdotally, it was noticed that *Trip8b*^{-/-} mice displayed more defensive aggressive behavior in social defeat sessions during the first half of CSD but eventually started to show more submissive postures similar to *Trip8b*^{+/+} mice by the end of the test (personal observations). Thus, there may be some benefit to repeating the experiments in Chapter 2 with a different stress paradigm, such as Chronic Restraint Stress (CRS) or CUS.

In all the HCN ablation models, the most reproducible and robust result is the large reduction in immobility in the FST and TST. Of these two tests, the FST has been particularly criticized as a test for depression-like behavior[173,225]. Besides the criticisms concerning the validity of the test, these groups posit that the test has more to do with coping than antidepressant-like behavior. In fact, one group has gone as far as to state that chronic stress paradigms that result in increased immobility in the FST, such as CRS or CUS, are actually conditioning procedures for passive coping behavior[173]. Though this interpretation seems extreme given the changes in anhedonia accompanied by these chronic stress procedures, the idea of the FST as a coping specific test may have some value and would fit well with the results presented in this thesis. However, to accept this interpretation, new experiments would be needed whereby coping behaviors and depression behaviors could be more clearly dissociated, ideally with the absence or presence of active coping propensities yielding susceptibility differences to chronic stress-induced behaviors. How this experimental design could be achieved, however, is unclear.

In line with this, one of the biggest unknowns regarding the active coping behavior observed in Chapter 3 is how this behavior in rodents relates to human disease. Though it's been mentioned that patients that engage in active coping show advantages in terms of disease resilience and treatment outcomes[105-107], it's not clear yet if the active coping behaviors that are identified in mice are analogous, despite similar terminology. When describing these murine coping behaviors in the literature, the authors often come from the perspective of ethologists, not physicians[109,123]. They note that a rodent's coping style confers certain evolutionary or adaptive benefits in one environment while the opposite coping style may be more advantageous in another. In this sense, neither active nor passive coping can be considered adaptive or maladaptive outside of the correct context. This contrasts with the human perspective of coping style, where active or proactive coping is almost always considered adaptive. Because of this difference, it is not clear whether the therapeutic benefits of coping style can really be assayed through mouse models, though some studies have correlated these active coping styles with prevention of certain pathological behaviors[185,186].

Some future experiments might have utility in resolving this issue. The conceptually more straightforward approach would be assay numerous mice on their coping styles, subject them to various chronic stress modalities, and then determine if coping style predicted susceptibility or resilience to developing pathological behaviors. However, the results from this would still be associative, as it would be difficult to establish whether the coping style in isolation was adaptive or whether more adaptive brain circuitry contributed to both the difference in coping style and disease susceptibility independently. For this reason, the philosophically more sound approach would be to condition mice towards active or passive coping behaviors and then determine their susceptibility to develop pathological behaviors after chronic stress. This could also be done in the reverse order to determine if coping style influences the recovery from chronic stress as well. While conceptually rather uncomplicated, methodologically this is a very difficult task. Most notably, unlike for humans where psychological counseling can teach active coping in a controlled and non-stressful environment, it may not be possible to train mice on one coping style or the other without applying significant stressors. Thus, it would again be difficult to dissociate the magnitude of the stressfulness of those training paradigms with the development or resolution of stress-induced behaviors. Thus, the dichotomy between intrinsic disease susceptibility and extrinsic coping

mechanisms to reduce the impact of chronic stress may be nearly impossible to dissociate in mice, though there may be some value in undergoing the experiments mentioned above if very carefully planned and executed.

GI motility, growth restriction, and HCN2

In Chapter 4, a novel HCN2 mutation was identified in the TRLS/2J mouse line, which led to a characteristic phenotype of epilepsy, motor dysfunction, antidepressant-like behavior, and small size. Though the small size of these mice could have resulted from dysfunction in numerous tissues, evidence was presented that it was dysfunction in the ENS that led to the small size in these mice. This was supported by the following pieces of evidence: 1) *Trls2*$^{-/-}$ mice had an appearance and biochemical phenotype that was consistent with malnutrition. These mice have a small frame, have weak bones, thin skin, and lower blood sugar than their littermates. Further, the response of their hormones from the pancreas, pituitary, and thyroid are all in line with what would occur with malnutrition. In addition, the timing of the growth restriction in these mice comes at about the time that mice begin eating solid food. Though difficulty with glycogen storage and glucose mobilization from the liver are possible, the lack of HCN2 expression in this organ makes this a less probable explanation. 2) *Trls2*$^{-/-}$ mice had reduced GI tract motility, with some mice taking nearly 8 or 9 hours to pass red feces on the Gastrointestinal Transit Time (GTT) assay. As these mice have also been observed to have distended stomachs on necropsy (personal observation), it's possible that gastroparesis leads to their small size. While more formal experiments of gastric emptying and accommodation were not feasible to complete by our lab, the reported expression of this channel in the ENS cells of this tissue make this possible. 3) Unlike the *Trls2*$^{-/-}$ mice, ChAT-neuron specific HCN2-KO mice did not have small size, making parasympathetic dysfunction less likely.

Despite these promising findings, there's no doubt that future experimentation would be needed to confirm this phenotype. Some experiments that would be incredibly beneficial include *ex vivo* recordings of slow muscle contractions from the GI tract of *Trls2*$^{-/-}$ mice, barium swallow studies to determine if gastroparesis or dysfunction with gastric accommodation are evident in *Trls2*$^{-/-}$ mice, electrophysiological recordings from ENS neurons in acute slice preparations or cultured *in vitro*, and

creation of *c-kit-cre* x *Hcn2$^{flx/flx}$* mice, which would remove HCN2 from the Interstitial Cells of Cajal (ICCs). Though the amount of future experiments needed to confirm this phenotype are expansive, if a mechanism whereby HCN2 regulates GI motility were found, this may have very important translational utility for patients with GI dysmotility, including those with diabetic gastroparesis, neurodegenerative slow GI motility in Parkinson's and Huntington's Diseases, congenital dysmotility syndromes in neonates, and Chronic Intestinal Pseudo-Obstruction.

One alternative explanation for the growth restriction in HCN2 mice comes from what is perhaps an unlikely source: deficits in respiratory physiology. Though the experiments were not complete at the time this thesis was published, a severe respiratory phenotype was observed in *Trls2$^{-/-}$* mice undergoing whole body plethysmography (data not shown). When compared to *Trls2$^{+/+}$* or *Trls2$^{+/-}$* mice, *Trls2$^{-/-}$* mice showed abnormally high breathing rates that were generally unresponsive to changes in CO2 nor hypoxia. In fact, while the breathing rate appropriately increased in *Trls2$^{+/+}$* and *Trls2$^{+/-}$* mice, *Trls2$^{-/-}$* mice actually showed a reduction in breathing rate induced by hypoxia (data not shown). Interestingly, children born with Congenital Central Hypoventilation Syndrome (CCHS) have a host of similar findings to HCN2-KO mice, including abnormal responses to hypercapnia and hypoxia, severe GI dysmotility, hypoglycemia, disordered sleep, and decreased perceptions of anxiety[226]. Interestingly, I$_h$ has been detected in the retrotrapezoid nucleus (RTN), the region putatively dysfunctional in the respiratory symptoms of CCHS, and ZD-7288 mediated blockade of I$_h$ leads to altered respiration in anesthetized rats. While it's unclear *Trls2$^{-/-}$* mice really have similar pathology to CCHS patients, it does present the possibility that the growth restriction in these animals is due to lack of chemoreception at the level of the RTN. As 90% of CCHS cases involve *Phox2b* gene mutations, and a *Phox2b*-cre mouse is widely available, it seems probable that crossing this line with *Hcn2$^{flx/flx}$* mice will lead to severe respiratory dysfunction. However, whether the small size will be reproduced in these mice remains to be seen.

REFERENCES

1.   Ursin H, Eriksen HR. The cognitive activation theory of stress. Psychoneuroendocrinology. 2004;29(5):567-92.
2.   McEwen BS. Stress, adaptation, and disease. Allostasis and allostatic load. Annals of the New York Academy of Sciences. 1998;840:33-44.
3.   Schneiderman N, Ironson G, Siegel SD. STRESS AND HEALTH: Psychological, Behavioral, and Biological Determinants. Annual review of clinical psychology. 2005;1:607.
4.   Koolhaas JM, Boer SFd, Buwalda B, Meerlo P. Social stress models in rodents: Towards enhanced validity. Neurobiology of Stress. 2017;6:104.
5.   McEwen BS, Gianaros PJ. Central role of the brain in stress and adaptation: Links to socioeconomic status, health, and disease. Annals of the New York Academy of Sciences. 2010;1186:190.
6.   Suri D, Vaidya VA. The adaptive and maladaptive continuum of stress responses - a hippocampal perspective. Rev Neurosci. 2015;26(4):415-42.
7.   Kessler Rc BP. LIfetime prevalence and age-of-onset distributions of dsm-iv disorders in the national comorbidity survey replication. Arch Gen Psychiatry. 2005;62(6):593-602.
8.   Briley M, Lépine. The increasing burden of depression. Neuropsychiatric Disease and Treatment. 2011.
9.   Knol MJ, Twisk JWR, Beekman ATF, Heine RJ, Snoek FJ, Pouwer F. Depression as a risk factor for the onset of type 2 diabetes mellitus. A meta-analysis. Diabetologia. 2006;49(5):837-45.
10.   Evans DL, Charney DS, Lewis L, Golden RN, Gorman JM, Krishnan KRR, Nemeroff CB, Bremner JD, Carney RM, Coyne JC, Delong MR, Frasure-Smith N, Glassman AH, Gold PW, Grant I, Gwyther L, Ironson G, Johnson RL, Kanner AM, Katon WJ, Kaufmann PG, Keefe FJ, Ketter T, Laughren TP, Leserman J, Lyketsos CG, McDonald WM, McEwen BS, Miller AH, Musselman D, O'Connor C, Petitto JM, Pollock BG, Robinson RG, Roose SP, Rowland J, Sheline Y, Sheps DS, Simon G, Spiegel D, Stunkard A, Sunderland T, Tibbits Jr P, Valvo WJ. Mood Disorders in the Medically Ill: Scientific Review and Recommendations. Biological Psychiatry. 2005;58(3):175-89.
11.   Duman RS, Aghajanian GK. Synaptic Dysfunction in Depression: Potential Therapeutic Targets. Science. 2012;338(6103):68-72.
12.   Trivedi MH, Rush AJ, Wisniewski SR, Nierenberg AA, Warden D, Ritz L, Norquist G, Howland RH, Lebowitz B, McGrath PJ, Shores-Wilson K, Biggs MM, Balasubramani GK, Fava M, Team SDS. Evaluation of Outcomes With Citalopram for Depression Using Measurement-Based Care in STAR*D: Implications for Clinical Practice. Am J Psychiatry. 2006;163(1):28-40.
13.   Arnone D, McIntosh AM, Ebmeier KP, Munafò MR, Anderson IM. Magnetic resonance imaging studies in unipolar depression: Systematic review and meta-regression analyses. European Neuropsychopharmacology. 2012;22(1):1-16.
14.   Duman RS, Monteggia LM. A Neurotrophic Model for Stress-Related Mood Disorders. Biological Psychiatry. 2006;59(12):1116-27.
15.   Krishnan V, Nestler EJ. The molecular neurobiology of depression. Nature. 2008;455(7215):894-902.
16.   Zeng L-L, Shen H, Liu L, Wang L, Li B, Fang P, Zhou Z, Li Y, Hu D. Identifying major depression using whole-brain functional connectivity: a multivariate pattern analysis. Brain. 2012;135(5):1498-507.
17.   Greicius MD, Flores BH, Menon V, Glover GH, Solvason HB, Kenna H, Reiss AL, Schatzberg AF. Resting-State Functional Connectivity in Major Depression: Abnormally Increased Contributions from Subgenual Cingulate Cortex and Thalamus. Biological Psychiatry. 2007;62(5):429-37.
18.   Hamilton JP, Chen G, Thomason ME, Schwartz ME, Gotlib IH. Investigating neural primacy in Major Depressive Disorder: multivariate Granger causality analysis of resting-state fMRI time-series data. Molecular Psychiatry. 2011;16(7):763-72.
19.   Seminowicz DA, Mayberg HS, McIntosh AR, Goldapple K, Kennedy S, Segal Z, Rafi-Tari S. Limbic–frontal circuitry in major depression: a path modeling metanalysis. NeuroImage. 2004;22(1):409-18.
20.   Mayberg HS, Brannan SK, Tekell JL, Silva JA, Mahurin RK, McGinnis S, Jerabek PA. Regional metabolic effects of fluoxetine in major depression: serial changes and relationship to clinical response. Biological Psychiatry. 2000;48(8):830-43.

21.   Cryan JF, Holmes A. The ascent of mouse: advances in modelling human depression and anxiety. Nat Rev Drug Discov. 2005;4(9):775-90.

22.   Surget A, Wang Y, Leman S, Ibarguen-Vargas Y, Edgar N, Griebel G, Belzung C, Sibille E. Corticolimbic Transcriptome Changes are State-Dependent and Region-Specific in a Rodent Model of Depression and of Antidepressant Reversal. Neuropsychopharmacology. 2008;34(6):1363-80.

23.   Duric V, Banasr M, Stockmeier CA, Simen AA, Newton SS, Overholser JC, Jurjus GJ, Dieter L, Duman RS. Altered expression of synapse and glutamate related genes in post-mortem hippocampus of depressed subjects. International Journal of Neuropsychopharmacology. 2013;16(1):69-82.

24.   Chen Y, Bender RA, Brunson KL, Pomper JK, Grigoriadis DE, Wurst W, Baram TZ. Modulation of dendritic differentiation by corticotropin-releasing factor in the developing hippocampus. PNAS. 2004;101(44):15782-7.

25.   Ivy AS, Rex CS, Chen Y, Dubé C, Maras PM, Grigoriadis DE, Gall CM, Lynch G, Baram TZ. Hippocampal Dysfunction and Cognitive Impairments Provoked by Chronic Early-Life Stress Involve Excessive Activation of CRH Receptors. J Neurosci. 2010;30(39):13005-15.

26.   Licznerski P, Duman RS. Remodeling of axo-spinous synapses in the pathophysiology and treatment of depression. Neuroscience. 2013;251:33-50.

27.   Katayama T, Jodo E, Suzuki Y, Hoshino KY, Takeuchi S, Kayama Y. Phencyclidine affects firing activity of basolateral amygdala neurons related to social behavior in rats. Neuroscience. 2009;159(1):335-43.

28.   Qiao H, An S-C, Ren W, Ma X-M. Progressive alterations of hippocampal CA3-CA1 synapses in an animal model of depression. Behavioural Brain Research. 2014;275:191-200.

29.   Kallarackal AJ, Kvarta MD, Cammarata E, Jaberi L, Cai X, Bailey AM, Thompson SM. Chronic Stress Induces a Selective Decrease in AMPA Receptor-Mediated Synaptic Excitation at Hippocampal Temporoammonic-CA1 Synapses. J Neurosci. 2013;33(40):15669-74.

30.   Murray EA, Wise SP, Drevets WC. Localization of Dysfunction in Major Depressive Disorder: Prefrontal Cortex and Amygdala. Biological Psychiatry. 2011;69(12):e43-e54.

31.   Felix-Ortiz Ada C, Beyeler A, Seo C, Leppla Christopher A, Wildes CP, Tye Kay M. BLA to vHPC Inputs Modulate Anxiety-Related Behaviors. Neuron. 2013;79(4):658-64.

32.   Felix-Ortiz AC, Tye KM. Amygdala Inputs to the Ventral Hippocampus Bidirectionally Modulate Social Behavior. The Journal of Neuroscience. 2014;34(2):586-95.

33.   Videbech P, Ravnkilde B. Hippocampal Volume and Depression: A Meta-Analysis of MRI Studies. Am J Psychiatry. 2004;161(11):1957-66.

34.   Campbell S, Marriott M, Nahmias C, MacQueen GM. Lower Hippocampal Volume in Patients Suffering From Depression: A Meta-Analysis. Am J Psychiatry. 2004;161(4):598-607.

35.   Arnone D, McKie S, Elliott R, Juhasz G, Thomas EJ, Downey D, Williams S, Deakin JFW, Anderson IM. State-dependent changes in hippocampal grey matter in depression. Molecular Psychiatry. 2012.

36.   Airan RD, Meltzer LA, Roy M, Gong Y, Chen H, Deisseroth K. High-Speed Imaging Reveals Neurophysiological Links to Behavior in an Animal Model of Depression. Science. 2007;317(5839):819-23.

37.   Padovan CM, Guimarães FS. Antidepressant-like effects of NMDA-receptor antagonist injected into the dorsal hippocampus of rats. Pharmacology Biochemistry and Behavior. 2004;77(1):15-9.

38.   Lu X-Y, Kim CS, Frazer A, Zhang W. Leptin: A potential novel antidepressant. PNAS. 2006;103(5):1593-8.

39.   McLaughlin RJ, Hill MN, Morrish AC, Gorzalka BB. Local enhancement of cannabinoid CB1 receptor signalling in the dorsal hippocampus elicits an antidepressant-like effect. Behavioural Pharmacology. 2007;18(5-6):431-8.

40.   MacQueen G, Frodl T. The hippocampus in major depression: evidence for the convergence of the bench and bedside in psychiatric research? Molecular Psychiatry. 2011;16(3):252-64.

41.   Price JL, Drevets WC. Neurocircuitry of Mood Disorders. Neuropsychopharmacology. 2010;35(1):192-216.

42.   Tahmasian M, Knight DC, Manoliu A, Schwerthöffer D, Scherr M, Meng C, Shao J, Peters H, Doll A, Khazaie H, Drzezga A, Bäuml J, Zimmer C, Förstl H, Wohlschläger AM, Riedl v, Sorg C. Aberrant intrinsic connectivity of hippocampus and amygdala overlap in the fronto-insular and dorsomedial-prefrontal cortex in major depressive disorder. Front Hum Neurosci. 2013;7.

43.   Admon R, Holsen LM, Aizley H, Remington A, Whitfield-Gabrieli S, Goldstein JM, Pizzagalli DA. Striatal Hypersensitivity During Stress in Remitted Individuals with Recurrent Depression. Biological Psychiatry.

44.   Sundermann B, Olde lütke Beverborg M, Pfleiderer B. Toward literature-based feature selection for diagnostic classification: a meta-analysis of resting-state fMRI in depression. Front Hum Neurosci. 2014;8.

45.   Strange BA, Witter MP, Lein ES, Moser EI. Functional organization of the hippocampal longitudinal axis. Nat Rev Neurosci. 2014;15(10):655-69.

46.   Fanselow MS, Dong H-W. Are the Dorsal and Ventral Hippocampus Functionally Distinct Structures? Neuron. 2010;65(1):7-19.

47.   Martínez-Téllez RI, Hernández-Torres E, Gamboa C, Flores G. Prenatal stress alters spine density and dendritic length of nucleus accumbens and hippocampus neurons in rat offspring. Synapse. 2009;63(9):794-804.

48.   Ferland CL, Schrader LA. Regulation of histone acetylation in the hippocampus of chronically stressed rats: a potential role of sirtuins. Neuroscience. 2011;174:104-14.

49.   Hunter RG, McCarthy KJ, Milne TA, Pfaff DW, McEwen BS. Regulation of hippocampal H3 histone methylation by acute and chronic stress. Proceedings of the National Academy of Sciences. 2009;106(49):20912-7.

50.   Alfarez DN, Joëls M, Krugers HJ. Chronic unpredictable stress impairs long-term potentiation in rat hippocampal CA1 area and dentate gyrus in vitro. European Journal of Neuroscience. 2003;17(9):1928-34.

51.   Cai X, Kallarackal AJ, Kvarta MD, Goluskin S, Gaylor K, Bailey AM, Lee H-K, Huganir RL, Thompson SM. Local potentiation of excitatory synapses by serotonin and its alteration in rodent models of depression. Nature Neuroscience. 2013;16(4):464-72.

52.   Burgdorf J, Zhang XL, Nicholson KL, Balster RL, Leander JD, Stanton PK, Gross AL, Kroes RA, Moskal JR. GLYX-13, a NMDA receptor glycine-site functional partial agonist, induces antidepressant-like effects without ketamine-like side effects. Neuropsychopharmacology. 2013;38(5):729-42; PMCID: 3671991.

53.   Krystal JH, Sanacora G, Duman RS. Rapid-Acting Glutamatergic Antidepressants: The Path to Ketamine and Beyond. Biological Psychiatry. 2013;73(12):1133-41.

54.   Autry AE, Adachi M, Nosyreva E, Na ES, Los MF, Cheng P-f, Kavalali ET, Monteggia LM. NMDA receptor blockade at rest triggers rapid behavioural antidepressant responses. Nature. 2011;475(7354):91-5.

55.   Berman RM, Cappiello A, Anand A, Oren DA, Heninger GR, Charney DS, Krystal JH. Antidepressant effects of ketamine in depressed patients. Biological Psychiatry. 2000;47(4):351-4.

56.   Zarate Ca, Jr. A randomized trial of an n-methyl-d-aspartate antagonist in treatment-resistant major depression. Arch Gen Psychiatry. 2006;63(8):856-64.

57.   Duncan WC, Sarasso S, Ferrarelli F, Selter J, Riedner BA, Hejazi NS, Yuan P, Brutsche N, Manji HK, Tononi G, Zarate CA. Concomitant BDNF and sleep slow wave changes indicate ketamine-induced plasticity in major depressive disorder. The International Journal of Neuropsychopharmacology. 2012;FirstView:1-11.

58.   Li N, Lee B, Liu R-J, Banasr M, Dwyer JM, Iwata M, Li X-Y, Aghajanian G, Duman RS. mTOR-Dependent Synapse Formation Underlies the Rapid Antidepressant Effects of NMDA Antagonists. Science. 2010;329(5994):959-64.

59.   Liu R-J, Lee FS, Li X-Y, Bambico F, Duman RS, Aghajanian GK. Brain-Derived Neurotrophic Factor Val66Met Allele Impairs Basal and Ketamine-Stimulated Synaptogenesis in Prefrontal Cortex. Biological Psychiatry. 2012;71(11):996-1005.

60.   Nosyreva E, Szabla K, Autry AE, Ryazanov AG, Monteggia LM, Kavalali ET. Acute Suppression of Spontaneous Neurotransmission Drives Synaptic Potentiation. The Journal of Neuroscience. 2013;33(16):6990-7002.

61.   Lenze EJ, Skidmore ER, Begley AE, Newcomer JW, Butters MA, Whyte EM. Memantine for late-life depression and apathy after a disabling medical event: a 12-week, double-blind placebo-controlled pilot study. Int J Geriatr Psychiatry. 2012;27(9):974-80.

62.   Zarate CA, Singh JB, Quiroz JA, De Jesus G, Denicoff KK, Luckenbaugh DA, Manji HK, Charney DS. A Double-Blind, Placebo-Controlled Study of Memantine in the Treatment of Major Depression. Am J Psychiatry. 2006;163(1):153-5.

63.   Gideons ES, Kavalali ET, Monteggia LM. Mechanisms underlying differential effectiveness of memantine and ketamine in rapid antidepressant responses. Proceedings of the National Academy of Sciences. 2014;111(23):8649-54.

64.   Kapur S, Seeman P. Ketamine has equal affinity for NMDA receptors and the high-affinity state of the dopamine d2 receptor. Biological Psychiatry. 2001;49(11):954-5.

65.   Hevers W, Hadley SH, Lüddens H, Amin J. Ketamine, But Not Phencyclidine, Selectively Modulates Cerebellar GABAA Receptors Containing α6 and δ Subunits. J Neurosci. 2008;28(20):5383-93.

66.   Zhou C, Douglas JE, Kumar NN, Shu S, Bayliss DA, Chen X. Forebrain HCN1 Channels Contribute to Hypnotic Actions of Ketamine. Anesthesiology. 2013.

67.   Chen X, Shu S, Bayliss DA. HCN1 Channel Subunits Are a Molecular Substrate for Hypnotic Actions of Ketamine. J Neurosci. 2009;29(3):600-9.

68.   Hu H, Vervaeke K, Storm JF. Two forms of electrical resonance at theta frequencies, generated by M-current, h-current and persistent Na+ current in rat hippocampal pyramidal cells. J Physiol. 2002;545(3):783-805.

69.   Narayanan R, Johnston D. Long-Term Potentiation in Rat Hippocampal Neurons Is Accompanied by Spatially Widespread Changes in Intrinsic Oscillatory Dynamics and Excitability. Neuron. 2007;56(6):1061-75.

70.   Narayanan R, Johnston D. The h Channel Mediates Location Dependence and Plasticity of Intrinsic Phase Response in Rat Hippocampal Neurons. J Neurosci. 2008;28(22):5846-60.

71.   Fan Y, Fricker D, Brager DH, Chen X, Lu H-C, Chitwood RA, Johnston D. Activity-dependent decrease of excitability in rat hippocampal neurons through increases in Ih. Nature Neuroscience. 2005;8(11):1542-51.

72.   Brager DH, Johnston D. Plasticity of Intrinsic Excitability during Long-Term Depression Is Mediated through mGluR-Dependent Changes in Ih in Hippocampal CA1 Pyramidal Neurons. J Neurosci. 2007;27(51):13926-37.

73.   Lewis AS, Estep C, Chetkovich DM. The fast and slow ups and downs of HCN channel regulation. Channels. 2010;4(3):73-89.

74.   Lewis AS, Vaidya SP, Blaiss CA, Liu Z, Stoub TR, Brager DH, Chen X, Bender RA, Estep CM, Popov AB, Kang CE, Van Veldhoven PP, Bayliss DA, Nicholson DA, Powell CM, Johnston D, Chetkovich DM. Deletion of the Hyperpolarization-Activated Cyclic Nucleotide-Gated Channel Auxiliary Subunit TRIP8b Impairs Hippocampal Ih Localization and Function and Promotes Antidepressant Behavior in Mice. J Neurosci. 2011;31(20):7424-40.

75.   Shin M, Brager D, Jaramillo TC, Johnston D, Chetkovich DM. Mislocalization of h channel subunits underlies h channelopathy in temporal lobe epilepsy. Neurobiology of Disease. 2008;32(1):26-36.

76.   Kim Chung S, Chang Payne Y, Johnston D. Enhancement of Dorsal Hippocampal Activity by Knockdown of HCN1 Channels Leads to Anxiolytic- and Antidepressant-like Behaviors. Neuron. 2012;75(3):503-16.

77.   Gu N, Vervaeke K, Hu H, Storm JF. Kv7/KCNQ/M and HCN/h, but not KCa2/SK channels, contribute to the somatic medium after-hyperpolarization and excitability control in CA1 hippocampal pyramidal cells. J Physiol. 2005;566(3):689-715.

78.   Wanat MJ, Hopf FW, Stuber GD, Phillips PEM, Bonci A. Corticotropin-releasing factor increases mouse ventral tegmental area dopamine neuron firing through a protein kinase C-dependent enhancement of Ih. J Physiol. 2008;586(8):2157-70.

79.   Lewis AS, Chetkovich DM. HCN channels in behavior and neurological disease: Too hyper or not active enough? Molecular and Cellular Neuroscience. 2011;46(2):357-67.

80.   Lewis AS, Schwartz E, Savio Chan C, Noam Y, Shin M, Wadman WJ, James Surmeier D, Baram TZ, Macdonald RL, Chetkovich DM. Alternatively Spliced Isoforms of TRIP8b Differentially Control H Channel Trafficking and Function. J Neurosci. 2009;29(19):6250-65.

81.   Brewster AL, Chen Y, Bender RA, Yeh A, Shigemoto R, Baram TZ. Quantitative Analysis and Subcellular Distribution of mRNA and Protein Expression of the Hyperpolarization-Activated Cyclic

Nucleotide-Gated Channels throughout Development in Rat Hippocampus. Cereb Cortex. 2007;17(3):702-12.

82.		Santoro B, Wainger BJ, Siegelbaum SA. Regulation of HCN Channel Surface Expression by a Novel C-Terminal Protein-Protein Interaction. J Neurosci. 2004;24(47):10750-62.

83.		Williams SR, Stuart GJ. Site Independence of EPSP Time Course Is Mediated by Dendritic I h in Neocortical Pyramidal Neurons. J Neurophysiol. 2000;83(5):3177-82.

84.		Harnett MT, Magee JC, Williams SR. Distribution and Function of HCN Channels in the Apical Dendritic Tuft of Neocortical Pyramidal Neurons. J Neurosci. 2015;35(3):1024-37.

85.		Qiu D-L, Chu C-P, Shirasaka T, Tsukino H, Nakao H, Kato K, Kunitake T, Katoh T, Kannan H. Corticotrophin-Releasing Factor Augments the IH in Rat Hypothalamic Paraventricular Nucleus Parvocellular Neurons In Vitro. J Neurophysiol. 2005;94(1):226-34.

86.		Giesbrecht CJ, Mackay JP, Silveira HB, Urban JH, Colmers WF. Countervailing Modulation of Ih by Neuropeptide Y and Corticotrophin-Releasing Factor in Basolateral Amygdala As a Possible Mechanism for Their Effects on Stress-Related Behaviors. J Neurosci. 2010;30(50):16970-82.

87.		Ludwig A, Budde T, Stieber J, Moosmang S, Wahl C, Holthoff K, Langebartels A, Wotjak C, Munsch T, Zong X, Feil S, Feil R, Lancel M, Chien KR, Konnerth A, Pape H-C, Biel M, Hofmann F. Absence epilepsy and sinus dysrhythmia in mice lacking the pacemaker channel HCN2. EMBO J. 2003;22(2):216-24.

88.		Santoro B, Piskorowski RA, Pian P, Hu L, Liu H, Siegelbaum SA. TRIP8b Splice Variants Form a Family of Auxiliary Subunits that Regulate Gating and Trafficking of HCN Channels in the Brain. Neuron. 2009;62(6):802-13.

89.		Piskorowski R, Santoro B, Siegelbaum Steven A. TRIP8b Splice Forms Act in Concert to Regulate the Localization and Expression of HCN1 Channels in CA1 Pyramidal Neurons. Neuron. 2011;70(3):495-509.

90.		Brager DH, Lewis AS, Chetkovich DM, Johnston D. Short- and long-term potentiation in CA1 neurons from mice lacking the h-channel auxiliary subunit TRIP8b. J Neurophysiol. 2013.

91.		Wang Z, Xu N-l, Wu C-p, Duan S, Poo M-m. Bidirectional Changes in Spatial Dendritic Integration Accompanying Long-Term Synaptic Modifications. Neuron. 2003;37(3):463-72.

92.		Magee JC. Dendritic Hyperpolarization-Activated Currents Modify the Integrative Properties of Hippocampal CA1 Pyramidal Neurons. J Neurosci. 1998;18(19):7613-24.

93.		Redlich R, Dohm K, Grotegerd D, Opel N, Zwitserlood P, Heindel W, Arolt V, Kugel H, Dannlowski U. Reward Processing in Unipolar and Bipolar Depression: A Functional MRI Study. Neuropsychopharmacology. 2015.

94.		Cao J-L, Covington HE, Friedman AK, Wilkinson MB, Walsh JJ, Cooper DC, Nestler EJ, Han M-H. Mesolimbic Dopamine Neurons in the Brain Reward Circuit Mediate Susceptibility to Social Defeat and Antidepressant Action. J Neurosci. 2010;30(49):16453-8.

95.		Friedman AK, Walsh JJ, Juarez B, Ku SM, Chaudhury D, Wang J, Li X, Dietz DM, Pan N, Vialou VF, Neve RL, Yue Z, Han M-H. Enhancing Depression Mechanisms in Midbrain Dopamine Neurons Achieves Homeostatic Resilience. Science. 2014;344(6181):313-9.

96.		Tsankova NM, Berton O, Renthal W, Kumar A, Neve RL, Nestler EJ. Sustained hippocampal chromatin regulation in a mouse model of depression and antidepressant action. Nature Neuroscience. 2006;9(4):519-25.

97.		Berton O, McClung CA, DiLeone RJ, Krishnan V, Renthal W, Russo SJ, Graham D, Tsankova NM, Bolanos CA, Rios M, Monteggia LM, Self DW, Nestler EJ. Essential Role of BDNF in the Mesolimbic Dopamine Pathway in Social Defeat Stress. Science. 2006;311(5762):864-8.

98.		Golden SA, Iii HEC, Berton O, Russo SJ. A standardized protocol for repeated social defeat stress in mice. Nat Protocols. 2011;6(8):1183-91.

99.		Marcelin B, Liu Z, Chen Y, Lewis AS, Becker A, McClelland S, Chetkovich DM, Migliore M, Baram TZ, Esclapez M, Bernard C. Dorsoventral Differences in Intrinsic Properties in Developing CA1 Pyramidal Cells. J Neurosci. 2012;32(11):3736-47.

100.		Bender RA, Brewster A, Santoro B, Ludwig A, Hofmann F, Biel M, Baram TZ. Differential and age-dependent expression of hyperpolarization-activated, cyclic nucleotide-gated cation channel isoforms 1–4 suggests evolving roles in the developing rat hippocampus. Neuroscience. 2001;106(4):689-98.

101.   Grigoryan G, Ardi Z, Albrecht A, Richter-Levin G, Segal M. Juvenile stress alters LTP in ventral hippocampal slices: Involvement of noradrenergic mechanisms. Behavioural Brain Research. 2015;278:559-62.

102.   Maggio N, Segal M. Persistent Changes in Ability to Express Long-Term Potentiation/Depression in the Rat Hippocampus After Juvenile/Adult Stress. Biological Psychiatry. 2011;69(8):748-53.

103.   Chen Y, Brunson KL, Adelmann G, Bender RA, Frotscher M, Baram TZ. Hippocampal corticotropin releasing hormone: pre- and postsynaptic location and release by stress. Neuroscience. 2004;126(3):533-40.

104.   Sarkar A, Chachra P, Kennedy P, Pena CJ, Desouza LA, Nestler EJ, Vaidya VA. Hippocampal HDAC4 Contributes to Postnatal Fluoxetine-Evoked Depression-Like Behavior. Neuropsychopharmacology. 2014;39(9):2221-32.

105.   Feder A, Nestler EJ, Charney DS. Psychobiology and molecular genetics of resilience. Nat Rev Neurosci. 2009;10(6):446-57.

106.   Charney DS. Psychobiological Mechanisms of Resilience and Vulnerability: Implications for Successful Adaptation to Extreme Stress. Am J Psychiatry. 2004;161(2):195-216.

107.   de Ridder D, Geenen R, Kuijer R, van Middendorp H. Psychological adjustment to chronic disease. The Lancet. 2008;372(9634):246-55.

108.   Southwick SM, Vythilingam M, Charney DS. The Psychobiology of Depression and Resilience to Stress: Implications for Prevention and Treatment. Annual Review of Clinical Psychology. 2005;1(1):255-91.

109.   Koolhaas JM, de Boer SF, Coppens CM, Buwalda B. Neuroendocrinology of coping styles: Towards understanding the biology of individual variation. Frontiers in Neuroendocrinology. 2010;31(3):307-21.

110.   Bjørkløf GH, Engedal K, Selbæk G, Kouwenhoven SE, Helvik A-S. Coping and Depression in Old Age: A Literature Review. DEM. 2013;35(3-4):121-54.

111.   Cairns KE, Yap MBH, Pilkington PD, Jorm AF. Risk and protective factors for depression that adolescents can modify: A systematic review and meta-analysis of longitudinal studies. Journal of Affective Disorders. 2014;169:61-75.

112.   Goossens PJJ, Klein EAMK-vd, Achterberg Tv. Coping Styles of Outpatients With a Bipolar Disorder. Archives of Psychiatric Nursing. 2008;22(5):245-53.

113.   Contractor AA, Armour C, Shea MT, Mota N, Pietrzak RH. Latent profiles of DSM-5 PTSD symptoms and the "Big Five" personality traits. Journal of Anxiety Disorders. 2016;37:10-20.

114.   Meyer B. Coping with Severe Mental Illness: Relations of the Brief COPE with Symptoms, Functioning, and Well-Being. Journal of Psychopathology and Behavioral Assessment. 2001;23(4):265-77.

115.   Humphreys K, Mankowski ES, Moos RH, Finney JW. Do enhanced friendship networks and active coping mediate the effect of self-help groups on substance abuse? Ann Behav Med. 1999;21(1):54-60.

116.   Moser AE, Annis HM. The role of coping in relapse crisis outcome: a prospective study of treated alcoholics. Addiction. 1996;91(8):1101-14.

117.   Stewart DE, Yuen T. A Systematic Review of Resilience in the Physically Ill. Psychosomatics. 2011;52(3):199-209.

118.   Chiavarino C, Rabellino D, Ardito RB, Cavallero E, Palumbo L, Bergerone S, Gaita F, Bara BG. Emotional coping is a better predictor of cardiac prognosis than depression and anxiety. Journal of Psychosomatic Research. 2012;73(6):473-5.

119.   Huang C-Y, Lai H-L, Lu Y-C, Chen W-K, Chi S-C, Lu C-Y, Chen C-I. Risk Factors and Coping Style Affect Health Outcomes in Adults With Type 2 Diabetes. Biological Research For Nursing. 2016;18(1):82-9.

120.   Gore-felton C, Koopman C. Behavioral Mediation of the Relationship Between Psychosocial Factors and Hiv Disease Progression. Psychosomatic Medicine. 2008;70(5):569-74.

121.   Tielemans NS, Visser-Meily JM, Schepers VP, Post MW, Heugten CMv. Proactive Coping Poststroke: Psychometric Properties of the Utrecht Proactive Coping Competence Scale. Archives of Physical Medicine and Rehabilitation. 2014;95(4):670-5.

122.   de Boer SF, Buwalda B, Koolhaas JM. Untangling the neurobiology of coping styles in rodents: Towards neural mechanisms underlying individual differences in disease susceptibility. Neuroscience & Biobehavioral Reviews. 2017;74:401-22.

123.   Coppens CM, Boer SFd, Koolhaas JM. Coping styles and behavioural flexibility: towards underlying mechanisms. Philosophical Transactions of the Royal Society B: Biological Sciences. 2010;365(1560):4021.

124.   De Boer SF, Koolhaas JM. Defensive burying in rodents: ethology, neurobiology and psychopharmacology. European Journal of Pharmacology. 2003;463(1–3):145-61.

125.   Joca SRL, Zanelati T, Guimarães FS. Post-stress facilitation of serotonergic, but not noradrenergic, neurotransmission in the dorsal hippocampus prevents learned helplessness development in rats. Brain Research. 2006;1087(1):67-74.

126.   Bambico FR, Nguyen N-T, Gobbi G. Decline in serotonergic firing activity and desensitization of 5-HT1A autoreceptors after chronic unpredictable stress. European Neuropsychopharmacology. 2009;19(3):215-28.

127.   Korte SM, Meijer OC, de Kloet ER, Buwalda B, Keijser J, Sluyter F, van Oortmerssen G, Bohus B. Enhanced 5-HT1A receptor expression in forebrain regions of aggressive house mice. Brain Research. 1996;736(1–2):338-43.

128.   van Riel E, Meijer OC, Veenema AH, Joëls M. Hippocampal serotonin responses in short and long attack latency mice. J Neuroendocrinol. 2002;14(3):234-9.

129.   Ebner K, Singewald GM, Whittle N, Ferraguti F, Singewald N. Neurokinin 1 Receptor Antagonism Promotes Active Stress Coping Via Enhanced Septal 5-HT Transmission. Neuropsychopharmacology. 2007;33(8):1929-41.

130.   Singewald GM, Rjabokon A, Singewald N, Ebner K. The Modulatory Role of the Lateral Septum on Neuroendocrine and Behavioral Stress Responses. Neuropsychopharmacology. 2011;36(4):793-804.

131.   Sheehan TP, Chambers RA, Russell DS. Regulation of affect by the lateral septum: implications for neuropsychiatry. Brain Research Reviews. 2004;46(1):71-117.

132.   Luo AH, Tahsili-Fahadan P, Wise RA, Lupica CR, Aston-Jones G. Linking Context with Reward: A Functional Circuit from Hippocampal CA3 to Ventral Tegmental Area. Science. 2011;333(6040):353-7.

133.   Degroot A, Kashluba S, Treit D. Septal GABAergic and hippocampal cholinergic systems modulate anxiety in the plus-maze and shock-probe tests. Pharmacology Biochemistry and Behavior. 2001;69(3):391-9.

134.   Clinton SM, Kerman IA, Orr HR, Bedrosian TA, Abraham AD, Simpson DN, Watson SJ, Akil H. Pattern of forebrain activation in high novelty-seeking rats following aggressive encounter. Brain Research. 2011;1422:20-31.

135.   Haller J, Tóth M, Halasz J, De Boer SF. Patterns of violent aggression-induced brain c-fos expression in male mice selected for aggressiveness. Physiology & Behavior. 2006;88(1):173-82.

136.   Park HG, Carmel JB. Selective Manipulation of Neural Circuits. Neurotherapeutics. 2016;13(2):311.

137.   Han Y, Heuermann RJ, Lyman KA, Fisher D, Ismail QA, Chetkovich DM. HCN-channel dendritic targeting requires bipartite interaction with TRIP8b and regulates antidepressant-like behavioral effects. Molecular Psychiatry. 2017;22(3):458-65.

138.   Marcelin B, Lugo JN, Brewster AL, Liu Z, Lewis AS, McClelland S, Chetkovich DM, Baram TZ, Anderson AE, Becker A, Esclapez M, Bernard C. Differential Dorso-Ventral Distributions of Kv4.2 and HCN Proteins Confer Distinct Integrative Properties to Hippocampal CA1 Pyramidal Cell Distal Dendrites. J Biol Chem. 2012;287(21):17656-61.

139.   Biel M, Wahl-Schott C, Michalakis S, Zong X. Hyperpolarization-Activated Cation Channels: From Genes to Function. Physiological Reviews. 2009;89(3):847-85.

140.   Nolan MF, Malleret G, Dudman JT, Buhl DL, Santoro B, Gibbs E, Vronskaya S, Buzsáki G, Siegelbaum SA, Kandel ER, Morozov A. A Behavioral Role for Dendritic Integration: HCN1 Channels Constrain Spatial Memory and Plasticity at Inputs to Distal Dendrites of CA1 Pyramidal Neurons. Cell. 2004;119(5):719-32.

141.   Nolan MF, Malleret G, Lee KH, Gibbs E, Dudman JT, Santoro B, Yin D, Thompson RF, Siegelbaum SA, Kandel ER, Morozov A. The Hyperpolarization-Activated HCN1 Channel Is Important for Motor Learning and Neuronal Integration by Cerebellar Purkinje Cells. Cell. 2003;115(5):551-64.

142. Chung WK, Shin M, Jaramillo TC, Leibel RL, LeDuc CA, Fischer SG, Tzilianos E, Gheith AA, Lewis AS, Chetkovich DM. Absence epilepsy in apathetic, a spontaneous mutant mouse lacking the h channel subunit, HCN2. Neurobiology of Disease. 2009;33(3):499-508.

143. Tsantoulas C, Mooney ER, McNaughton PA. HCN2 ion channels: basic science opens up possibilities for therapeutic intervention in neuropathic pain. Biochemical Journal. 2016;473(18):2717-36.

144. Matt L, Michalakis S, Hofmann F, Hammelmann V, Ludwig A, Biel M, Kleppisch T. HCN2 channels in local inhibitory interneurons constrain LTP in the hippocampal direct perforant path. Cell Mol Life Sci. 2011;68(1):125-37.

145. Emery EC, Young GT, Berrocoso EM, Chen L, McNaughton PA. HCN2 Ion Channels Play a Central Role in Inflammatory and Neuropathic Pain. Science. 2011;333(6048):1462-6.

146. Schnorr S, Eberhardt M, Kistner K, Rajab H, Käer J, Hess A, Reeh P, Ludwig A, Herrmann S. hcn2 channels account for mechanical (but not heat) hyperalgesia during long-standing inflammation. Pain. 2014;155(6):1079-90.

147. Zhang Y, Liu Y, Qu J, Hardy A, Zhang N, Diao J, Strijbos PJ, Tsushima R, Robinson RB, Gaisano HY, Wang Q, Wheeler MB. Functional Characterization of HCN Channels in Rat Pancreatic β Cells. The Journal of endocrinology. 2009;203(1):45.

148. Kretschmannova K, Kucka M, Gonzalez-Iglesias AE, Stojilkovic SS. The Expression and Role of Hyperpolarization-Activated and Cyclic Nucleotide-Gated Channels in Endocrine Anterior Pituitary Cells. Molecular Endocrinology. 2012;26(1):153.

149. Calejo AI, Jorgačevski J, Rituper B, Guček A, Pereira PM, Santos MAS, Potokar M, Vardjan N, Kreft M, Gonçalves PP, Zorec R. Hyperpolarization-Activated Cyclic Nucleotide-Gated Channels and cAMP-Dependent Modulation of Exocytosis in Cultured Rat Lactotrophs. Journal of Neuroscience. 2014;34(47):15638-47.

150. Shahi PK, Choi S, Zuo DC, Kim MY, Park CG, Kim YD, Lee J, Park KJ, So I, Jun JY. The possible roles of hyperpolarization-activated cyclic nucleotide channels in regulating pacemaker activity in colonic interstitial cells of Cajal. Journal of Gastroenterology. 2014;49(6):1001.

151. Si X, Huang L, Gong Y, Lu J, Lin L. Role of calcium in activation of hyperpolarization-activated cyclic nucleotide-gated channels caused by cholecystokinin octapeptide in interstitial cells of cajal. Digestion. 2012;85(4):266-75.

152. Mao Y, Wang B, Kunze W. Characterization of Myenteric Sensory Neurons in the Mouse Small Intestine. J Neurophysiol. 2006;96(3):998-1010.

153. Xiao J, Nguyen TV, Ngui K, Strijbos PJLM, Selmer IS, Neylon CB, Furness JB. Molecular and functional analysis of hyperpolarisation-activated nucleotide-gated (HCN) channels in the enteric nervous system. Neuroscience. 2004;129(3):603-14.

154. Guo T, Li J, Li J, Kong D, Bi C, He Z, Tang D, Jin X, Jin L. Association between hyperpolarization-activated channel in interstitial cells of Cajal and gastrointestinal dysmotility induced by malignant ascites. Oncology Letters. 2017;13(3):1601.

155. Buniel M, Glazebrook PA, Ramirez-Navarro A, Kunze DL. Distribution of voltage-gated potassium (Kv) and hyperpolarization-activated (HCN) channels in sensory afferent fibers in the rat carotid body. The Journal of comparative neurology. 2008;510(4):367.

156. Hurtado R, Smith CS. Hyperpolarization-activated cation and T-type calcium ion channel expression in porcine and human renal pacemaker tissues. Journal of Anatomy. 2016;228(5):812-25.

157. Bolívar JJ, Tapia D, Arenas G, Castañón-Arreola M, Torres H, Galarraga E. A hyperpolarization-activated, cyclic nucleotide-gated, (Ih-like) cationic current and HCN gene expression in renal inner medullary collecting duct cells. American Journal of Physiology - Cell Physiology. 2008;294(4):C893-C906.

158. Carrisoza-Gaytán R, Rangel C, Salvador C, Saldaña-Meyer R, Escalona C, Satlin LM, Liu W, Zavilowitz B, Trujillo J, Bobadilla NA, Escobar LI. The hyperpolarization-activated cyclic nucleotide-gated HCN2 channel transports ammonium in the distal nephron. Kidney International. 2011;80(8):832-40.

159. Yang S, Xiong C-j, Sun H-m, Li X-s, Zhang G-q, Wu B, Zhou D-s. The distribution of HCN2-positive cells in the gastrointestinal tract of mice. Journal of Anatomy. 2012;221(4):303.

160. Mathers CD, Loncar D. Projections of Global Mortality and Burden of Disease from 2002 to 2030. PLoS Med. 2006;3(11).

161. Weissman Mm BRC. CRoss-national epidemiology of major depression and bipolar disorder. JAMA. 1996;276(4):293-9.

162.   Cryan JF, Mombereau C. In search of a depressed mouse: utility of models for studying depression-related behavior in genetically modified mice. Molecular Psychiatry. 2004;9(4):326-57.

163.   Kolber BJ, Boyle MP, Wieczorek L, Kelley CL, Onwuzurike CC, Nettles SA, Vogt SK, Muglia LJ. Transient Early-Life Forebrain Corticotropin-Releasing Hormone Elevation Causes Long-Lasting Anxiogenic and Despair-Like Changes in Mice. J Neurosci. 2010;30(7):2571-81.

164.   Shin M, Chetkovich DM. Activity-dependent Regulation of h Channel Distribution in Hippocampal CA1 Pyramidal Neurons. J Biol Chem. 2007;282(45):33168-80.

165.   Shin M, Simkin D, Suyeoka GM, Chetkovich DM. Evaluation of HCN2 abnormalities as a cause of juvenile audiogenic seizures in Black Swiss mice. Brain Research. 2006;1083(1):14-20.

166.   Peña CJ, Kronman HG, Walker DM, Cates HM, Bagot RC, Purushothaman I, Issler O, Loh Y-HE, Leong T, Kiraly DD, Goodman E, Neve RL, Shen L, Nestler EJ. Early life stress confers lifelong stress susceptibility in mice via ventral tegmental area OTX2. Science. 2017;356(6343):1185-8.

167.   Notomi T, Shigemoto R. Immunohistochemical localization of Ih channel subunits, HCN1–4, in the rat brain. The Journal of Comparative Neurology. 2004;471(3):241-76.

168.   Bagot RC, Cates HM, Purushothaman I, Lorsch ZS, Walker DM, Wang J, Huang X, Schlüter OM, Maze I, Peña CJ, Heller EA, Issler O, Wang M, Song W-m, Stein JL, Liu X, Doyle MA, Scobie KN, Sun HS, Neve RL, Geschwind D, Dong Y, Shen L, Zhang B, Nestler EJ. Circuit-wide transcriptional profiling reveals brain region-specific gene networks regulating depression susceptibility. Neuron. 2016;90(5):969.

169.   Magariños AM, Li CJ, Toth JG, Bath KG, Jing D, Lee FS, McEwen BS. Effect of Brain-Derived Neurotrophic Factor Haploinsufficiency on Stress-Induced Remodeling of Hippocampal Neurons. Hippocampus. 2011;21(3):253.

170.   Edgar N, Sibille E. A putative functional role for oligodendrocytes in mood regulation. Transl Psychiatry. 2012;2:e109.

171.   Krishnan V, Han M-H, Graham DL, Berton O, Renthal W, Russo SJ, LaPlant Q, Graham A, Lutter M, Lagace DC, Ghose S, Reister R, Tannous P, Green TA, Neve RL, Chakravarty S, Kumar A, Eisch AJ, Self DW, Lee FS, Tamminga CA, Cooper DC, Gershenfeld HK, Nestler EJ. Molecular Adaptations Underlying Susceptibility and Resistance to Social Defeat in Brain Reward Regions. Cell. 2007;131(2):391-404.

172.   Guilloux J-P, Seney M, Edgar N, Sibille E. Integrated behavioral z-scoring increases the sensitivity and reliability of behavioral phenotyping in mice: Relevance to emotionality and sex. Journal of Neuroscience Methods. 2011;197(1):21-31.

173.   de Kloet ER, Molendijk ML. Coping with the Forced Swim Stressor: Towards Understanding an Adaptive Mechanism. Neural Plasticity. 2016;2016:e6503162.

174.   O'Leary OF, Felice D, Galimberti S, Savignac HM, Bravo JA, Crowley T, El Yacoubi M, Vaugeois J-M, Gassmann M, Bettler B, Dinan TG, Cryan JF. GABAB(1) receptor subunit isoforms differentially regulate stress resilience. PNAS. 2014;111(42):15232-7.

175.   Fischell J, Van Dyke AM, Kvarta MD, LeGates TA, Thompson SM. Rapid Antidepressant Action and Restoration of Excitatory Synaptic Strength After Chronic Stress by Negative Modulators of Alpha5-Containing GABAA Receptors. Neuropsychopharmacology. 2015;40(11):2499-509.

176.   Zanos P, Moaddel R, Morris PJ, Georgiou P, Fischell J, Elmer GI, Alkondon M, Yuan P, Pribut HJ, Singh NS, Dossou KSS, Fang Y, Huang X-P, Mayo CL, Wainer IW, Albuquerque EX, Thompson SM, Thomas CJ, Zarate CA, Jr, Gould TD. NMDAR inhibition-independent antidepressant actions of ketamine metabolites. Nature. 2016;533(7604):481.

177.   Nolan MF, Dudman JT, Dodson PD, Santoro B. HCN1 Channels Control Resting and Active Integrative Properties of Stellate Cells from Layer II of the Entorhinal Cortex. J Neurosci. 2007;27(46):12440-51.

178.   Schaefer AT, Angelo K, Spors H, Margrie TW. Neuronal Oscillations Enhance Stimulus Discrimination by Ensuring Action Potential Precision. PLoS Biol. 2006;4(6).

179.   Lörincz A, Notomi T, Tamás G, Shigemoto R, Nusser Z. Polarized and compartment-dependent distribution of HCN1 in pyramidal cell dendrites. Nature Neuroscience. 2002;5(11):1185-93.

180.   Kim CS, Brager DH, Johnston D. Perisomatic changes in h-channels regulate depressive behaviors following chronic unpredictable stress. Molecular Psychiatry. 2017.

181.   O'Leary OF, Cryan JF. A ventral view on antidepressant action: roles for adult hippocampal neurogenesis along the dorsoventral axis. Trends in Pharmacological Sciences. 2014;35(12):675-87.

182.   Pinto V, Costa JC, Morgado P, Mota C, Miranda A, Bravo FV, Oliveira TG, Cerqueira JJ, Sousa N. Differential impact of chronic stress along the hippocampal dorsal–ventral axis. Brain Struct Funct. 2015;220(2):1205-12.

183.   Bagot RC, Parise EM, Peña CJ, Zhang H-X, Maze I, Chaudhury D, Persaud B, Cachope R, Bolaños-Guzmán CA, Cheer JF, Cheer J, Deisseroth K, Han M-H, Nestler EJ. Ventral hippocampal afferents to the nucleus accumbens regulate susceptibility to depression. Nat Commun. 2015;6:7062.

184.   Russo SJ, Murrough JW, Han M-H, Charney DS, Nestler EJ. Neurobiology of resilience. Nature Neuroscience. 2012;15(11):1475-84.

185.   Wood SK, Walker HE, Valentino RJ, Bhatnagar S. Individual Differences in Reactivity to Social Stress Predict Susceptibility and Resilience to a Depressive Phenotype: Role of Corticotropin-Releasing Factor. Endocrinology. 2010;151(4):1795.

186.   Vidal J, Buwalda B, Koolhaas JM. Male Wistar rats are more susceptible to lasting social anxiety than Wild-type Groningen rats following social defeat stress during adolescence. Behavioural Processes. 2011;88(2):76-80.

187.   Koolhaas JM, Coppens CM, Boer SFd, Buwalda B, Meerlo P, Timmermans PJA. The Resident-intruder Paradigm: A Standardized Test for Aggression, Violence and Social Stress. JoVE (Journal of Visualized Experiments). 2013(77):e4367-e.

188.   Degroot A, Nomikos GG. Genetic deletion and pharmacological blockade of CB1 receptors modulates anxiety in the shock-probe burying test. European Journal of Neuroscience. 2004;20(4):1059-64.

189.   Boucher AA, Arnold JC, Hunt GE, Spiro A, Spencer J, Brown C, McGregor IS, Bennett MR, Kassiou M. Resilience and reduced c-Fos expression in P2X7 receptor knockout mice exposed to repeated forced swim test. Neuroscience. 2011;189:170-7.

190.   Casey BJ, Craddock N, Cuthbert BN, Hyman SE, Lee FS, Ressler KJ. DSM-5 and RDoC: progress in psychiatry research? Nat Rev Neurosci. 2013;14(11):810-4.

191.   Insel T, Cuthbert B, Garvey M, Heinssen R, Pine DS, Quinn K, Sanislow C, Wang P. Research Domain Criteria (RDoC): Toward a New Classification Framework for Research on Mental Disorders. Am J Psychiatry. 2010;167(7):748-51.

192.   Tiscornia G, Singer O, Ikawa M, Verma IM. A general method for gene knockdown in mice by using lentiviral vectors expressing small interfering RNA. PNAS. 2003;100(4):1844.

193.   Paddison PJ, Caudy AA, Bernstein E, Hannon GJ, Conklin DS. Short hairpin RNAs (shRNAs) induce sequence-specific silencing in mammalian cells. Genes Dev. 2002;16(8):948-58.

194.   Kheirbek MA, Drew LJ, Burghardt NS, Costantini DO, Tannenholz L, Ahmari SE, Zeng H, Fenton AA, Hen R. Differential Control of Learning and Anxiety along the Dorsoventral Axis of the Dentate Gyrus. Neuron. 2013;77(5):955-68.

195.   Tannenholz L, Jimenez JC, Kheirbek MA. Local and regional heterogeneity underlying hippocampal modulation of cognition and mood. Front Behav Neurosci. 2014;8.

196.   Romanelli MN, Sartiani L, Masi A, Mannaioni G, Manetti D, Mugelli A, Cerbai E. HCN Channels Modulators: The Need for Selectivity. Curr Top Med Chem. 2016;16(16):1764-91.

197.   Heuermann RJ, Jaramillo TC, Ying S-W, Suter BA, Lyman KA, Han Y, Lewis AS, Hampton TG, Shepherd GMG, Goldstein PA, Chetkovich DM. Reduction of thalamic and cortical Ih by deletion of TRIP8b produces a mouse model of human absence epilepsy. Neurobiology of Disease. 2016;85:81.

198.   Lyman KA, Han Y, Chetkovich DM. Animal models suggest the TRIP8b-HCN interaction is a therapeutic target for major depressive disorder. Expert Opinion on Therapeutic Targets. 2017;21(3):235-7.

199.   Stieber J, Herrmann S, Feil S, Löster J, Feil R, Biel M, Hofmann F, Ludwig A. The hyperpolarization-activated channel HCN4 is required for the generation of pacemaker action potentials in the embryonic heart. Proceedings of the National Academy of Sciences. 2003;100(25):15235-40.

200.   Karst SY, Ward-Bailey P, Samples R, Johnson K, Donahue LR, Davisson M. Tremor and reduced lifespan 2 Jackson: a new remutation on Chromosome 10. MGI Database. 2008.

201.   Fazeli PK, Klibanski A. Determinants of GH resistance in malnutrition. J Endocrinol. 2014;220(3):R57-R65.

202.   Shi ZX, Levy A, Lightman SL. The effect of dietary protein on thyrotropin-releasing hormone and thyrotropin gene expression. Brain Research. 1993;606(1):1-4.

203.   Amendola E, De Luca P, Macchia PE, Terracciano D, Rosica A, Chiappetta G, Kimura S, Mansouri A, Affuso A, Arra C, Macchia V, Di Lauro R, De Felice M. A Mouse Model Demonstrates a Multigenic Origin of Congenital Hypothyroidism. Endocrinology. 2005;146(12):5038-47.

204.   Johnson KR, Marden CC, Ward-Bailey P, Gagnon LH, Bronson RT, Donahue LR. Congenital Hypothyroidism, Dwarfism, and Hearing Impairment Caused by a Missense Mutation in the Mouse Dual Oxidase 2 Gene, Duox2. Molecular Endocrinology. 2007;21(7):1593-602.

205.   Takabayashi S, Umeki K, Yamamoto E, Suzuki T, Okayama A, Katoh H. A Novel Hypothyroid Dwarfism Due to the Missense Mutation Arg479Cys of the Thyroid Peroxidase Gene in the Mouse. Molecular Endocrinology. 2006;20(10):2584-90.

206.   Roepke TK, King EC, Reyna-Neyra A, Paroder M, Purtell K, Koba W, Fine E, Lerner DJ, Carrasco N, Abbott GW. Kcne2 deletion uncovers its crucial role in thyroid hormone biosynthesis. Nature Medicine. 2009;15(10):1186-94.

207.   Hauck AL, Swanson KS, Kenis PJA, Leckband DE, Gaskins HR, Schook LB. Twists and turns in the development and maintenance of the mammalian small intestine epithelium. Birth Defects Research Part C: Embryo Today: Reviews. 2005;75(1):58-71.

208.   Stenson WF. Postnatal growth in the intestine. Current Opinion in Gastroenterology. 2013;29(2):107-11.

209.   McMenamin CA, Travagli RA, Browning KN. Inhibitory neurotransmission regulates vagal efferent activity and gastric motility. Exp Biol Med (Maywood). 2016;241(12):1343-50.

210.   Nakamura Y, Shi X, Numata T, Mori Y, Inoue R, Lossin C, Baram TZ, Hirose S. Novel HCN2 Mutation Contributes to Febrile Seizures by Shifting the Channel's Kinetics in a Temperature-Dependent Manner. PLoS ONE. 2013;8(12):e80376.

211.   DiFrancesco JC, Barbuti A, Milanesi R, Coco S, Bucchi A, Bottelli G, Ferrarese C, Franceschetti S, Terragni B, Baruscotti M, DiFrancesco D. Recessive Loss-of-Function Mutation in the Pacemaker HCN2 Channel Causing Increased Neuronal Excitability in a Patient with Idiopathic Generalized Epilepsy. Journal of Neuroscience. 2011;31(48):17327-37.

212.   Dibbens LM, Reid CA, Hodgson B, Thomas EA, Phillips AM, Gazina E, Cromer BA, Clarke AL, Baram TZ, Scheffer IE, Berkovic SF, Petrou S. Augmented currents of an HCN2 variant in patients with febrile seizure syndromes. Annals of Neurology. 2010;67(4):542-6.

213.   Império GEd, Ramos IP, Santiago LA, Pereira GF, Almeida NAdS, Fuziwara CS, Pazos-Moura CC, Kimura ET, Olivares EL, Ortiga-Carvalho TM. The Impact of a Non-Functional Thyroid Receptor Beta upon Triiodotironine-Induced Cardiac Hypertrophy in Mice. CPB. 2015;37(2):477-90.

214.   Xie TY, Ngo ST, Veldhuis JD, Jeffery PL, Chopin LK, Tschöp M, Waters MJ, Tolle V, Epelbaum J, Chen C, Steyn FJ. Effect of Deletion of Ghrelin-O-Acyltransferase on the Pulsatile Release of Growth Hormone in Mice. J Neuroendocrinol. 2015;27(12):872-86.

215.   Chitkara DK, di Lorenzo C. From the bench to the 'crib'-side: implications of scientific advances to paediatric neurogastroenterology and motility. Neurogastroenterology & Motility. 2006;18(4):251-62.

216.   Mostafa RM, Moustafa YM, Hamdy H. Interstitial cells of Cajal, the Maestro in health and disease. World Journal of Gastroenterology : WJG. 2010;16(26):3239.

217.   Vittal H, Farrugia G, Gomez G, Pasricha PJ. Mechanisms of Disease: the pathological basis of gastroparesis—a review of experimental and clinical studies. Nature Clinical Practice Gastroenterology & Hepatology. 2007;4(6):336-46.

218.   Pellegrini C, Antonioli L, Colucci R, Ballabeni V, Barocelli E, Bernardini N, Blandizzi C, Fornai M. Gastric motor dysfunctions in Parkinson's disease: Current pre-clinical evidence. Parkinsonism & Related Disorders. 2015;21(12):1407-14.

219.   Jost WH. Gastrointestinal dysfunction in Parkinson's Disease. Journal of the Neurological Sciences. 2010;289(1):69-73.

220.   Ukleja A. Altered GI Motility in Critically Ill Patients: Current Understanding of Pathophysiology, Clinical Impact, and Diagnostic Approach. Nutr Clin Pract. 2010;25(1):16-25.

221.   Abell TL, Malinowski S, Minocha A. Nutrition Aspects of Gastroparesis and Therapies for Drug-Refractory Patients. Nutr Clin Pract. 2006;21(1):23-33.

222.   O'Donnell AM, Coyle D, Puri P. Decreased expression of hyperpolarisation-activated cyclic nucleotide-gated channel 3 in Hirschsprung's disease. World Journal of Gastroenterology : WJG. 2015;21(18):5635-40.

223.   Tu H, Zhang L, Tran TP, Muelleman RL, Li YL. Diabetes alters protein expression of hyperpolarization-activated cyclic nucleotide-gated channel subunits in rat nodose ganglion cells. Neuroscience. 2010;165(1):39-52.

224.   Chan CS, Glajch KE, Gertler TS, Guzman JN, Mercer JN, Lewis AS, Goldberg AB, Tkatch T, Shigemoto R, Fleming SM, Chetkovich DM, Osten P, Kita H, Surmeier DJ. HCN channelopathy in external globus pallidus neurons in models of Parkinson's disease. Nature Neuroscience. 2010;14(1):85-92.

225.   Commons KG, Cholanians AB, Babb JA, Ehlinger DG. The Rodent Forced Swim Test Measures Stress-Coping Strategy, Not Depression-like Behavior. ACS Chem Neurosci. 2017;8(5):955-60.

226.   Weese-Mayer DE, Marazita ML, Rand CM, Berry-Kravis EM. Congenital Central Hypoventilation Syndrome. In: Pagon RA, Adam MP, Ardinger HH, Wallace SE, Amemiya A, Bean LJH, et al., editors. GeneReviews(®). Seattle (WA): University of Washington, Seattle; 1993.